ENGINEERING AMPHIPHILIC FABRICS FOR MICROFLUIDIC APPLICATIONS

A Dissertation
Presented to
The Academic Faculty

by

Tracie LeeAnne Owens

In Partial Fulfillment
of the Requirements for the Degree
Doctor of Philosophy in the
School of Chemical & Biomolecular Engineering

Georgia Institute of Technology
December 2011

ENGINEERING AMPHIPHILIC FABRICS FOR MICROFLUIDIC APPLICATIONS

Approved by:

Dr. Victor Breedveld, Advisor
School of Chemical & Biomolecular Engineering
Georgia Institute of Technology

Dr. Tom Fuller
School of Chemical & Biomolecular Engineering
Georgia Institute of Technology

Dr. Haskell Beckham, Co-Advisor
School of Materials Science and Engineering
Georgia Institute of Technology

Dr. Sankar Nair
School of Chemical & Biomolecular Engineering
Georgia Institute of Technology

Dr. Yulin Deng
School of Chemical & Biomolecular Engineering
Georgia Institute of Technology

Dr. Spyros Pavlostathis
School of Civil & Environmental Engineering
Georgia Institute of Technology

Date Approved: November 9, 2011

To my parents Timothy and Ernestine Owens for their love, support and for emphasizing the importance of an education

ACKNOWLEDGEMENTS

I would like to thank all those who have contributed to this work and my academic development. First, I want to thank Dr. Victor Breedveld for his guidance and support during my undergraduate and graduate research. Learning from his unique approach to problem solving has made me a better engineer and I am so happy to have had the opportunity to work with him. I would also like to thank Dr. Haskell Beckham for his support and guidance. He has an extensive background in chemistry and textile manufacturing. An understanding of these topics was critical to the success of my graduate research. I am grateful that he was always available to answer my questions and steer me in the right direction during my thesis work. I also wish to thank Dr. Johannes Leisen. This research was based on his ideas about the potential benefits of flow in amphiphilic fabrics. He has also provided valuable suggestions during the course of my graduate studies that have contributed to the success of my thesis work.

I would also like to thank my committee members: Dr. Yulin Deng, Dr. Tom Fuller, Dr. Sankar Nair, and Dr. Spyros Pavlostathis, for their insight and suggestions. I want to thank the Complex Fluids Research Group members I have worked with as an undergraduate and graduate student. Past lab colleagues: Dr. Raymond Tu, Dr. Santosh Rahane, Dr. Jun Sato, Dr. Ryan Slopek, Dr. Jae Kyu Cho, Dr. Balamurali Balu, and Dr. Kayode Olanrewaju, and current lab colleagues: Emily Peterson, Kyung-Hee Oh, Lester Li, and Sri Charan Yarlagadda. I extend thanks to all of the members of Dr. Beckham's research group. I would also like to thank Jun Suk Lee who was an undergraduate student that worked with me on some of the wicking experiments.

I would also wish to thank the organizations that were involved with the manufacturing of the amphiphilic fabrics studied in this thesis: Patrick Yarns and the Textile Technology Center of Gaston College. Additional thanks goes to the Chemistry Department at Spelman College for allowing me to use their Flame Atomic Absorbance Spectrometer (FAAS). A special thanks is extended to Dr. Cornelia Gillyard who put me in contact with Dr. Peter Chen who provided guidance on the use of the FAAS. I thank Dr. Chen for all his help.

I certainly cannot imagine graduate school without the support of my friends and family. I am so grateful to my good friends Mallarie McCune, Mayisha Ealey, Kendra Maxwell, Belinda Williams and Jessica Taylor.

Words cannot describe the love and appreciation I have for my family. There is no amount of thanks I can extend to my parents, Timothy and Ernestine Owens, to match their support. I will always be grateful to them for everything they have done for me and I feel truly blessed to be their daughter. I also must thank my sisters Chanda and Edie Owens. They have been there for me through everything, and I thank them for seeing me through my thesis work as well. I also want to thank my niece MacKenzie Taylor Owens. She is such a sweet little girl and can always make me laugh. I wish to thank my cousin Edynn Prevost, my aunts Idanell Barnett and Edith Prevost, and my Uncle Louis Barnett, whose advice and support I can always count on. Finally, to every member of the Owens and Walker families thank you and I love you.

TABLE OF CONTENTS

Page

ACKNOWLEDGEMENTS i

LIST OF TABLES viii

LIST OF FIGURES ix

LIST OF SYMBOLS AND ABBREVIATIONS xv

SUMMARY xix

CHAPTER

1 Introduction 1

1.1 Control of Fluid Flow at Micrometer Length-Scales 1

1.1.1 Interfacial Forces and Capillary Action 1

1.1.2 Surface Area to Volume Ratio 4

1.1.3 Laminar Flow 6

1.1.4 Mass Diffusion 6

1.2 Microfluidics 7

1.2.1 History 8

1.2.2 Fabrication of Microfluidic Devices 10

1.2.3 Soft Lithography 11

1.2.4 Microfluidic Applications, Advances and Limitations 12

1.3 Textiles 16

1.3.1 History 16

1.3.2 Textile Applications 18

1.3.3 Textile Manufacturing 19

1.3.4 Fabric Performance Parameters 31

1.3.5 Wicking Studies 34

1.4 Motivation and Research Objectives 38

1.5 Thesis Organization 42

2 Validation of the Integrated Upward-Horizontal-Downward Wicking test for Providing Intensive Properties of Textile Fabrics 43

2.1 Introduction 43

2.2 Experimental 45

2.2.1 45

2.2.1 Theory 45

2.2.2 Upward-Horizontal-Downward Wicking 48

2.2.3 Fabric and Fluids 51

2.3 Results and Discussion 53

2.4 Conclusions 63

3 Control of Microfluidic Flow in Amphiphilic Fabrics 64

3.1 Introduction 64

3.2 Experimental 66

3.2.1 Fabric Design 66

3.2.2 Materials 70

3.2.3 Methods 71

3.3 Results and Discussion 74

3.3.1 Drop Tests 74

3.3.2 Upward Wicking Tests 79

3.3.3 Parallel Flow of Immiscible Phases - Horizontal Two-phase Wicking Tests 83

3.4 Conclusions 85

4 Analysis of the Structural Features Affecting Microfluidic Flow in Amphiphilic Fabrics 87

4.1 Introduction 87

4.2 Experimental 89

4.2.1 Fabric Design 89

4.2.2 Materials 97

4.2.3 Methods 98

4.3 Results and Discussion 100

4.4 Conclusions 109

5 Amphiphilic Fabrics as Liquid-Liquid Contactors for Solvent Extractions 110

5.1 Introduction 110

5.2 Experimental 113

5.2.1 Fabric Design 113

5.2.2 Materials 114

5.2.3 Methods 115

5.3 Results and Discussion 125

5.3.1 Qualitative Extraction Studies 125

5.3.2 Quantitative Extraction Studies 127

5.4 Conclusions 134

6 Conclusions and Recommendations 137

6.1 Conclusions 137

6.2 Recommendations 141

REFERENCES 145

VITA 151

LIST OF TABLES

Page

Table 2.1 Fluid Properties at 20 °C 53

LIST OF FIGURES

Page

Figure 1.1 Illustrates the phases of capillary action. (a) wetting; a liquid wets the wall of a capillary with contact angle $\theta < 90^{o}$; when $\sigma_{SL} > \sigma_{SV} - \sigma_{LV}$ (b) liquid transport; the extent liquid will be transport into a capillary due to tension forces alone is inversely related to the radius of the capillary. 3

Figure 1.2 An illustration of the difference between the interaction of the bulk fluid with the wall of a capillary in (a) macrochannel (b) microchannel. 5

Figure 1.3 Relationship between distance and time for the mass diffusion of a particle or molecule in a liquid. The bottom region of the plot corresponds to shorter distances, or the micrometer length-scale, while the upper region of the plot corresponds to longer distances, or the macro length-scale. 7

Figure 1.4 Illustrates the similarity in void structure between the channels of a microfluidic device and the channels of an amphiphilic fabric. (a) microfluidic device that can be used to perform sandwich immunoassays[12]. The screws in this system (marked with dashed circles) act as manual operating valves. Green-dyed water marks the channels (b) fabric woven with hydrophilic (blue) yarns and hydrophobic (red) yarns [Figure 1.4b was provided by AstenJohnson]. 16

Figure 1.5 Typical filament extrusion processes (a) principal of melt spinning (b) principal of dry spinning (c) principal of wet spinning [34]. 21

Figure 1.6 Synthetic fibers engineered with different cross sectional shapes. (a) round nylon fibers (b) triangular nylon fiber (c) square rayon fibers [35]. 22

Figure 1.7 Schematic of feed mechanism to create blended fibers. (a) bicomponent side by side fiber (b) bicomponent matrix & fibrils fiber (c) bicomponent shear core fiber [35]. 22

Figure 1.8 Typical methods for manufacturing spun yarn. (a) principal of ring spinning [34] (b) principal of open-end spinning [29](c) principal of air-jet spinning [29]. 24

Figure 1.9 Schematics of knitted fabric constructions [35]. Illustrates a basic knit construction (a) plain knit and two complex knit constructions (b) milanese knit and (c) tricot knit 27

Figure 1.10 Illustrates the basic action at the loom of a weaving machine [34]. The harness or shaft moves the warp yarns up or down, a weft yarn is inserted, the reed pushes the weft yarn tightly into the fabric. 29

Figure 1.11 Schematics of woven fabric pattern[24, 35]. Illustrates three basic weaving patterns: (a) plain weave (b) twill weave (c) satin weave 30

Figure 1.12 Letters of the alphabet embroidered into a plain weave fabric [37]. 31

Figure 1.13 Experimental set-ups for monitoring fluid transport into fabrics. (a) drop test (b) upward wicking test (c) horizontal wicking test (d) downward wicking test 37

Figure 2.1 Schematic of (a) the experimental set-up for conducting the upward-horizontal-downward wicking test, and (b) the key components and parameters. Wicking is gravimetrically monitored through a fabric strip with upward (h), horizontal (H_L) and downward (D_L) segments. The h governs the saturation level through H_L and D_L. The test is repeated on the same fabric at different h values to determine permeability and effective capillary radius as a function of saturation. 50

Figure 2.2 Micrograph of the plain stitch knit fabric used for all of the wicking tests. Technical face of the fabric is shown at two magnifications [53]. 51

Figure 2.3 Saturation versus upward wicking height measured for the horizontal and downward segments of the fabric strip using three separate alkane fluids: dodecane, tetradecane and hexadecane. 54

Figure 2.4 Horizontal (a) and downward (b) wicking rates versus upward wicking height for dodecane, tetradecane and hexadecane. Lines are shown as guides. 55

Figure 2.5 Capillary pressure (a) and permeability (b) versus saturation for dodecane, tetradecane, and hexadecane. Lines are shown as guides. 57

Figure 2.6 Permeability versus effective capillary radius for dodecane, tetradecane and hexadecane. Lines are shown as guides. 58

Figure 2.7 Predicted (solid line) and experimental (□) horizontal (a) and downward (b) wicking rates versus upward wicking height for 1-octanol. 60

Figure 2.8 Predicted (solid line) and experimental (+) horizontal (a) and downward (b) wicking rates versus upward wicking height for water. The experimental wicking rates for water were measured at 90% relative humidity and were taken from the literature [49]. 62

Figure 3.1 Schematics of five fabric samples examined in this study. The red (dark) yarns represent hydrophobic (or lipophilic) yarns (L), while the blue (light) yarns represent hydrophilic yarns (H): (a) 1H-1L/4L, (b) 2H-2L/4L, (c) 2H-2L/2H-2L, (d) 4H/4L (e) 4H/4H (purely hydrophilic control fabric). Highlighted are examples of a "channel" and an "intersection", key structural features of the amphiphilic fabrics with regards to fluid transport. 68

Figure 3.2 Experimental set-ups for monitoring fluid transport into fabrics: (a) drop test in which an overhead camera was used to capture flow path and a side-view camera was used to capture drop volume as a function of time, (b) upward wicking test from a reservoir in which a balance and camera were used, and (c) horizontal wicking test in which the end of a fabric strip was cut at the border between groups of parallel adjacent hydrophilic and hydrophobic yarns so that feeder strips could supply water and dodecane from two separate reservoirs. 72

Figure 3.3 Single drops of water absorb into fabrics at rates and along paths governed by the arrangement and density of hydrophilic yarns: (a) fabric schematics, (b) UV-illuminated images in which hydrophilic polyester yarns are bright, and (c) time-resolved images of drop absorption. Each column represents a single fabric sample. Bottom row shows side view images of the water drop after 50 seconds. 75

Figure 3.4 Quantitative analysis of water drop volume reduction versus time: (a) fabric schematics, (b) side view images of water drops 35 seconds after placement on fabrics; numbers below images are rates of drop volume reduction determined from (c) drop volume, normalized to initial volume, versus time for ●:1H-1L/4L, ■: 2H-2L/4L, ♦: 2H-2L/2H-2L, and ▲: 4H/4L; lines are linear least-squares fits and slopes are rates of drop volume reduction listed in (b). For the fully hydrophilic 4H/4H fabric, the drop was completely absorbed within 1 s. 77

Figure 3.5 Upward wicking of water: (a) fabric schematics, (b) images showing flow patterns and wetting fronts after 100 seconds, and (c) initial upward wicking rates determined from linear least squares fit to first 30 seconds of mass versus time data. 81

Figure 3.6 Co-flow of aqueous and hydrocarbon fluid in amphiphilic fabric 5H-5L/2H-2L: (a) fabric schematic, (b) UV-illuminated image of fabric that shows hydrophilic microchannels as bright regions, and (c) time-resolved overhead images that show water (stains yellow) wicks along the hydrophilic microchannels (pre-wicked into fabric already at $t = 0$) and dodecane (stains faint purple), which initially appears from the top left of image at 37 s as a darkening of the yarns, wicks along the hydrophobic microchannels. By 65 s, dodecane has wet the entire fabric not already wet by water, including perhaps some hydrophilic microchannels. By 46 min, water has filled all

hydrophilic microchannels and the image exactly resembles the UV-illuminated image of the dry fabric shown in (b). 84

Figure 4.1 Schematic of 18 fabric samples examined in this study. The red (dark) yarns represent hydrophobic (or lipophilic) yarns (L), while the blue (light) yarns represent hydrophilic yarns (H). The fabrics are grouped according to class, which is defined by the ratio of the number of hydrophilic to hydrophobic yarns in the repeat pattern of each fabric. (a) Class 1: H/L= 0.33, (b) Class 2: H/L=0.71, (c) Class 3: H/L=1, (d) Class 4: H/L=1.4 (e) Class 5: H/L=3, (f) Class 6: H/L= ∞. 91

Figure 4.2 Schematic of fabrics used to investigate the effect of "channels" on liquid flow. Highlighted is an example of a channel, and the number of channels in each fabric: 1H-1L/4L (0 channel); 2H-2L/4L (1 channel); 4H/4L (4 channels). 93

Figure 4.3 Schematic of fabrics used to investigate the effect of "intersections" on liquid flow. Highlighted is an example of an intersection. (a) Fabrics with 1 channel: 2H-2L/4L (0 intersections); 2H-2L/1H-1L (4 intersections); 2H-2L/4H (8 intersections). (b) Fabrics with 4 channels: 4H/4L (0 intersections); 4H/1H-1L (8 intersections); 4H/4H (16 intersections). 94

Figure 4.4 Schematic of fabrics used to investigate the effect of blockage yarns on liquid flow. Fabrics were evaluated in sets of 3. (a) Displays the control fabrics for each fabric set. Control fabrics were used to provide a base wicking rate, as they have a similar structure; they were not used to quantify the effect of blockages because they have fewer hydrophilic yarns and thus a different H/L ratio. (b) Shows the fabrics in each data set with 1 blockage (2H-2L/1H-1L, 5H-5L/1H-1L, 4H/2H-2L) and 2 blockages (2H-2L/2H-2L, 5H-5L/2H-2L, 4H/2H-2L). Also highlighted in (b) is an example of a "blockage" yarn. 95

Figure 4.5 Schematic of fabrics used to investigate the effect of yarn orientation on liquid flow; (a) displays fabrics with purely horizontal yarn orientation (4L/1H-1L, 4L/2H-2L, 4L/4H) and (b) displays fabrics with purely vertical yarn orientation (1H-1L/4L, 2H-2L/4L, 4H/4L). 97

Figure 4.6 Upward wicking experimental set-up for monitoring fluid transport into fabrics. Upward wicking tests were done from a reservoir; a balance and camera were used to record each test. 100

Figure 4.7 Analysis of fabric class (*i.e.* H/L ratio); upward wicking rates of all 18 fabric samples, ranked in order of increasing wicking rate. Shown above and below the bar graph are the schematics of all fabrics tested; the number to the left of each schematic is the fabric rank, the color of each number designates the class of the fabric sample. The inserted graph displays the average upward wicking rate of each class (Δ) versus H/L ratio. 102

Figure 4.8 Analysis of the effect of channels; upward wicking rate is plotted versus number of features: in the repeat unit: hydrophilic channels (■) and hydrophilic yarns (►). 103

Figure 4.9 Analysis of the effect of intersections on wicking rate; upward wicking rate is plotted versus number of intersections for fabrics with 1 channel (♦) and 4 channels (▼) in the repeat unit, respectively (see Figure 4.3). 104

Figure 4.10 Analysis of the effect of blockages. Upward wicking rate is displayed versus number of blockages for fabrics with 1 channel (●),1.6 channels (■) and 4 channels (▲); the open symbol in each group of fabrics represents the control fabric (see Figure 4.4) 106

Figure 4.11 Analysis of the effect of yarn orientation. Depicts the wetting front of fabrics 4L/1H-1L, 4L/2H-2L, 4L/4H, which do not facilitate upward wicking, after 1 minute of submersion into a liquid reservoir, compared with fabrics 1H-1L/4L, 2H-2L/4L, and 4H/4L resp., which do facilitate upward wicking. 108

Figure 5.1 Schematics of fabrics used for solvent extraction studies; (a) 5H-5L/4L (b) 5H-5L/1H-1L (c) 5H-5L/2H-2L (d) 2H-2L/2H-2L. The repeat unit of each fabric is enclosed within the dashed lines. 114

Figure 5.2 Two-phase horizontal wicking set-up. 117

Figure 5.3 Typical concentration profile at the interface between two liquids as solute A diffuses from liquid 1 to liquid 2. 119

Figure 5.4 Two-phase vertical wicking set-up. 124

Figure 5.5 Progression of acetic acid extraction into water within amphiphilic fabrics. (a) fabric schematics, (b) fabric images showing water (stains yellow-green) pre-wicked into fabrics (c) time-resolved overhead images of acetic acid extraction; in the image at 0 s hexane has reached the pre-wicked hydrophilic yarns which are saturated with water/thymol blue mixture; as acetic acid is transferred from the hexane phase into the aqueous phase, the water pH is lowered and the indicator changes color from yellow-green (pH 7) to pink (pH 2). 126

Figure 5.6 Extraction efficiency versus initial copper ion concentration (a) schematic of the three fabrics used for copper ion extraction studies; values below each schematic are superficial velocity and Reynolds number for each fabric, the aqueous phase residence time for each fabric shown was ~5 min, ~8 min, ~24 min, respectively (b) extraction efficiencies for the three fabrics tested (c) comparison of extraction efficiency between fabric 5H-5L/2H-2L and batch extractions with and without applied energy (*i.e.* agitation) 129

Figure 5.7 Possible flow patterns in amphiphilic microchannel at slow and fast aqueous flow rates. (a) aqueous slug flow at low flow rates reduces contact area between organic and aqueous phases, whereas (b) aqueous stream flow maximizes contact area between organic and aqueous phases; flow concept derived from research done by Dessimoz *et. al* [76]. 132

LIST OF SYMBOLS AND ABBREVIATIONS

γ	Liquid surface tension
η	Fluid viscosity
ε	Fabric porosity
θ	Contact angle of liquid wetting a surface
ρ	Fluid density
σ_{SL}	Surface energy at interface between solid and liquid
σ_{SV}	Surface energy at interface between solid and vapor
σ_{LV}	Surface energy at interface between liquid and vapor
a	Interfacial contact area between liquid 1 and liquid 2
a_d	Dry specific contact area between liquid 1 and liquid 2
A	Total dry contact area between liquid 1 and liquid 2
$C_{A_b}^{(1)}$	Concentration of solute A in the bulk of liquid phase 1
$C_{A_b}^{2}$	Concentration of solute A in the bulk of liquid phase 2
$[Cu_{aq}]_i$	Concentration of copper ions in the aqueous phase before extraction

$[Cu_{aq}]_f$	Concentration of copper ions in the aqueous phase after extraction
ν	Linear velocity of a fluid
D	Diffusion coefficient
D_h	Hydraulic diameter
D_L	Downward wicking length
d	Distance
$\% E$	Extraction efficiency
g	Gravitational constant
H_L	Horizontal wicking length
h	height
K_L	Mass transfer coefficient
k	Permeability
L_h	Horizontal wicking length at time t
L_d	Downward wicking length at time t
$L(t)$	Length at time t
$m(t)$	Mass at time t

N_A	Molar flux of solute A
P_c	Capillary Pressure
P_h	Hydrostatic pressure
R	Radius of a capillary
R_c	Effective capillary radius
Re	Reynolds number
S	Fabric saturation
t	Time
V	Volume of fluid in fabric during extraction
V_f	Fluid volume taken up by fabric
V_s	Superficial velocity
V_t	Total fabric volume
W_c	Horizontal wicking rate
PDMS	Polydimethylsiloxane
POC	Point of care
SAV	Surface area to volume ratio

UHD	Upward-horizontal-downward wicking test
PET	Polyester
D2EHPA	di-(2-ethylhexyl)phosphoric acid
FAAS	Flame atomic absorption spectroscopy

SUMMARY

Manipulation of the size, shape, connectivity and surface chemistry of microchannel networks can be used to optimize a microfluidic device to suit a wide range of applications in analytical chemistry and diagnostics. This is possible because the small dimensions of microfluidic chips cause them to have large surface-area-to-volume ratios, strong channel wall-fluid interactions, and rapid mass diffusion of particles within liquid phases. The research described in this thesis was inspired by work in microfluidics; fabrics were systematically engineered to exhibit amphiphilic properties to achieve microfluidic co-flow of immiscible liquid phases. These fabrics show potential for use as media for large-scale chemical processing applications, in particular liquid-liquid extractions with reduced energy costs and increased efficiency. The goal of this thesis was to conduct fundamental experimental studies showing the feasibility of controlling microscopic liquid flow in amphiphilic fabrics and investigate their use as contactors for liquid-liquid extractions.

A fundamental knowledge of the dynamics of liquid transport in fabrics was necessary to begin work in the development of the amphiphilic fabrics. Chapter 2 of this thesis outlines the key parameters used to quantify liquid transport in textiles: permeability (k), effective capillary radius (R_c), capillary pressure (P_c) and saturation (S). This chapter also details the validation of a new upward-horizontal-downward (UHD) wicking test that has been shown to provide intensive properties of a fabric, which can be used to make wicking rate predictions. The test will be very useful for estimating scale-up and process conditions once the amphiphilic fabrics are ready for commercialized use.

Using knowledge about the dynamics of liquid transport in fabrics that was gained in Chapter 2, amphiphilic fabrics were designed and engineered. Woven textile fabrics were constructed from hydrophilic and hydrophobic spun yarns to give planar substrates containing amphiphilic microchannels with defined orientations and locations. In Chapter 3, we investigated control of microscopic liquid flow in these fabrics; water wicking into five different amphiphilic fabrics was observed and measured using video microscopy and upward wicking tests. Hydrophilic intra- and inter-yarn microchannels were shown to selectively transport aqueous fluids, with the flow path and flow rate governed by the placement of the hydrophilic yarns in the fabric. Additionally, simultaneous wicking of an aqueous and hydrocarbon fluid into the hydrophilic and hydrophobic microchannels of an amphiphilic fabric was successfully demonstrated.

The next step was to identify which fabric designs would be best for liquid-liquid extraction applications. Therefore, a quantitative understanding of the relationship between wicking rate and fabric design was needed. In Chapter 4, upward wicking tests were performed with 18 different amphiphilic fabrics. Comparisons of the upward wicking rate with respect to each fabric design revealed there are five structural features that affect liquid flow: the H/L ratio (balance between hydrophobic and hydrophilic yarns), density of inter-yarn channels between yarns of the same type, density of intersections between like yarns, yarn blockages due to intersecting yarns of the opposite type, and yarn orientation. Water wicking rate is directly related to H/L ratio, channels, and intersections, and inversely related to the number of yarn blockages. Yarn orientation was found to be very important to upward flow; preventing wicking if there

were no hydrophilic yarns oriented in the flow direction. In light of these observations, several fabrics were easily identified as candidates for extraction experiments.

The final objective in the development of the amphiphilic fabrics was to show their potential as liquid-liquid contactors for solvent extraction applications. In Chapter 5, the progression of the extraction of acetic acid from hexane into water using three different amphiphilic fabric patterns was observed via video microscopy. The indicator thymol blue was added to change the color of the water upon the extraction of acetic acid. Results from this qualitative study showed that there is sufficient contact between aqueous and organic phases wicking into an amphiphilic fabric, such that a liquid-liquid extraction can proceed. Confident in the feasibility of conducting extractions with amphiphilic fabrics, the efficiency of the extraction of copper ions from water using solutions of di-(2-ethyl-hexyl)phosphoric acid in dodecane was quantified. Extractions were carried out in three different amphiphilic fabrics with initial aqueous copper ion concentrations ranging from 50-200 ppm. Extraction efficiencies ranging from 75 to 98% were achieved.

CHAPTER 1

INTRODUCTION

1.1 Control of Fluid Flow at Micrometer Length-Scales

The characteristics of fluid flow on the micrometer length-scale open up a pathway for control and manipulation of fluid volumes within microchannels, so that chemistry and chemical analysis can be conducted more efficiently. This is because the physical phenomena that dominate in microchannels differ from those experienced at the macroscale. The unique attributes of fluid flow on the microscale include significant surface tension contributions, a large surface area to volume ratio, laminar flow, and rapid mass diffusion [1]. A thorough understanding of these phenomena was critical to the development of the amphiphilic fabrics chronicled in this thesis; the introductory chapter therefore starts with a review of the underlying physics.

1.1.1 Interfacial Forces and Capillary Action

Wetting of a microchannel or capillary, commonly known as capillary action, occurs because surface tension forces at the microscale are very significant. Capillary action occurs through two steps, first wetting of two walls, then transport of liquid into the capillary [2]. A fluid will wet the walls of a capillary when the forces of adhesion between the liquid and the wall are greater than the forces of cohesion between the molecules of the liquid [2, 3]. This can quantitatively be described by Young's equation [4]: $\sigma_{SV} - \sigma_{SL} / \sigma_{LV} = \cos \theta$, and is also illustrated in Figure 1.1a. In Young's

equation σ_{LV} is the surface energy at the interface between a liquid and a vapor, commonly known as surface tension (γ) for a liquid and its own vapor, σ_{SL} is the surface energy at the interface between a liquid and a solid, σ_{SV} is the surface energy at the interface between a solid and a vapor, and θ is the contact angle between the vapor, liquid, solid interface. For a wetting fluid; $\theta < 90°$ or $\sigma_{SL} > \sigma_{SV} - \sigma_{LV}$. The magnitude of σ_{SL} is governed by the surface chemistry of the solid. Therefore, in a network of microchannels we can control which channels are wetted by a particular fluid and which are not by varying the surface chemistry of select channels.

If surface chemistry favors wetting, the extent to which liquid will travel into a capillary due to interfacial forces alone can be described using the component of the force of adhesion that points along the channel axis, $F_A = \gamma \cos\theta \, \partial L$, where γ is the surface tension of the liquid and ∂L is the contact line over which the force of adhesion is acting. For the force of adhesion in a circular capillary ∂L is given by $2\pi R$, where R is the radius of the capillary. The balancing force to the force of adhesion in a vertical capillary is gravity: $F_g = \rho \pi R^2 h g$, where ρ is the density of the fluid, h is the height liquid has traveled in the capillary and g is the acceleration of gravity. As liquid moves up the capillary walls the weight of the fluid column opposes the force of adhesion. Hence, the height liquid will travel into a capillary due to the force of adhesion is directly related to the magnitude of the surface tension and inversely related to the radius of the capillary. As capillary radius is reduced to the micrometer scale, the extent liquid will travel through the capillary due to tension forces alone is significant [1, 5]. Furthermore, as we change the size and shape of the radius of a microchannel the rate of liquid transport into the channel will be affected (cf. Figure 1.1b) [1].

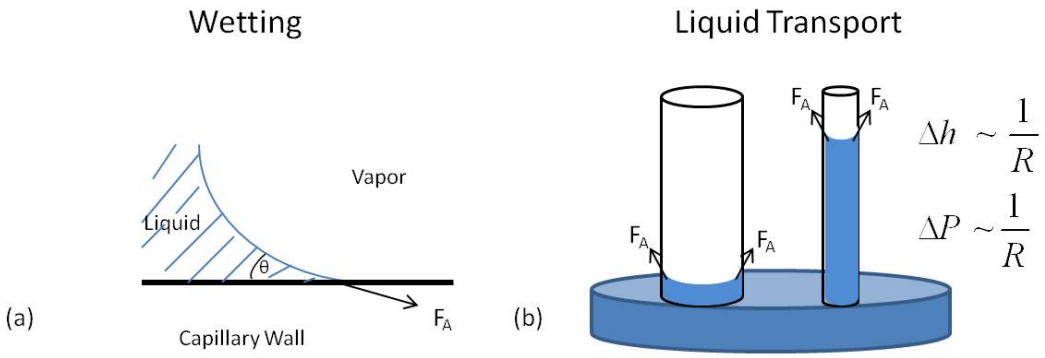

Figure 1.1 Illustrates the phases of capillary action. (a) wetting; a liquid wets the wall of a capillary with contact angle $\theta < 90^o$; when $\sigma_{SL} > \sigma_{SV} - \sigma_{LV}$ (b) liquid transport; the extent liquid will be transport into a capillary due to tension forces alone is inversely related to the radius of the capillary.

An alternative framework for describing capillary flow, which is used commonly in literature, uses the concept of capillary pressure [5, 6]. When a liquid wets a capillary, a curved interface forms between the liquid and the vapor phase in the capillary [3, 7, 8]. The curvature of this interface creates a pressure drop across the interface, which is commonly referred to as capillary pressure or Laplace pressure: $P_c = 2\gamma\cos\theta / R$. The physics of a static fluid tells us that the pressure at every point along a horizontal line within the static fluid must be the same [9]. The Laplace pressure lowers the pressure behind the curved interface of a wetting liquid. Due to the Laplace pressure, once a liquid wets a capillary, the pressure within the liquid at the same vertical height inside the capillary differs from the pressure at the same height outside the capillary. Hence, the liquid level in the capillary will change until the pressures are balanced. As capillary

radius is reduced to the micrometer-scale, the Laplace pressure, and the extent to which liquid will travel in the capillary due to capillary pressure are significant. Similar to the force of adhesion, the balancing force of capillary pressure in a vertical capillary is the force of gravity. As liquid moves up the capillary walls the weight of the fluid column opposes the movement due to the capillary pressure and eventually flow will cease. However, if we consider horizontal or downward capillary flow, flow of a Newtonian fluid will never cease, because F_g is not acting in the direction opposite to capillary forces.

Quantitatively, there is no difference between the two conceptual explanations ($F_A = \pi R^2 P_c$). However, the pressure explanation becomes less intuitive when we evaluate capillary action in more complex geometries. To define a pressure difference between liquid at the same vertical height inside a capillary and liquid at the same height outside of the capillary, the capillary must have a simple geometry, so that the radius of curvature is well-defined, and closed to the atmosphere. However, capillary action has been observed in many complex porous structures, such as fabrics and soil, which are not closed conduits, but open to the atmosphere [2, 8]. These counterexamples illustrate clearly that the force of adhesion framework is more meaningful as the driving force for capillary action in the context of this thesis.

1.1.2 Surface Area to Volume Ratio

As the radius of a channel decreases, the surface area to volume ratio (SAV) can increase by orders of magnitude [1]. A large surface area to volume ratio indicates that the bulk volume of liquid in the channel is in close contact with the walls of the channel.

Take, for example, two cylindrical channels filled with liquid as shown in Figure 1.2. Assume that one channel has a radius of 1 centimeter and the other a radius of 100 micrometer. The surface area to volume ratio is given by $SAV = 2\pi RL/\pi R^2 L \sim 1/R$, so $SAV_{1cm}/SAV_{100\mu m}=1/100$. The fluid volume in the microchannel has ~ 100 times stronger interaction with the channel walls than the fluid volume in the macrochannel. This is better illustrated in Figure 1.2. For a macrochannel, Figure 1.2a shows that the boundary layer that represents the interaction between the fluid and the channel wall includes a much smaller fraction of the fluid volume than the smaller channel in Figure 1.2b. This example underlines the importance of surface chemistry of the channel walls for controlling fluid flow in microscopic channels.

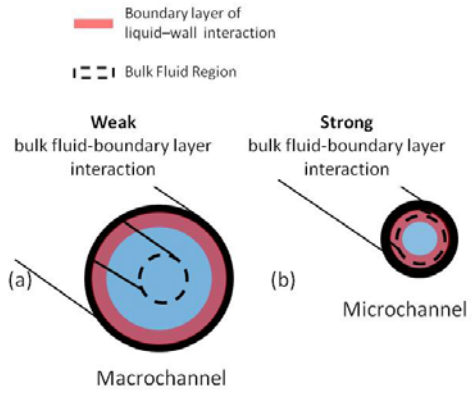

Figure 1.2 An illustration of the difference between the interaction of the bulk fluid with the wall of a capillary in (a) macrochannel (b) microchannel.

1.1.3 Laminar Flow

Laminar flow occurs when the inertial forces of the fluid flow are insufficient to disturb the streamlines; as a result, the velocity profile in laminar flow is well-defined with stable, parallel streamlines [9]. Consequently, two or more streams of fluid flowing in contact with each other under laminar flow will only mix by diffusion [1]; mixing due to convective motion of the streams is insignificant. A fluid will have laminar flow when its Reynolds number, *Re*, is low. Reynolds number is described by $Re = \rho v D_h / \eta$ where ρ is the fluid density, v the characteristic velocity of the fluid, η the fluid viscosity, and D_h is the hydraulic diameter [9]. Due to the small size of microchannels, flow is virtually always laminar.

1.1.4 Mass Diffusion

In microchannels, typical fluid layer thicknesses range from micrometers to nanometers [10]. Diffusion can be modeled in one dimension by the equation $d^2 = 2Dt$, where d is the average distance a particle moves in a time t, and D is the diffusion coefficient of the particle; distance varies to the square power (Figure 1.3) [1, 10]. Hence, in a thin film of liquid mass diffusion occurs rapidly (cf. Figure 1.3). Consequently, by conducting chemistry and chemical analysis in microchannels lower reagent volumes and shorter times for chemical analysis can be achieved [10].

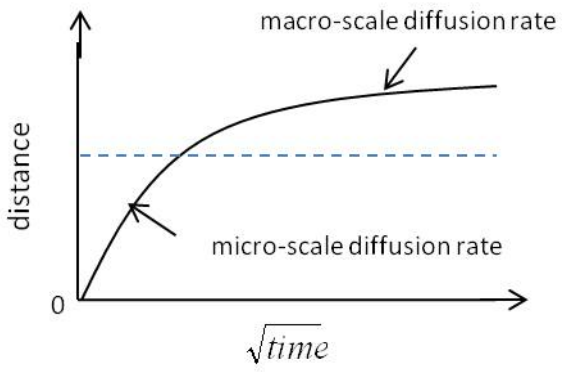

Figure 1.3 Relationship between distance and time for the mass diffusion of a particle or molecule in a liquid. The bottom region of the plot corresponds to shorter distances, or the micrometer length-scale, while the upper region of the plot corresponds to longer distances, or the macro length-scale.

1.2 Microfluidics

Due to the special characteristics of fluid flow at micrometer length-scales, manipulation of microchannel properties can be used to direct fluid to precise locations within a network of microchannels. By constructing devices that consist of networks of microchannels and fluid reservoirs, one can carry out several simultaneous chemical reactions and analysis, using smaller reagent volumes and achieving faster analysis than with traditional, larger-scale laboratory techniques. Additionally, capillary action can potentially be used to eliminate the need to apply energy to transport fluid in a microchannel network. By varying the design of networks of microchannels and optimizing microchannel size, shape and surface chemistry, microfluidic devices can be made to suit a wide range of applications in analytical chemistry and diagnostics. This is

the fundamental principle on which a relatively new field of research, usually referred to as microfluidics, has been based.

1.2.1 History

Microfluidics is the field of research and engineering that studies geometrically constrained fluids within micrometer-sized structures, usually in the form of intricate networks of interconnected channels and reservoirs on small “microfluidic chips” [1, 11]. The origin of microfluidics stems from four fields of study: molecular analysis, biodefense, molecular biology and microelectronics [12].

The success of microanalytical methods in the 1970s to 1980s, such as gas-phase chromatography (GPC), high-pressure liquid chromatography (HPLC) and capillary electrophoresis (CE) showcased the advantages of using very small quantities of samples and reagents to carry out chemical separations and analysis with high resolution and sensitivity [12]. With the successes of these microanalytical methods, the most obvious next step was to develop more compact and versatile systems that could extend the use of these methods to other applications in chemistry and biochemistry.

The emergence of chemical and biological weapons during the Cold War emphasized the need for field-deployable microfluidic systems designed to serve as detectors to screen for chemical and biological threats against US military personnel [12]. The US Department of Defense supported a series of programs in the 1990s with the goals of developing microfluidic technology. In many academic research labs, small chips were engineered with networks of interconnected microchannels and reservoirs for use as portable analytical devices. With these devices, sampling and sensing could be

carried out simultaneously, allowing for sensitive laboratory testing and screening to be done quickly and easily at military field locations.

The third motivational factor that stimulated the development of microfluidic technology came from new interests in genomics in the 1980s, in particular high-throughput DNA sequencing [12]. These applications created the need for analytical methods with much greater throughput, and higher sensitivity and resolution than had previously been thought of for molecular biology. Repetitions of basic microfluidic structures within a single chip had potential to meet such challenges.

The final driving force that encouraged advances in microfluidic technology was the success of photolithography in the fabrication of silicon microelectronics, and micro-electromechanical systems (MEMS) [12]. These methods proved directly applicable to the fabrication of microfluidic systems. The first microfluidic devices were fabricated using photolithography and etching techniques adapted from the microelectronics industry. Since then, fabrication technology has moved toward more effective methods involving cheaper polymer substrates.

The field of microfluidics is still relatively new and its potential fairly untapped. New microfluidic fabrication techniques and application areas are still rapidly evolving. To achieve the full potential impact of microfluidic technology, the next step is to develop solutions which can move the field of study from mainly academic research to large-scale and commercially relevant applications.

1.2.2 Fabrication of Microfluidic Devices

There are various methods to fabricate microfluidic devices. Each method has advantages and disadvantages; the most suitable method depends on the end application of the device. The first microfluidic devices, developed by Manz, Harrison, Ramsey, and others were fabricated in the early 1990s using techniques adapted from the microelectronics industry [13]. These techniques involved fabricating microfluidic chips made of silicon and glass via wet etching and laser ablation [14].

Generally, wet etching begins with coating a silicon or glass substrate with a thin layer of photoresist, a light-sensitive material that becomes soluble or insoluble in a solvent after exposure to light. The substrate is then covered with an optical mask that is patterned with the desired network geometry of channels and reservoirs. After exposure to light, the uncured photoresist is removed, revealing the surface of the substrate that is now covered with a photoresist impression of the microfluidic channel structure. The exposed areas of the substrate are then etched away in a chemical bath, after which the remaining photoresist is removed. The resulting substrate has channels etched into its surface in the pattern defined by the mask. These channels are finally sealed by bonding the substrate to another, flat substrate with pre-drilled holes to provide inlet and exit ports that can be used to connect the channel network to the outside world.

In laser ablation, microchannels are etched into a substrate, usually polymeric, by either exposing the substrate to a laser through a mask or by moving the substrate across a focused laser beam on a mechanical stage according to the defined etching pattern.

Micromachining techniques are precise, but also costly, labor intensive, and require highly specialized skills, equipment, and facilities. They are generally not suitable

for exploratory work in microfluidics [1, 12]. Furthermore, silicon does not possess the desirable physical properties for most microfluidic applications; it is opaque and therefore not compatible with the optical analysis techniques required for many biological studies [1].

1.2.3 Soft Lithography

Soft lithography is a more versatile method for microfluidic chip fabrication than laser ablation or wet etching of silicon or glass substrates. In this approach, microchannels are molded into a two-part polymer (elastomer and curing agent), generally polydimethylsiloxane (PDMS), because of its ease of curing [14, 15]. The PDMS mold is created from a photoresist master, usually a silicon wafer with micrometer thick imprints of the channel structure. The master is produced using one of the techniques described in the previous subsection. A mixture of PDMS and curing agent is then poured on top of the master. The master with the liquid PDMS layer is degassed in a desiccator for roughly 20 minutes to remove air bubbles, and cured in an oven at 60-80^{o}C. During curing, the liquid PDMS solidifies, thus imprinting the pattern of the photoresist master into its surface. The PDMS mold is removed from the master by peeling it away for the surface and inlet/outlet ports are created on the device by punching holes in the PDMS after removal from the master. To seal the channels and reservoirs, the PDMS mold is bonded to a flat glass substrate. To functionalize the surfaces prior to bonding, they are usually briefly exposed to an oxygen plasma before being brought into contact. PDMS has good optical qualities and soft lithography is a faster, less expensive, and less specialized fabrication method than micromachining. A

key advantage is that masters can be used repeatedly to create PDMS molds with the same channel structure. Hence, most research laboratories fabricate microfluidic devices using soft lithography; however, depending on the applications, other techniques can be useful [1, 14].

1.2.4 Microfluidic Applications, Advances and Limitations

A large portion of microfluidic applications are centered around medical diagnosis (*i.e.* cell-based assays and disease screens) and fundamental biological studies. For example, for sensitive applications such as single cell analysis, cell surface markers can be used in microfluidic devices to detect and trap specific cells. For this application, microfluidic channels are coated with antibodies specific to cell surface markers to capture cells of interest for detection and diagnosis of diseases like cancer and studies of neurological disorders. Nagrath *et. al.* designed a device with antibody coated pillars that can capture circulating tumor cells (CTCs) overexpressing epithelial cell adhesion molecule (EpCAM) from blood samples [16]. Microfluidics has also been shown to be useful for multi-step analytical applications, such as DNA analysis. Miniaturizing the steps of DNA amplification has been studied by several researchers [11]. Recently, progress has been made on applying this technology to detect bacterial pathogens. Chen *et. al.* designed a polycarbonate microfluidic system for detecting bacterial pathogens in oral fluid samples. The integrated system has several fluid modules for cell lysis, nucleic acid extraction and isolation, Polymerase Chain Reaction (PCR), and labeling of the PCR product for detection on a lateral flow strip [17]. The “on chip” analysis reduces the sample volume, the risk of sample contamination and clinician infection, improving

analysis and diagnosis speed more than typical pathogen detection methods. Additionally, the use of a lateral flow strip provides fast, convenient and low-cost point-of-care and home testing.

Other applications of microfluidics seem to reduce time, and reagent costs for high-throughput biological studies. For example, Hansen *et. al.* developed a microfluidic device which integrated 48 different solvents of varying viscosity, surface tension, ionic strength, and pH, to carry out 144 simultaneous reactions, for the purpose of understanding and modeling macromolecular structures, protein–ligand interactions, and the physical manifestation of certain diseases and design of drugs [18]. Significant savings in sample consumption and experimentalist time were achieved through the use of this device.

Although the field of microfluidics shows great promise there are some limitations to microfluidic applications. The soft-lithography manufacturing process limits commercially viable use to specialized high-value applications with small volumetric throughput of liquids. Recent advances towards cheaper microfluidic devices have largely been driven by the desire to deploy point-of-care (POC) diagnostic screening kits in developing countries for detection of common diseases [11]. These efforts have focused on replacement of PDMS with alternative substrate materials. Cheap, porous materials that can efficiently wick liquids via capillary action, like paper and cotton yarns, have emerged as primary candidates, because capillary action eliminates the need for external power sources to generate flow [1]. Paper, however, wicks fluid isotropically; control over the rate and direction of liquid flow within this substrate requires the use of hydrophobic barrier materials (*e.g.*, SU-8 photoresist or wax-like

ink) [19-21] to create flow channels inside the hydrophilic paper, or careful design of the shape of the paper substrate [22, 23]. Capitalizing on the inherent directionality of the voids in cotton yarns, other researchers have integrated yarns (*i.e.*, threads) as fluid channels into polymer substrates to create low-cost microfluidic devices for medical diagnostics [24-26]. Additionally, the use of threads with different wettability (*i.e.*, hydrophobic and hydrophilic yarns) in polymer substrates has been employed as a method to manipulate liquid transport and stimulate mixing of phases [25].

Paper- and yarn-based microfluidic structures not only offer more scalable production methods for microliter scale medical diagnostic devices; because of their economics, they also open up a pathway towards applications with much larger volumetric flow rates, while maintaining the inherent advantages of microfluidics. Take for example the large-scale liquid–liquid extraction processes commonly used in crude oil refinement, pharmaceutical production, and wastewater treatment [27]. A liquid-liquid extraction is a process that facilitates the removal of a chemical species (solute) from one liquid phase (raffinate) to another (extract), based on the solute having a higher relative solubility in the other. Once the raffinate and the extract phases are brought into contact, the solute will diffuse into the extract. This process is commonly used commercially as a separation method for removal of contaminates from product streams. Large-scale industrial extractions are typically done in multistage continuous extractors. Dispersion devices (*i.e.*, mixer, impeller, sprayer) are integrated into the extraction column to increase the contact area between immiscible phases, where the extraction can occur. The cost required to install these devices, as well as the energy required to maintain them makes industrial-scale extraction equipment quite expensive. It should be noted that the

fundamental physical characteristics of microfluidic flow are very amenable to the requirements of liquid-liquid extractions. The efficiency of extraction processes is often determined by the interfacial contact area between immiscible liquid phases (larger contact area is better), as well as the diffusion of solute from the bulk of each liquid to the liquid-liquid interface (faster diffusion and shorter diffusion paths being the goal). Microfluidic flow provides for large surface area to volume ratios and rapid mass diffusion. Thus, faster, more efficient extractions with smaller reagent volumes could potentially be achieved if microfluidic devices can be mass-produced sufficiently cheaply to be economically viable for processes with large volumetric flow rates, such as, industrial-scale liquid-liquid extractions.

Fabrics are engineered porous structures that consist of yarns, which themselves are bundles of fibers or filaments (cf. Figure 1.4b). A woven fabric therefore contains two types of microscopic voids that can accommodate microfluidic flow: (1) the *intra*-yarn spaces between fibers or filaments within a yarn, and (2) the *inter*-yarn spaces between the yarns in a fabric (cf. Figure 1.4b). By weaving hydrophobic and hydrophilic yarns together in a single fabric, we can thus create a network of microchannels with heterogeneous surface properties, which should allow for simultaneous flow of immiscible liquid phases with a large interfacial contact area. The textile manufacturing industry has developed scalable technologies to produce patterned fabrics that combine yarns of different types in repetitive geometrical structures with various degrees of complexity, ranging from simple plain weave structures to more complex architectures for specialty applications. It is also well-known that variations in fabric construction parameters and material properties can significantly affect fluid movement in fabrics. The

premise of this thesis is to extend the design of fabrics in a novel direction, aiming to control the fluid flow inside fabrics with precision and specificity akin to microfluidic devices and use them as contactors for large-scale liquid-liquid extractions. Hence, it is useful to now discuss the textile industry, textile manufacturing, and fluid flow in fabrics.

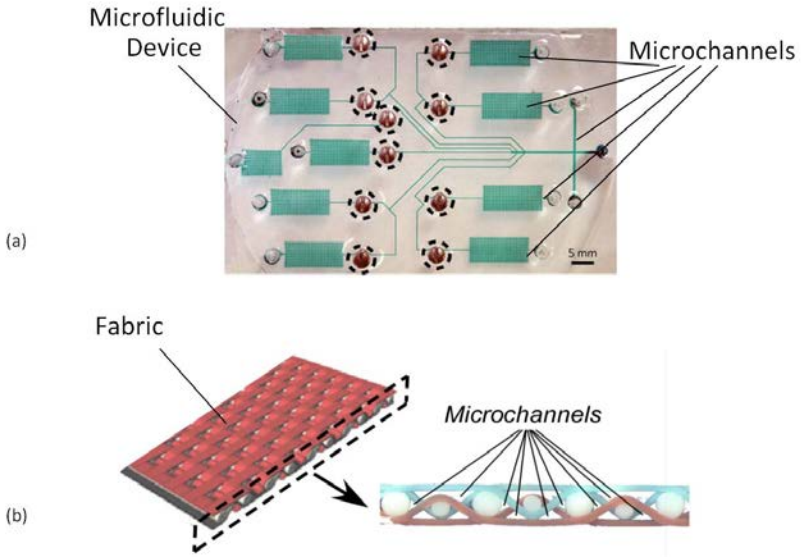

Figure 1.4 Illustrates the similarity in void structure between the channels of a microfluidic device and the channels of an amphiphilic fabric. (a) microfluidic device that can be used to perform sandwich immunoassays[12]. The screws in this system (marked with dashed circles) act as manual operating valves. Green-dyed water marks the channels (b) fabric woven with hydrophilic (blue) yarns and hydrophobic (red) yarns [Figure 1.4b was provided by AstenJohnson].

1.3 Textiles

1.3.1 History

The term textile refers to a material made up of a network of fibers, interlocked or bound together. The fabrication of textiles is one of the oldest technologies in existence.

Archeological studies have been made which show imprints of woven fabric materials on clay pots that date back some 27,000 years [28, 29]. No one knows exactly when weaving fabrics actually started, but by 6000 B.C the art of weaving and dyeing had developed into a viable industry around the world [29]. Even in these early times craftsmen could produce fabrics that were decorated and adorned with intricate geometric patterns.

The first record of a weaving device is a picture of a horizontal loom on an Egyptian dish dated 4400 B.C [28]. As more complex civilizations of people evolved, more improvement in textile technology developed and international trading emerged. Chinese silk was the most prized material of the international trades in the early centuries 45-400 A.D [28]. During the 15^{th} century trade fairs were set up in Europe that provided a place for active exchange of silks and wools. In fact, the purpose of Columbus's quest to the west, which initiated the major colonization of America, was to map out a quicker and easier trade route to the East; the purpose was to obtain textiles, especially silks, from the Orient. The textile industry was revolutionized during what is referred to as the "Industrial Revolution"; during this era, textile production was taken from essentially hand processes to mechanization for mass production. Important inventions, such as spinning machines, automated weaving looms and the cotton gin planted the seeds for the industrialization of the textile industry [30]. In more recent years new applications in textiles have been made possible by the ability of scientists to engineer textile fibers, yarns and fabrics. Fabric designs can be modified using computer aided design programs (CAD), which allow designers to modify designs interactively; CAD use can speed up manufacturing by supplying electronic links to production [29]. Computer Aided

Manufacturing (CAM) systems can also help with textile production; looms, knitting machines and dyeing processes can all be controlled by the computer. Presently, due to trade barriers established in the early 20th century, domestic textile production has suffered severe economic losses; a shift toward production of higher value textile products has occurred [31]. These products include industrial fabrics and products in the growing industry of technical textiles.

Textile manufacturing is a mature, worldwide industry that is well-developed and has the infrastructure to support the development of any number of fabrics designed for specific end applications.

1.3.2 Textile Applications

Textiles can be manufactured for two purposes: aesthetic or technical use. Aesthetic textiles are mainly used because of their appearance for products such as clothing, furnishings, carpets, towels and window covering. Technical textiles are manufactured for their technical and performance properties rather than their aesthetic or decorative characteristics [31].

There are several different categories of technical textiles [31]. For example, sterile clothing for patients and medical staff has been development from advances in medical textiles. Fabrics have been manufactured with nano-coatings, fluorocarbon coatings, and surface roughness to create ultrahydrophobic, or self-cleaning fabrics [32]. Additionally, microencapsulation of antimicrobial agents within textile fibers, yarns and fabrics has been shown to prevent bacterial and fungal infections in patients [31-33].

Geotextiles are implemented for civil and environmental solutions during construction of buildings, roads and dams. Ground drains are commonly lined with textiles that act as filtration media to permit water flow, but prevent passage of soil particles [31]. Ultimately, the use of the geotextile minimizes the movement of ground surfaces preventing subsidence. Textiles are also used for packaging and containment. Bags and sacks are manufactured from cotton and flax, to provide reusable bags of superior strength (*e.g.* bags that can handle a capacity of up to 2 tones) to store and ship powdered and granular materials ranging from fertilizer, sand, cement, sugar and flour to dyestuffs [31].

Fluid flow within textiles has been primarily studied, modified and exploited for use in so-called moisture management applications in which fluids are transported away from their source for storage or evaporation. The emergence of performance fabrics like UnderArmour® and Coolmax® by Dupont for use in sportswear apparel, has shown that moisture uptake in fabrics can be controlled using optimized weave or knit construction and surface chemistry.

Knowledge of how to manufacture textiles was critical for the development of textiles for the aforementioned applications. Therefore, a review of textile manufacturing processes is useful for the development of the amphiphilic fabrics studied in this thesis.

1.3.3 Textile Manufacturing

Fibers

Fibers come in two forms: staple and filament. Staple fibers are short typically, one to tens of inches long. Filament fibers are long, typically hundreds of meters long. Natural fibers, including cotton, flax, wool and asbestos, are all staple fibers with lengths

ranging from 1-40 inches [34]. Silk is the only natural fiber that occurs in nature in filament form and its length ranges from 900-1200 meters [35]. Natural fibers varying according to their strength and recoverability, and many of them readily swell upon moisture absorbance. Hence, natural fiber properties should be carefully evaluated before being used in any particular end application. Synthetic fibers are made from chemicals (*i.e.* synthetic polymers) that are solidified into filament form. There are several different kinds of synthetic fibers, but the most widely used synthetic fibers are polyesters, polyamides (Nylon), and polyolefins [34, 35]. Polyester fibers have excellent strength, abrasion and wrinkle resistance. They are used consistently for apparel and furnishing. They are also used industrially for various technical applications. Polyamide fibers are commonly known as Nylon. Nylon has low moisture absorption, but excellent elastic recovery, abrasion resistance and strength. Nylon is used in swimwear and outerwear and for manufacturing carpets and parachutes. Polyolefin fibers fall into two categories: polyethylene and polyproylene. These fibers are lightweight and have high elasticity. Polyolefins have been used in athletic wear, and linings for outerwear, but also for erosion control as liner fabrics.

Manufacturing Synthetic Fibers: Filament Extrusion

Filament extrusion is the technique used to manufacture synthetic fibers. In extrusion the desired polymers for the filament are melted or dissolved into a liquid. The liquid polymer is then forced through a device called a spinning nozzle or spinneret; a metal disk containing one to several thousand tiny holes through which filaments are formed. As the liquid polymer is forced through the spinneret it solidifies, either because

of cooling (melt spinning), solvent evaporation (dry spinning), or phase separation (wet spinning) (cf. Figure 1.5) [34]. Once the filaments are formed they are twisted together to form a filament yarn that can be finished using some type of texturing, or they are cut into staple fibers and then processed into a spun yarn.

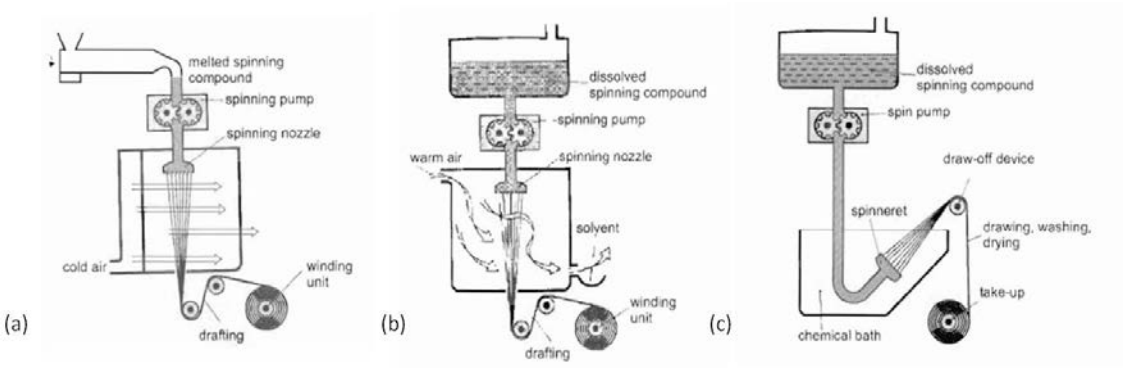

Figure 1.5 Typical filament extrusion processes (a) principal of melt spinning (b) principal of dry spinning (c) principal of wet spinning [34].

There are a number of design parameters that can be varied to produce the desired fiber or filament with a specific size, shape or chemistry. For example, commonly the holes of the spinneret are varied to produce fibers of different shape, diameter or structural make-up (cf. Figure 1.6). Furthermore, the feeding mechanism to the extrusion process can be varied to produce blended fibers with heterogeneous properties (cf. Figure 1.7). Blended fibers combine two or more polymers into a single strand. Examples of such constructions are a side by side arrangement, in which half the fiber is composed of one polymer A and the other half is composed of polymer B, a matrix and fibrils arrangement, in which polymer B is integrated like a porous matrix into polymer

A, and a sheath core arrangement, in which polymer A composes the outside core of the fiber and polymer B composes the inside core. These fiber blends can be engineered to create the desired fibers to meet specific needs.

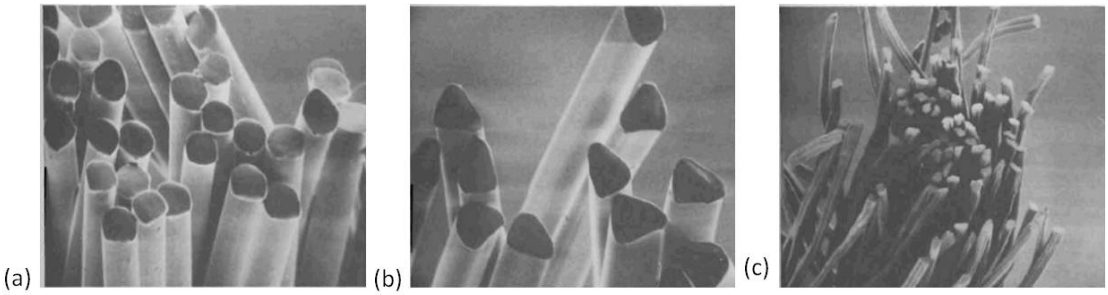

Figure 1.6 Synthetic fibers engineered with different cross sectional shapes. (a) round nylon fibers (b) triangular nylon fiber (c) square rayon fibers [35].

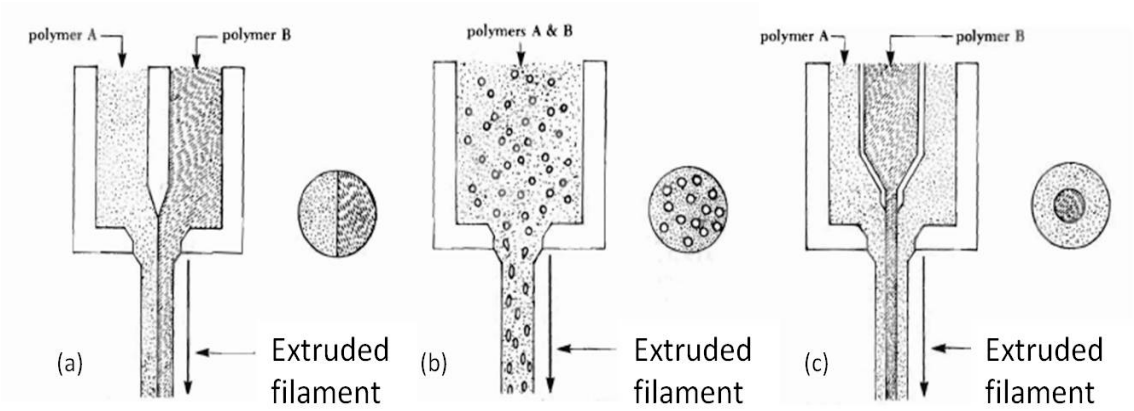

Figure 1.7 Schematic of feed mechanism to create blended fibers. (a) bicomponent side by side fiber (b) bicomponent matrix & fibrils fiber (c) bicomponent shear core fiber [35].

Yarn

Yarn is a long continuous mass of intertwined fibers. A yarn can be produced from two methods: either as a spun yarn or a filament yarn [34]. All filament yarns are made from synthetic fibers, with the exception of silk. Filament yarns are made by slightly twisting or grouping filaments together. Spun yarn is yarn that is manufactured from staple fibers tightly wound or twisted together using a yarn spinning process. Spun yarn can be made with natural fibers or synthetic fibers that have been cut into staple form.

Yarn Spinning

Ring spinning, open-end spinning, and air-jet spinning are the three most common technologies used to manufacture spun yarn (cf. Figure 1.8) [29, 34]. These methods vary in terms of the method used to apply twist to the yarn. Depending on the spinning method, the yarns characteristics (*e.g.* tenacity/elongation, evenness, hairiness, and twist angle) can be tuned to produce a yarn with specific physical properties. Once the fibers have been harvested or synthesized, cleaned (for natural fibers), separated and aligned into an array of staple fibers called a sliver, either spinning method can be initiated.

For ring spinning, a sliver of fibers, usually having a diameter of 15-30 mm, has to be further reduced into a roving, which is a sliver of fibers with a diameter on the order of 3 mm. In the ring spinning process, a roving is rotated around a ring. As the fibers are spun into a circle twist is inserted. This newly made yarn is then collected onto a narrow tube called a bobbin. This can be better explained by visualizing a piece of string with a weighted object hanging from it. If the weight is spun into a circle twist is applied to the

string. Ring spun yarns are strong, they have excellent tenacity/elongation and evenness. However, they can have hairy surfaces.

In open-end spinning, a sliver of fibers is fed into a rotor. The fibers collect at the widest end of the rotor and as the rotor spins, twist is inserted to hold the fibers together, creating a yarn. The yarn is continuously removed and simultaneously wound onto a tube for storage, also called a bobbin or package. Yarns made from open-end spinning are typically cheaper to produce, but they are not as strong as ring spun yarns. These yarns have less elongation, evenness and hairiness than ring-spun yarns.

The air jet-spinning method uses air nozzles to entangle a silver of fibers into a yarn. The finished yarn is wound directly onto a package. Air jet spinning produces yarn with good evenness and low hairiness or pile up of stray fibers at the yarn surface, however like open-end yarns, air-jet yarns are weaker than ring spun yarns.

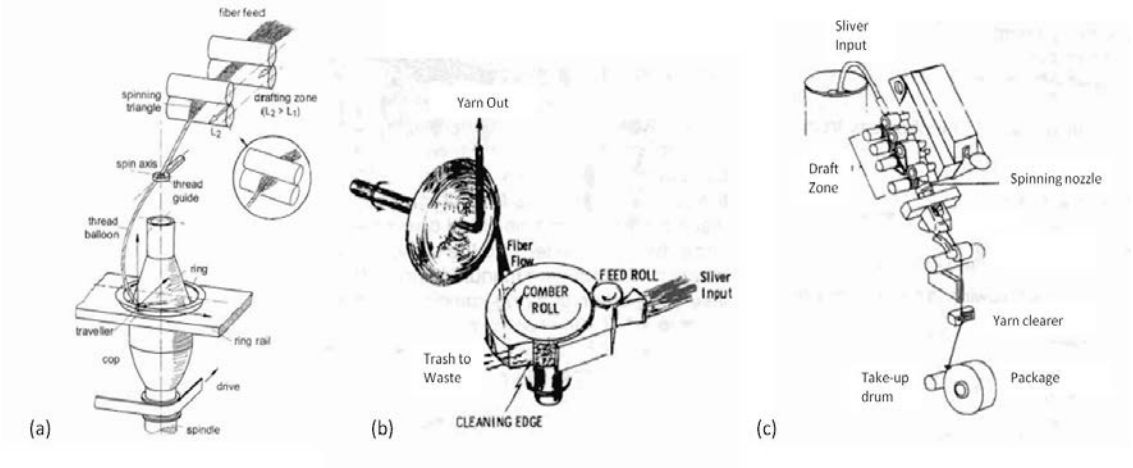

Figure 1.8 Typical methods for manufacturing spun yarn. (a) principal of ring spinning [34] (b) principal of open-end spinning [29](c) principal of air-jet spinning [29].

Fabric Construction

Textiles can be manufactured in three ways: as a knitted fabric, a woven fabric or a nonwoven material [29]. Knitted fabrics are made from interlocking one or more continuous strands of yarn into a series of loops or stitches (cf. Figure 1.9)[36]. Knitted fabrics are engineered mainly for apparel and domestic uses and a few industrial applications. Common knitted apparel include socks, pantyhose, and underwear garments. Knitted fabrics are used in technical applications for automotive upholstery. Knitted fabrics are used for these applications because they easily mold to the shape of an object, they possess wrinkle resistant qualities, and have excellent stretch and recoverability.

Woven fabrics are made from two sets of yarns that intersect at right angles, each yarn crossing over or under subsequent intersecting yarns according to a predetermined weaving pattern. There are many weaving patterns, but three basic weaves form the basic designs from which all other weaving patterns are produced: plain weave, twill weave and satin weave (c.f. Figure 1.11). Woven fabrics are used for household products such as sheets and towels. They are typically more durable than knitted fabric which makes them more suitable for various industrial applications. Examples include soil reinforcement, filtration, and erosion control applications. The benefit of woven fabrics in terms of durability arises from their stiffness: stress can be absorbed by the warp and weft yarns, and hence by fibers, without much mechanical elongation [31].

Nonwovens are any material made directly from fibers and held together as a fabric by adhesives, seal fusion or mechanical entanglement of fibers. Nonwoven fabrics have

many applications, aesthetic and technical, and these applications span a wide range of industries. For example, they are used in upholstery for the backing and cushioning of couches, in the personal care industry for diapers and sanitary napkins, in the health care industry for surgical caps and gowns, and even in civil engineering for soil stabilization. Nonwoven fabrics are not the focus of the experimentation conducted in this thesis because they lack uniformity in their woven structure. Further discussion of them is therefore outside the scope of this work.

Knitting Technology

Knitted fabrics are manufactured using two methods: warp knitting and weft knitting [29]. The methods differ according to the direction the yarns are formed into the fabric. In a warp knit, the interlocking loops of yarns or stitches are knitted vertically into the fabric. For weft knit fabrics, the stitches are knitted horizontally into the fabric. In the textile industry the set of horizontal stitches in a knitted fabric is referred as the “course” of the fabric. The set of vertical stitches in a knitted fabric is referred to as the “wale” of the fabric. All stitches in the course of a warp knit fabric are produced at the same time, while the stitches in the course of a weft knit fabric are produced one at a time [29]. Warp knits generally have less stretch and more durability than weft knit fabrics. Industrial production of knitted fabrics is automated using a knitting machine. Industrial knitting machines can produce knitted fabrics at 1000 to 4 million stitches per minute.

Examples of various knitting constructions are shown in Figure 1.9. The most basic knitting construction, the plain knit, as well as more complex knit structures such as the milanese knit and the tricot knit are shown. The plain knit is a weft knit process

producing a plain, flat surface knit with even patterned loops. The milanese knit is a warp knit process in which stitches are composed of two loops one from different sets of warp threads, both moving diagonally from one stitch to another, and alternatively horizontally along the fabric. The crossing of the yarns creates a diamond effect on the face of the fabric. The tricot knit is also a warp knit, it produces a fine textured fabric with lengthwise ribs on the face of the fabric and horizontal crosswise ribs on the back.

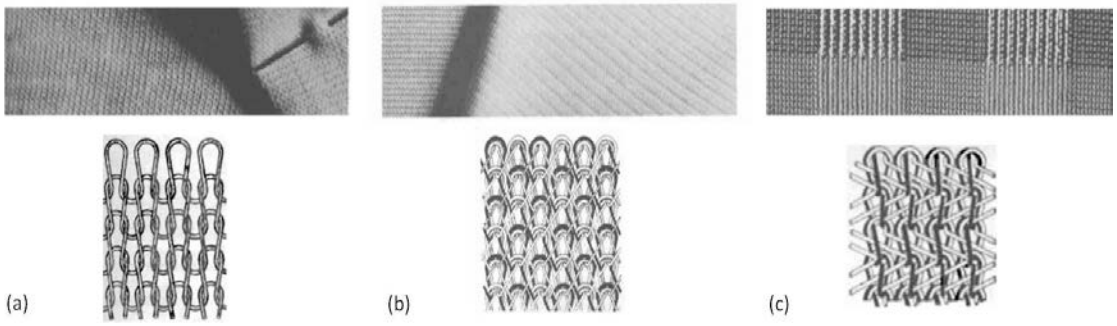

Figure 1.9 Schematics of knitted fabric constructions [35]. Illustrates a basic knit construction (a) plain knit and two complex knit constructions (b) milanese knit and (c) tricot knit

Weaving Technology

Woven fabrics consist of two sets of yarns intersecting at right angles; there is a set of vertical yarns and horizontal yarns. In the textile industry the set of vertical yarns in a woven fabric is referred as the “warp” of the fabric. The set of horizontal yarns in a woven fabric is referred to as the “weft” of the fabric.

Similar to knitting, industrial production of woven fabrics is automated; the only manual task to complete in order to weave a fabric is installing the yarns into the weaving

machine [29].The first task is to mount bobbins of yarn onto a creel in a clearly defined order according to the desired pattern of the fabric. A creel is a large metal frame where bobbins of yarn, which is a large supply or package of yarn wound around a cylindrical tube, can be mounted in a clearly defined order according to the desired pattern of the fabric. This metal frame is composed of several posts that contain pivoting supports that hold the yarn packages in place. Each post has mechanisms to control the yarn take up and rings to guide the yarn to the weaving machine. Once all the yarns are installed on the creel, each yarn thread is fed through a reed. A reed is a comb like device that keeps every single yarn separated as it is wound onto a warp beam. Each yarn thread is fed between the teeth of the reed, which are called dents. Once aligned on the warp beam the yarn threads are carried to the loom where the weaving processes begins.

At the loom, before inserting the weft yarns each warp yarn must be threaded through its own drop wire, heddle eye, and reed dent. The drop wire is a device that stops the weaving process if any yarn should break. The heddle eyes are held in a frame called a harness or shaft. Each harness can raise and lower a single warp yarn so that the weft yarns can be inserted according to the specified weaving pattern. Finally, the yarns are threaded through another reed to maintain an even distribution of yarns across the fabric. This reed is also used to push back the weft yarns once they have been inserted into the fabric. The weaving process thus consists of a repetitive motion; warp yarns being moved up and down creating an opening to insert a weft yarn, weft yarns are then inserted, and the reed pushes the weft yarn back tightly into the fabric. The process repeats until all the weft yarns have been inserted into the warp yarns. This can be better visualized by

referring to Figure 1.10, which depicts a loom as a weft yarn is being inserted into the warp yarns.

The major difference between weaving machines is the way the weft yarns are inserted into the warp yarns. Weft yarns can be inserted using a number of mechanisms. These include the use of water or air jets that carry the weft yarn across the warp of the fabric from the force applied to the fluid. Similarly, a gripper projectile, a small hook-like device that grips the end of a weft yarn, can be projected across the fabric while it carries the weft yarn with it. A rapier can also be used, which is a mechanically operated arm that will simply carry the weft yarn across the fabric. Each mechanism varies with regards to the speed of weaving and the type of yarns that can be used. Woven fabrics can be produced at the highest rate with air jets, which can achieve speeds of up to 2,200 meters of weft yarn inserted per minute. The other methods have speeds ranging from 950-2,000 meters of weft yarn inserted per minute [29].

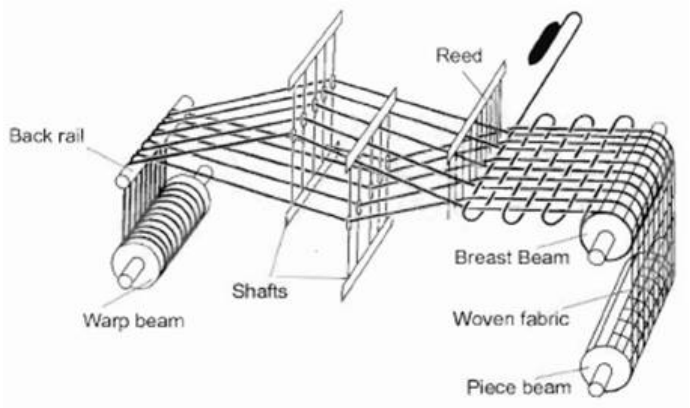

Figure 1.10 Illustrates the basic action at the loom of a weaving machine [34]. The harness or shaft moves the warp yarns up or down, a weft yarn is inserted, the reed pushes the weft yarn tightly into the fabric.

Examples of various weaving patterns are shown in Figure 1.11; the most basic weaving patterns (plain weave, twill weave, and satin weave) are shown. In the plain weave, weft and warp yarns are intersect orthogonally, with the weft yarn passing alternatively over and under subsequent warp yarns. Such a fabric is firm and drapes well, but it tends to wrinkle more than other weaves [35]. In the twill weave, weft yarns are interlaced over and under two or more warp yarns in a fixed staggered manner, forming a diagonal line on the fabric surface. Fabrics with twill weaves are dense and durable, with good wrinkle recovery [35]. Satin weaves are characterized by warp floats across the surface of the fabric due the action of the weft yarn passing over then under several warp yarns. Satin fabrics have high luster, and high light reflection, and smooth surfaces [35]. However floating warp yarns make the fabric nondurable, due to floating yarns being subject to snagging pulling or breaking. Much more complex weave patterns are also routinely produced on industrial scales, but a full discussion is beyond the scope of this thesis.

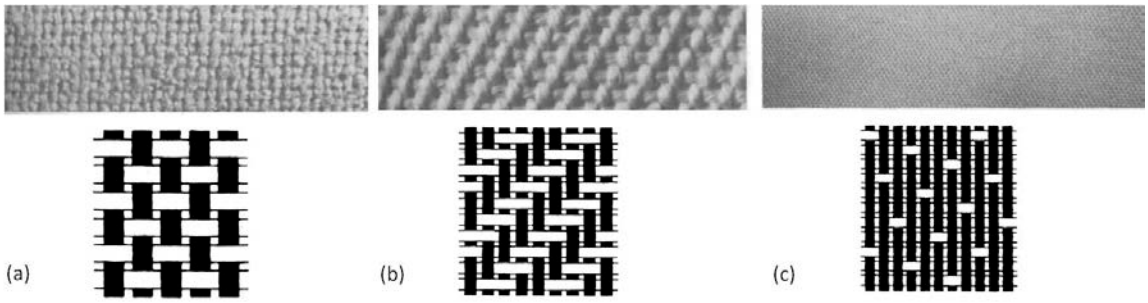

Figure 1.11 Schematics of woven fabric pattern[24, 35]. Illustrates three basic weaving patterns: (a) plain weave (b) twill weave (c) satin weave

Embroidery of woven fabrics opens up even more fabric design options. Embroidery is conducted by interlacing stitches of additional yarns onto the face of a woven fabric according to a desired pattern. Similar to knitting and weaving, there are industrial scale embroidery machines that can mass-produce custom designed embroidered fabrics. The pattern can vary widely, ranging from text to pictures (cf. Figure 1.12).

Figure 1.12 Letters of the alphabet embroidered into a plain weave fabric [37].

1.3.4 Fabric Performance Parameters

The ability of a fabric to transport moisture is critical to many textile applications. For example, clothing for sportswear must be made with fabric that can quickly transport water away from the body to keep the athlete dry and comfortable. Once a prototypical fabric has been manufactured, it is necessary to characterize its fluid transport properties to ensure suitability for its intended end applications. The transport properties can be evaluated through wicking tests in which the mass or volume of fluid absorbed into a fabric is measured as a function of time. From this information, performance parameters

of a fabric can be determined. This section summarizes the key parameters that define the ability of a fabric to transport moisture, and subsequently provides details on how wicking tests are currently being performed.

Transport of liquid into textiles occurs primarily due to capillary action (cf. Section 1.1.1). There are four key parameters that describe capillary flow: effective capillary radius (R_c), capillary pressure (P_c), permeability (k) and saturation (S). Capillary pressure depends on the liquid surface tension and wetting contact angle, saturation also depends on the fluid properties. Permeability and effective capillary radius are intensive parameters that only depend on the fundamental properties of the fabric itself. In experiments, liquid flow rates are commonly used to describe the absorption characteristics of a fabric. However, the experimental data can be analyzed in terms of fabric performance parameters that solely depend on the fabric's pore structure and materials, so called intensive properties. These properties are extremely useful, because they can be used to make generalized predictions about liquid transport into the fabric for all Newtonian fluids, as long as viscosity and wetting properties are known. Performance parameters that are defined with respect to the properties of the liquid, are referred to as extensive properties and these quantities have limited predictive power; they depend on liquid properties and are thus only relevant for a particular fluid.

Generally, fabrics contain a distribution of pore sizes, but in a first approximation the distribution can be characterized as bimodal, with smaller pores inside the yarns (*i.e.* inter-fiber or intra-yarn microchannels) and larger pores between the yarns (*i.e*. inter-yarn, macrochannels) [38]; the distribution of capillary radii can be represented in the form of a single average effective capillary radius (R_c). The effective capillary radius is

an intensive property that provides an idea of the average size of the void spaces within a fabric.

As described in Section 1.1.1, capillary pressure (P_c) may not be the most intuitive concept to describe the driving force for wicking flow in porous fabrics that are open to the atmosphere, but the concept is quantitatively equivalent to the more easily interpreted force of adhesion framework. More importantly, capillary pressure is conventionally used in literature to quantify liquid transport due to capillary forces in porous media like soil and rock, which are mostly not open to the atmosphere. As a consequence, a large body of literature has developed that uses capillary pressure as a measure for the ability of a porous medium to absorb liquid due to interfacial tension forces. Capillary pressure is larger for a medium that can easily wick fluids and smaller for a medium that cannot. It is an extensive property, which depends both on the fabric structure and the properties of the wicking fluid, in particular the contact angle of the fluid with the fabric material and the surface tension of the liquid.

Permeability (k), on the other hand, is an intensive measure of the ability of a porous medium to facilitate fluid flow [39] . It essentially describes the size of the cross sectional area of fabric that is available for fluid flow and only depends on the geometry of the fabric's void space [40].

Finally, saturation (S) is a measure of the amount of fluid held within the void space of a porous medium. A wet fabric will have large saturation values, while a drier fabric will have a low saturation. By definition, the saturation can only range from 0 to 1 (or 100%) for a porous medium.

1.3.5 Wicking Studies

Most of the above performance parameters of a fabric can be evaluated from data collected and analyzed during a wicking test. There are several wicking techniques, including drop tests and longitudinal wicking tests [2]. A drop test is conducted by placing a drop of liquid onto a sample of fabric and recording the time it takes for the drop to absorb into the fabric (cf. Figure 1.13a). This test is ideal to quickly determine the wicking rate of a particular fluid into a sample of fabric. It can also provide a good understanding of the dynamics of liquid absorption from a finite reservoir. However, the test is complicated by radial spreading of the liquid drop, which makes it difficult to quantify performance parameters of the fabric, such as, permeability, effective capillary radius and capillary pressure.

There are three types of longitudinal wicking tests, upward (vertical), horizontal, and downward wicking. Longitudinal wicking refers to in-plane wicking along the length of the fabric strip. Spreading of liquid in a longitudinal test is thus unidirectional. In each test a strip of fabric is hung or draped over a support structure. This structure can be any device from which the fabric can be hung or draped so that it is oriented in the desired direction of flow. In this thesis, the support structure for each longitudinal wicking test will be referred to as the holding bridge. The mass of liquid absorbed into the fabric can be recorded through several means: using an analytical balance, through a gravimetric absorbency test system (GATS), electronically through the use of electrical sensors, or even optically from images of the progression of the wetting front in the fabric over time [41-43]. For this thesis, a review of the testing methods involving an analytical balance are most useful.

In an upward wicking test a fabric is hung vertically from a holding bridge. A liquid reservoir is placed on top of a balance so that the mass of liquid absorbed into the fabric can be recorded; both the liquid reservoir and the balance are placed on top of a lab jack, which can be raised until the fabric is submerged in the reservoir to a ~1 cm depth at the start of each experiment. The general set-up can be viewed in Figure 1.13b. The absorption rate can also be recorded by placing a camera in front of the fabric and recording the total length of wetted fabric over time. It is important to use only the data recorded for short times and distances to determine the upward wicking rate. At long times, the slowing effects of gravity become apparent in the data. Similar to the drop tests result, an upward wicking test can also be used to quickly determine the wicking rate of a particular fluid into a sample of fabric. However, it is difficult to accurately determine intrinsic performance properties from upward wicking data. Due to the dynamics of liquid transport into a vertical capillary (cf. section 1.1.1) it is easier for liquid held within the smaller radii of the fabric to wick to higher vertical heights, than liquid held within larger radii. Hence, the saturation of the fabric is a function of the upward wicking height; saturation decreases at increased wicking heights. Effective capillary radius, capillary pressure, and permeability are all a function of saturation. The only way to accurately evaluate these parameters is to perform the test repeatedly at fixed wicking heights, a task which is not feasible using an upward wicking set-up.

In a horizontal wicking test, a fabric strip is positioned onto a holding bridge by attaching the originating end to a rod that can be submerged into a fluid reservoir that is sitting on top of a balance and a lab jack; the fabric is then laid flat on top of the bridge and secured to the bridge using self-adhesive tape. The general set-up can be viewed in

Figure 1.13c. After the liquid reservoir is filled, the lab jack is raised until the fabric is submerged into the reservoir at the start of each experiment. Once the wetting front has reached the horizontal portion of the fabric, the mass of liquid absorbed into the fabric is recorded. The test is stopped once the liquid has penetrated the fabric throughout the entire horizontal length. Analysis of horizontal wicking experiments can take significantly more time than evaluating a fabric using a drop or upward wicking test, but from the test an intrinsic performance property of a fabric, effective capillary radius, and capillary pressure can be determined.

The common downward wicking method was introduced by Bernard Miller [44]. In Miller's approach a fabric strip is positioned onto a holding bridge by attaching the originating end to a rod that can be submerged into a fluid reservoir that is sitting on top of a balance and a lab jack, the fabric is then laid over a distance at an acute angle from the surface, then draped over a rod and allowed to hang downward. The general set-up can be viewed in Figure 1.13d. Once the liquid reservoir is filled, the lab jack is raised until the fabric is submerged at the start of each experiment. Once the wetting front in the fabric begins its descent downward the mass of liquid absorbed into the fabric is recorded. These data can then be used in combination with Darcy's law to determine the intrinsic permeability of the fabric. This method was developed to make up for the limitations of the vertical wicking test; the wetting front in a downward test is not slowed by gravity.

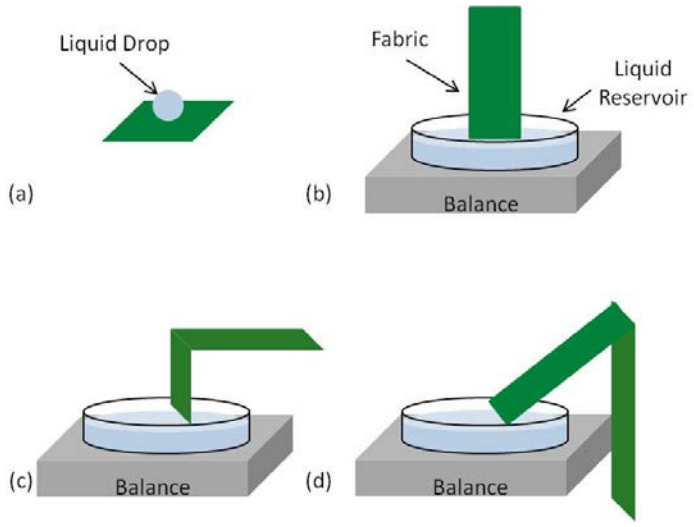

Figure 1.13 Experimental set-ups for monitoring fluid transport into fabrics. (a) drop test (b) upward wicking test (c) horizontal wicking test (d) downward wicking test

1.4 Motivation and Research Objectives

The benefits of microfluidic flow include spontaneous capillary wetting, rapid mass diffusion, laminar flow, and large surface area to volume ratios. As a result of these special properties, chemistry and chemical analysis of fluids performed at micrometer length-scales can be faster, cheaper, more precise and require smaller analytical reagent volumes than when traditional laboratory scale analysis equipment is used. To capitalize on these benefits, researchers have engineered microfluidic structures to improve the efficiency of high-throughput chemical analysis, drug and disease screenings, fundamental biological studies, and single cell analysis studies. However, common fabrication methods limit the use of microfluidic device applications to processes that use only small feed flow rates. This is unfortunate because the benefits of microfluidic flow could be useful in commercial applications with large feed flow rates.

Conducting an industrial scale liquid-liquid extraction using a microfluidic structure is of particular interest, because the efficiency of an extraction process is often determined by the interfacial contact area between immiscible liquid phases (larger contact area is better), as well as the diffusion of solute from the bulk of each liquid to the liquid-liquid interface (faster diffusion and shorter diffusion paths being the goal). As stated previously, the fundamental physical characteristics of microfluidic flow are very amenable to these requirements.

To extend the benefits of microfluidic flow beyond the laboratory to larger scale applications like liquid-liquid extractions, a high-volume production method and a pathway to system scale-up are needed. The focus of this thesis is to investigate the feasibility of fabrics as large-scale microfluidic structures, because existing textile

manufacturing technologies offer proven economy-of-scale advantages. The intent is to extend the design of fabrics in a novel direction, aiming to control the fluid flow inside fabrics with precision and specificity akin to microfluidic structures. As mentioned above in the background information of this thesis, the porous construction of a woven fabric naturally provides an intimately interconnected network of microchannels in the form of spaces within and between constituent yarns. Hence, in a woven fabric there are two types of microscopic voids that can accommodate microfluidic flow: (1) the *intra*-yarn spaces between fibers or filaments within a yarn, and (2) the *inter*-yarn spaces between the yarns in a fabric. By weaving hydrophobic and hydrophilic yarns together into a single fabric, we can create a network of microchannels with heterogeneous surface properties. The placement of these yarns should enable control of liquid flow within the channels of the fabric. Hydrophilic yarns should act as barriers to organic flow and hydrophobic yarns should act as barriers to aqueous flow. Furthermore, simultaneous flow of immiscible liquid phases throughout the large surface area of the fabric can be achieved when organic and aqueous phases flow in parallel along hydrophobic and hydrophilic yarns placed side by side. If we can engineer a sheet of amphiphilic fabric large enough to perform solvent extractions on an industrially relevant scale, the process could be conducted without dispersion devices, reducing installation and energy costs, while still maintaining intimate contact between phases to achieve an efficient extraction.

Standard textile production technologies provide an extensive design space with regards to fabric construction and yarn properties (*i.e.*, material, size, shape, surface chemistry). For example, the surface chemistry of fibers can be engineered by varying the monomers from which polymer fibers are constructed or by coating naturally

hydrophobic fibers with thin films that have hydrophilic qualities. Also, bicomponent synthetic fibers can be produced that consist of two different polymers dispersed side by side, or one dispersed as a matrix of filaments inside the other (*i.e.* matrix & fibrils fiber). Finally, fibers can be produced with different cross sectional shapes (e.g. triangular, square, or circular). From these fibers and yarns, knitted fabrics, woven fabrics, and embroidered woven fabrics can be manufactured with simple designs, such as a plain weave where warp and weft yarns are interlaced orthogonally, with each weft yarn alternating going over and under subsequent warp yarns, or with complex designs such as the milanese knit. Knitted fabrics can be produced at speeds of up 4 million stitches per minute and woven fabrics at 2,200 weft yarn insertions per minute. A wide variety of microfluidic channel designs can therefore be engineered and manufactured on industrial scales using existing textile facilities.

It is well-known that variations in fabric construction parameters and material properties significantly affect fluid movement in fabrics. Hence, liquid flow rates could be controlled by the size, shape, arrangement (*e.g.* fabric design), and number of hydrophilic and hydrophobic yarns in an amphiphilic fabric. Fabrics are porous mediums that can support fluid transport in or out of their porous matrix according to clearly defined capillary laws. Wicking experiments can easily be conducted to quantify the absorption performance of a fabric. Hence, liquid flow in novel amphiphilic fabrics can be quantified and understood using wicking experiments and knowledge of fluid flow through porous mediums. The results of laboratory scale studies could then be used to make predictions about the performance of these fabrics upon scale-up to industrial scale processes.

The overarching goal of this work was to conduct fundamental experimental studies showing the feasibility of controlling microscopic liquid flow in amphiphilic fabrics. The specific objectives followed to achieve this goal are below:

1. **Identify a wicking technique that can be used to quantify the intensive performance properties of fabric with respect to fabric saturation, so that wicking rates of water and all other Newtonian fluids can be predicted for a fabric under various experimental conditions based on limited experimental characterization data.**

2. **Manufacture a limited set of prototypical woven fabrics with amphiphilic characteristics, which vary with regards to the arrangement and placement of hydrophilic and hydrophobic yarns within each woven structure. Demonstrate the feasibility of controlling microscopic liquid flow in amphiphilic fabrics by characterizing the liquid transport properties of each fabric via drop tests and upward wicking tests. Investigate the feasibility of parallel flow of immiscible phases within an amphiphilic fabric.**

3. **Through systematic analysis of the variation of wicking rates for a large number of different amphiphilic fabric designs, identify the design features that affect liquid transport into amphiphilic fabrics. Use the results of the systematic study to determine which amphiphilic fabrics designs are most suitable for liquid-liquid extractions studies.**

4. **Investigate the interfacial dynamics between liquid phases in amphiphilic fabrics by (1) visually confirming that solvent extraction can successfully proceed within amphiphilic fabrics and (2) quantifying the efficiency of these liquid-liquid extractions with respect to solute concentration and fluid flow rate.**

1.5 Thesis Organization

Chapter 2 (Objective 1) describes the key parameters used to quantify liquid transport in textiles: permeability (k), effective capillary radius (R_c), capillary pressure (P_c) and saturation (S), and details the validation of a new upward-horizontal-downward (UHD) wicking test. *Chapter 3* (Objective 2) details the investigation of control of microscopic liquid flow in novel amphiphilic fabrics via drop tests and upward wicking tests. Additionally, simultaneous wicking of an aqueous and hydrocarbon fluid into the hydrophilic and hydrophobic microchannels of an amphiphilic fabric was investigated with a two-phase horizontal wicking test. *Chapter 4* (Objective 3) outlines the investigation of the relationship between wicking rate and fabric design through results from upward wicking tests performed with 18 different amphiphilic fabrics. *Chapter 5* (Objective 4) details experiments using amphiphilic fabrics as liquid-liquid contactors for solvent extraction. *Chapter 6* presents the overall summary and conclusions of the project.

CHAPTER 2

VALIDATION OF THE INTEGRATED UPWARD-HORIZONTAL-DOWNWARD WICKING TEST FOR PROVIDING INTENSIVE PROPERTIES OF TEXTILE FABRICS[1]

2.1 Introduction

Liquid transport in textiles is relevant for a number of applications, including performance athletic apparel, dyeing and finishing, and filtration. To quantify liquid transport in textiles, a variety of wicking tests have been employed in which the mass or volume of fluid wicked into the sample is measured as a function of time [45]. The results of these tests cannot be used for engineering design or prediction and no standard technique is widely accepted. A particularly important limitation of classical wicking tests is their inability to account for differences in wicking properties as a function of fluid saturation. Saturation (S), defined as the fraction of void space that is filled with fluid, governs the effective capillary radius (R_c) and permeability (k) of the capillary network available for fluid transport. As saturation increases, effective capillary radius

[1] The contents of this chapter has been accepted for publication:
Owens, T. L., Leisen, J., Breedveld, V., and Beckham, H. W. "Validation of the Integrated Upward-Horizontal-Downward Wicking Test for Providing Intensive Properties of Textile Fabrics", *The Journal of the Textile Institute* (2011).

and permeability increase. Therefore, to fully characterize the fluid transport properties of a capillary network, permeability and effective capillary radius should be determined across a range of saturation values. Once the full k-S-R_c properties of a given porous medium are determined, these can be analytically related to wicking rates. In other words, with knowledge of the k-S-R_c properties of a fabric, wicking rates through the fabric can be calculated and predicted. Such an approach to characterization of porous media is standard practice in many fields apart from textile engineering [3, 46-48].

Recently, Simile and Beckham reported a new wicking test that allows one to extract k-S-R_c properties of textile fabrics [49]. Their test, based on some ideas published by Ghali *et al.* [50], gravimetrically monitors in-plane fluid flow from a reservoir through sequential upward, horizontal and downward segments of a rectangular fabric strip. The upward segment governs the saturation, the horizontal segment is used to extract the effective capillary radius from which the capillary pressure can be calculated, and the downward segment is used to determine the permeability. For a single wicking test run at a fixed upward wicking height, k and R_c are determined for a single S. The test is repeated for different upward wicking heights to generate k-S-R_c properties for a range of saturations.

In developing the integrated upward-horizontal-downward (UHD) test, Simile and Beckham used water as the wicking fluid. This presented challenges since water evaporation from a high-surface-area fabric can be of similar magnitude as the wicking rate, especially during the relatively long (*i.e.*, > 30 minutes) duration of the UHD tests. If characterization of fluid-transport properties of a porous medium is the desired goal, it is important that fluid transport occurs only through the porous medium and not into the

surrounding environment. Simile and Beckham mitigated the evaporation by conducting the wicking tests inside an environmental chamber at relative humidities of around 90%. Testing at such high relative humidities leads to special requirements for electronic components and may not be suitable for highly hygroscopic materials. An alternative is to use a much less volatile fluid in the UHD test, determine the k-S-R_c properties of the fabric and use them to predict the wicking rates of water and other Newtonian fluids. This should be possible, assuming the test accurately provides the intrinsic k-S-R_c properties of a given fabric, since the analytical relationships used to process the data contain variables for the fluid properties. In this thesis chapter, we conducted the UHD test on a knit fabric using fluids with different physicochemical properties to determine whether the obtained k-S-R_c properties were valid and useful for predicting wicking rates of other fluids.

2.2 Experimental

2.2.1 Theory

The principle concepts and theoretical background used in developing the UHD test have been reported in detail [49]. Here, for the convenience of the reader, we briefly summarize the key concepts and analytical expressions used in conducting the test and processing the data. The analytical expressions are based on simple laws of capillarity and their use requires that we model the complex pore structure of a textile fabric as a network of capillary tubes with a distribution of radii. Generally, fabrics contain a distribution of pore sizes, which is often characterized as bimodal with smaller pores inside the yarns (*i.e.*, interfiber, microchannels) and larger pores between the yarns (*i.e.*,

interyarn, macrochannels) [38]. When such a capillary network is hydraulically connected to a fluid reservoir, fluid will wick into the void space if the forces of adhesion between the liquid and the capillary wall are greater than the forces of cohesion between the molecules of the liquid. This is quantitatively indicated by a contact angle $\theta < 90°$. The contact angle is a measure of the fluid-solid interaction and is a parameter in the Laplace equation relating capillary pressure (P_c) to effective capillary radius (R_c) [51]:

$$P_c = \frac{2\gamma \cos\theta}{R_c} \tag{1}$$

where γ is the fluid surface tension. In a fabric, a wide distribution of capillary radii exists, which can be represented by an average *effective* capillary radius R_c that can be found from horizontal wicking data using the Washburn equation (without gravitational effects) [52]:

$$L_h^2 = \frac{\gamma R_c \cos\theta}{2\eta} t \tag{2a}$$

where L_h is the horizontal distance that the fluid front moves during time t, and η is the fluid viscosity. If the horizontal wicking length, which is readily measured, is plotted versus the square root of wicking time, a linear relation is expected:

$$L_h = \left(\frac{\gamma R_c \cos\theta}{2\eta} \right)^{1/2} \sqrt{t} \qquad (2b)$$

The slope of this plot, $dL_h / d\sqrt{t}$ is defined as the wicking rate W_c, which can be calculated directly from experimental data. The effective capillary radius R_c can then be expressed in terms of measurable quantity W_c:

$$R_c = W_c^2 \left(\frac{2\eta}{\gamma \cos\theta} \right) \qquad (3)$$

Because the effective capillary radius determined in the UHD technique is a characteristic value of the part of the pore network through which fluid is flowing, R_c is a function of the saturation S, which in turn is simply governed by the upward wicking height. Gravity ensures that saturation decreases with increasing upward wicking height as the larger pores cannot carry fluid to the same heights as smaller pores; as a result, the effective capillary radius also decreases. Saturation can be calculated using the following equation:

$$S = \left(\frac{V_f}{\varepsilon V_t} \right) \qquad (4)$$

where V_f is the volume of fluid held in the fabric at the end of a wicking run, ε is the fabric porosity, and V_t is the total external volume of the fabric (*length* × *width* × *thickness*).

Permeability (k) is a quantitative measure of the ability of a porous medium to facilitate fluid flow [39] and is also a function of saturation. Permeability can be measured using a simple form of Darcy's law for downward wicking [40, 49, 53, 54]:

$$k = \frac{\frac{dL_d}{dt} H_L \eta \, \varepsilon S}{\left(P_c - P_h\right)} \tag{5}$$

where dL_d/dt is the velocity of the fluid front during downward wicking, H_L is the total horizontal wicking distance, P_h is the hydrostatic pressure and is given by ρgh, where g is the gravitational constant, ρ is the density, and h is the upward wicking height. The factor $\varepsilon \cdot S$, which is the fractional fluid content, is included to properly correct for the difference between Darcy velocity (*i.e.*, apparent, superficial velocity) and the measured liquid front velocity.

2.2.2 Upward-Horizontal-Downward Wicking

The experimental set-up is shown in Figure 2.1a and the key geometric parameters of the upward, horizontal and downward wicking segments are defined in Figure 2.1b. The framework to support the fabric strip was constructed using a Fischertechnik construction set. The fabric strip was positioned onto the framework by attaching the originating end onto a rod that is submerged into the fluid reservoir at the start of a wicking experiment; a weight (8.6 g) was hung at the bottom of the downward section to keep the fabric taut. The entire set-up was placed in a laboratory fume hood and covered with a panel of Plexiglass to protect the fabric strip and balance from air

currents. Wicking was monitored gravimetrically as a function of time by placing the fluid reservoir on an analytical balance (Sartorius Acculab VIC) that was interfaced to a computer running Labtronics Balance Talk XL software. For each wicking run, the horizontal section (H_L) was ~13 cm and the downward section (D_L) was ~10 cm (cf. Figure 2.1). The variable upward wicking height h was adjusted between 1.5 and 7 cm using a lab jack to position the balance and fluid reservoir. Data were collected gravimetrically in the horizontal and downward sections as $m(t)$ and converted into $L(t)$ data; this calculation is straightforward since the fluid wicked through a fabric strip of constant cross-sectional area and porosity. The upward height governs the saturation S at the start of the horizontal segment; a key assumption of the UHD test is that S then remains constant throughout the horizontal and downward segments; previous studies in our group have shown that this is a reasonable assumption [53].

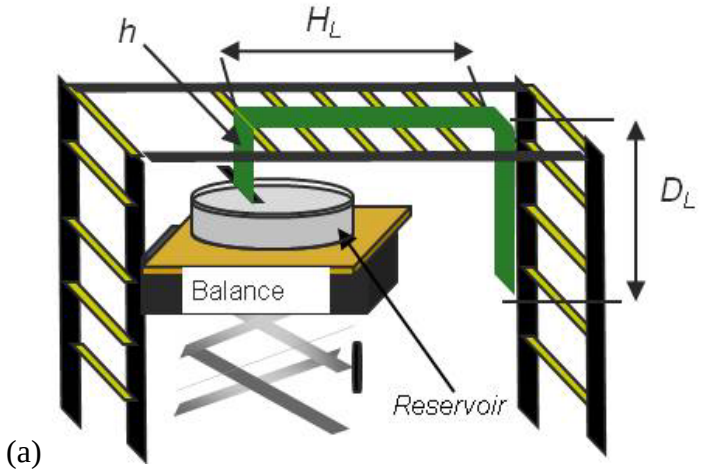

(a)

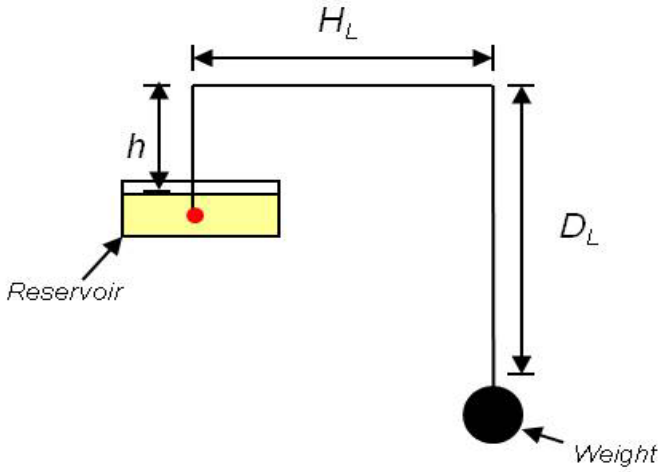

(b)

Figure 2.1 Schematic of (a) the experimental set-up for conducting the upward-horizontal-downward wicking test, and (b) the key components and parameters. Wicking is gravimetrically monitored through a fabric strip with upward (h), horizontal (H_L) and downward (D_L) segments. The h governs the saturation level through H_L and D_L. The test is repeated on the same fabric at different h values to determine permeability and effective capillary radius as a function of saturation.

Data from the horizontal section of the test can be used to find R_c and P_c through the Washburn (equation 3) and Laplace (equation 1) equations, respectively. Wicking data from the downward section of the test is used with the Darcy equation (equation 5) to determine permeability, *k*. The saturation, *S*, was determined for each upward height *h* using the fluid mass in the horizontal and downward sections of the fabric at the end of a wicking run.

2.2.3 Fabric and Fluids

A 100% polyester plain stitch knit fabric (Milliken & Company) was used for all wicking tests. The fabric weight was 0.013 g/cm^2 (5.7 oz/yd^2), thickness was 0.05 cm, wale/course yarn count was 33/38 per inch, and the porosity ε was measured to be 0.77. Micrographs of the fabric are shown in Figure 2.2. Fabric strips (2.2 × 34 cm) were cut and stirred in a bath of dodecane at 20 °C for 22 h to remove the commercial hydrophilic surface finish. Prior to use and between each wicking run, the fabric strips were dried at 70 °C for 24 hours and stored in a dry box.

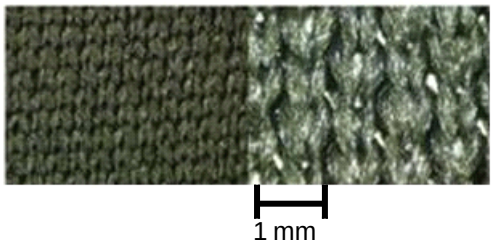

Figure 2.2 Micrograph of the plain stitch knit fabric used for all of the wicking tests. Technical face of the fabric is shown at two magnifications [53].

The fluids employed were anhydrous *n*-dodecane, *n*-tetradecane, *n*-hexadecane, 1-octanol (Sigma Aldrich, purity > 99%) and distilled water. Data from the wicking experiments with water were taken from the literature [49]; for these experiments, the hydrophilic coating was not removed from the fabric. Fluid characteristics are summarized in Table 2.1. The viscosities of the alkanes were measured using an MCR 300 controlled stress rheometer (Anton Paar). The surface tensions and densities were taken from the literature [55]. The contact angles were measured on a polyester film. A numerical sensitivity analysis revealed that contact angle variations have significant effects on the *k*-*S* curve. Higher contact angles shift the curve up while lower contact angles shift the curve down. Therefore, it is important to have a good estimation of contact angle on the surface of the fabric to determine the proper intrinsic permeability.

For each of the alkanes, two repetitions were conducted at upward heights of 2.5, 3.5 and 7 cm, while only one test was conducted at 1.5 and 5 cm. For octanol, three repetitions were conducted at each upward height. Errors in the experimental variables of end time for horizontal wicking, η, L_h, L_d, and h were estimated within reasonable ranges (*e.g.*, accuracy of η as +/- 3% due to slight temperature variations and rheometer sensitivity, accuracy of h as +/- 0.2 cm) and the resulting changes in k, S, and R_c were computed and reported. All wicking tests were conducted at 21.5 ± 1 °C.

Table 2.1 Fluid Properties at 20 °C

fluid	viscosity (mPa·s)	surface tension (dyne/cm)	density (g/cm^3)	contact angle on PET film
n-dodecane	1.52	25.4	0.75	< 5°
n-tetradecane	2.39	26.6	0.76	< 5°
n-hexadecane	3.57	27.6	0.77	< 5°
1-octanol	8.95	27.5	0.83	< 5°
water	1.00	72.9	1.0	76°

2.3 Results and Discussion

Wicking experiments were conducted using a homologous series of alkanes: dodecane, tetradecane and hexadecane. These fluids were chosen because they have low volatilities and similar chemical structures but exhibit differences in physical properties (cf. Table 2.1). Horizontal and downward wicking rates were collected for these fluids at different upward wicking heights. As shown in Figure 2.3, increasing upward wicking height corresponds to decreasing saturation. The similar saturations for each alkane at the same upward wicking height are a reflection of their similar densities.

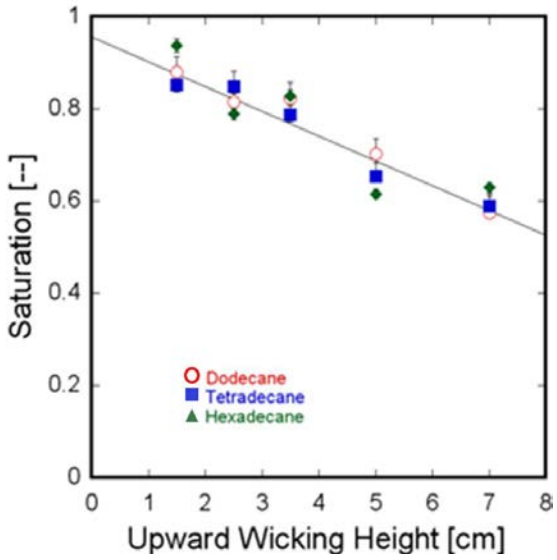

Figure 2.3 Saturation versus upward wicking height measured for the horizontal and downward segments of the fabric strip using three separate alkane fluids: dodecane, tetradecane and hexadecane.

The horizontal and downward wicking rates of each alkane are shown in Figure 2.4 as a function of upward wicking height. Wicking rates, which are different for the different fluids, decrease with increasing upward height. As saturation decreases, the capillary network transporting fluid is characterized by smaller average effective pores, and fluid movement through smaller pores is slower (cf. equation 3). For a given saturation, the alkane that exhibits the highest wicking rate is dodecane and the slowest wicking alkane is hexadecane. This is consistent with the fluid viscosities: dodecane < tetradecane < hexadecane.

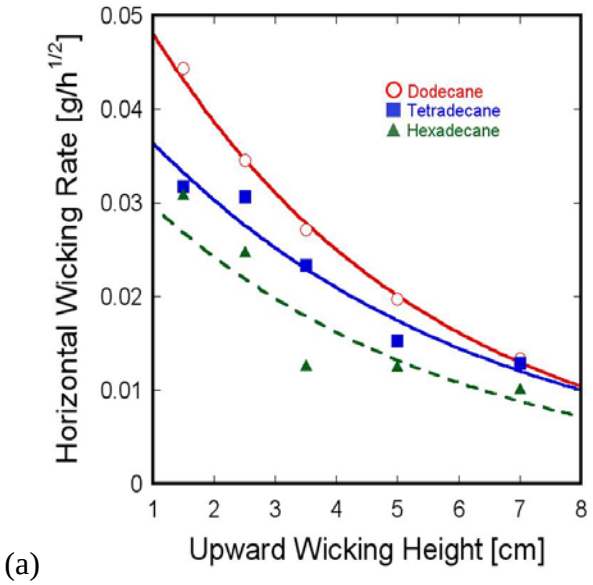

(a)

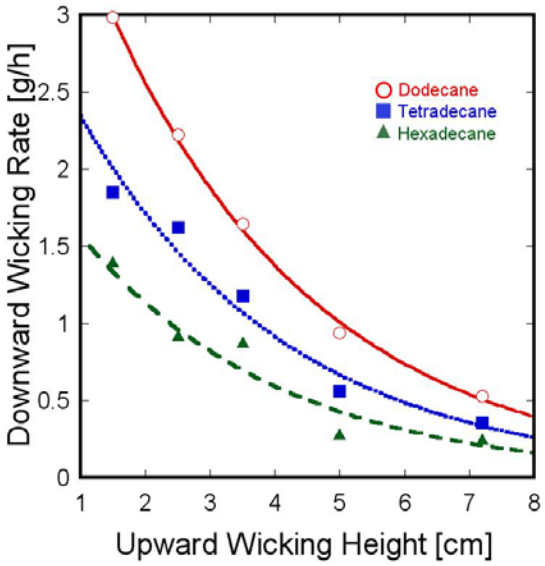

(b)

Figure 2.4 Horizontal (a) and downward (b) wicking rates versus upward wicking height for dodecane, tetradecane and hexadecane. Lines are shown as guides.

The wicking rate data were analyzed using equations 1 through 5 to yield plots of capillary pressure versus saturation (cf. Figure 2.5a) and permeability versus saturation (cf. Figure 2.5b). As saturation increases, capillary pressure decreases and permeability increases, trends consistent with wicking liquids through other porous materials such as sand [40]. Most importantly, both sets of data fall on single master curves. Figure 4 shows that fluids with different physical properties exhibit different wicking rates. Because the wicking rate is an extensive property that depends on fluid properties, this was expected. However, Figures 2.5a and Figure 2.5b show that P_c and k versus S are the same for all three liquids. Permeability is an intrinsic property of the fabric and should not vary with liquid properties. Capillary pressure depends on the fluid-solid interaction through the contact angle; since the contact angle is approximately the same for these three alkanes, the data in Figure 2.5b fall on a single curve. The relevant intensive property is the effective capillary radius, used to calculate P_c, which is expected to yield a single master curve when plotted versus saturation.

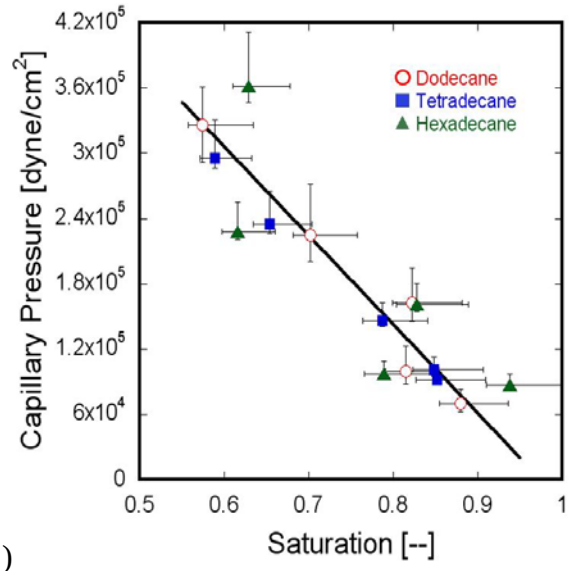

(a)

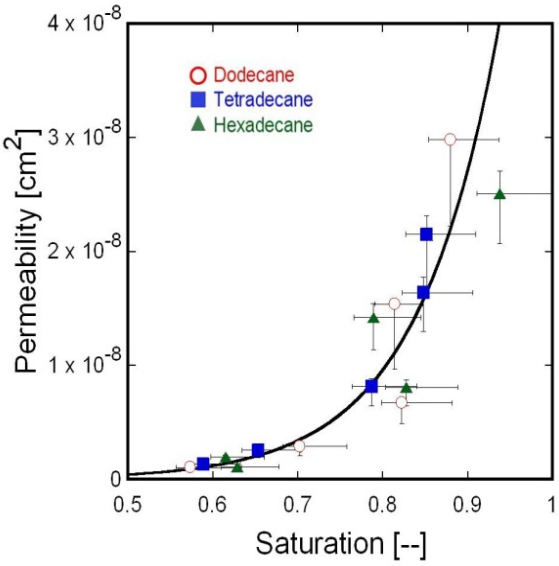

(b)

Figure 2.5 Capillary pressure (a) and permeability (b) versus saturation for dodecane, tetradecane, and hexadecane. Lines are shown as guides.

These data can be examined with respect to effective capillary radius (R_c) to provide information that is directly useful in designing fabric structures with engineered

wicking behavior. Figure 2.6 shows permeability as a function of effective capillary radius. In general, permeability and wicking rate increase with increasing R_c, which can be controlled by choice of fiber and yarn size, fiber cross-section, twist level, and cover factor in knit and woven fabrics. Since capillary pressure and therefore the ability of a fabric to support capillary flow, decreases with increasing R_c, further work is needed to determine an optimum effective capillary size.

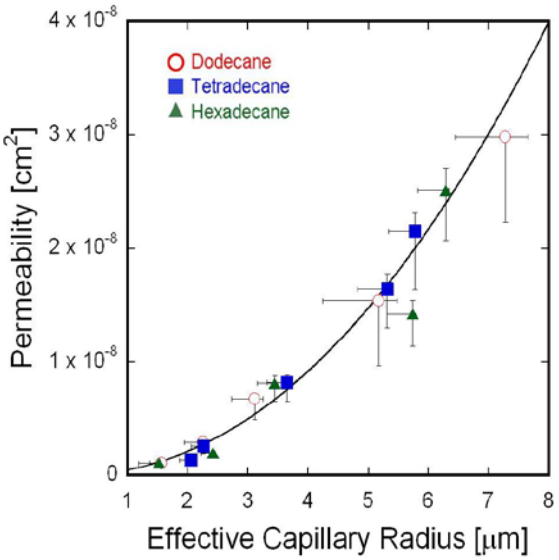

Figure 2.6 Permeability versus effective capillary radius for dodecane, tetradecane and hexadecane. Lines are shown as guides.

The UHD wicking test provides effective capillary radius and permeability as functions of saturation, properties that are intrinsic to the fabric. Such properties, determined from a set of wicking runs using a single fluid, can be used to make predictions about wicking rates of other fluids. Figure 2.7 shows predicted curves for horizontal and downward wicking rates as functions of upward wicking height (h) for

octanol along with experimental values at four *h* values. The experimental wicking rates agree very well with the predicted curves. Note that the wicking rates for octanol are much smaller than the ones measured for the three alkanes (cf. Figure 2.4), reflecting the higher viscosity ($\eta_{octanol} > 5\times\eta_{dodecane}$, cf. Table 2.1) for this alcohol that is capable of hydrogen bonding.

The predicted curves were created using the *k*-versus-*S* and *k*-versus-R_c relationships shown in Figures 2.5b and Figure 2.6, respectively. From R_c values and octanol properties, horizontal wicking rates were determined using the Washburn equation (equation 3). Downward wicking rates were determined from *k* values using Darcy's Law (equation 5) with P_c values calculated from R_c values using the Laplace equation (equation 1). These wicking rates are directly correlated to saturation through the *k*-*S*-R_c relationships embodied in Figures 2.5b and Figure 2.6. Plots of wicking rates versus saturation are sufficient to compare experiment to predictions. Since we had experimental data for *S* versus *h* for octanol, we used the upward wicking heights corresponding to each saturation for the predicted curves shown in Figure 2.7.

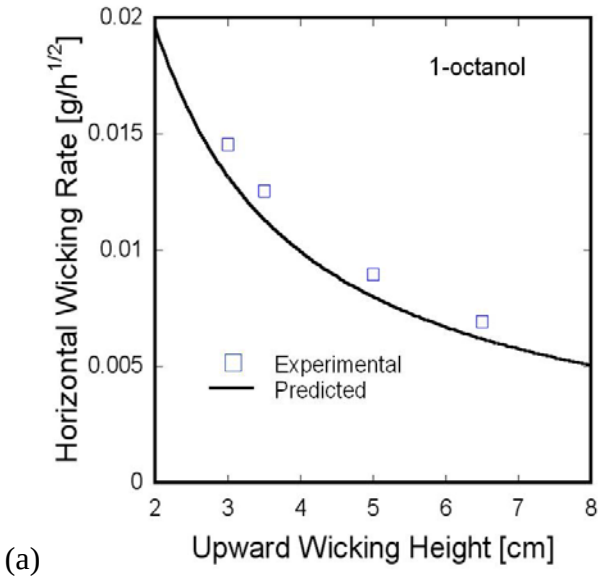

(a)

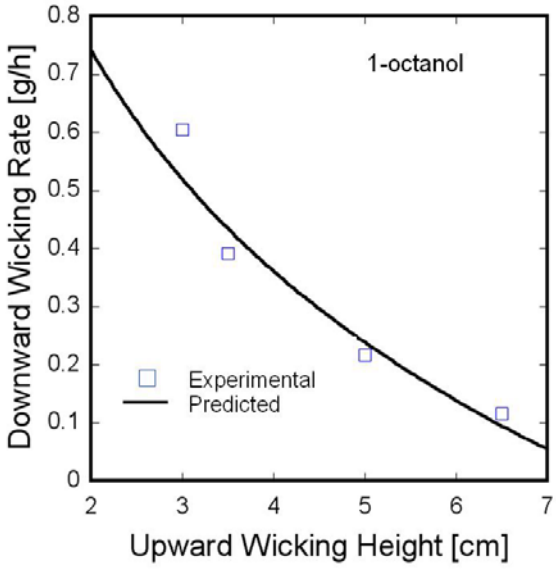

(b)

Figure 2.7 Predicted (solid line) and experimental (□) horizontal (a) and downward (b) wicking rates versus upward wicking height for 1-octanol.

As described earlier, the UHD wicking test was developed using water as the test fluid. Water was used because it is the principle fluid of concern for most textile applications (*e.g.*, performance athletic apparel). However, testing with water was challenging due to its volatility. Thus, it would be quite useful if tests could be conducted with a relatively nonvolatile fluid, like hexadecane, and the results used to predict wicking behavior for water in the same fabric. Using the same procedure as that described for octanol, the horizontal and downward wicking rates of water were predicted as functions of upward wicking height. These results are shown in Figure 2.8 along with some experimental values determined by Simile in a high-humidity environment to mitigate evaporation [49]. The agreement between experimental and predicted wicking rates was made possible by using a contact angle of water on polyester of 48°. The contact angle of water on a flat polyester film was measured to be 76°, but this polyester film was not coated with the hydrophilic finish that was present on the fibers of the polyester fabric examined in this study. Thus, while the contact angle of water on the polyester fabric should be less than 76°, the actual value was not measured. The UHD test may be an interesting route to obtain contact angles of fluids on fabrics that are otherwise difficult to accurately assess.

The wicking rates for water are an order of magnitude greater than those measured for the alkanes. This is consistent with a smaller viscosity and a larger surface tension, which is almost three times greater than the surface tension of the alkanes. Surface tension is directly proportional to wicking rates (cf. equations 1, 3 and 5).

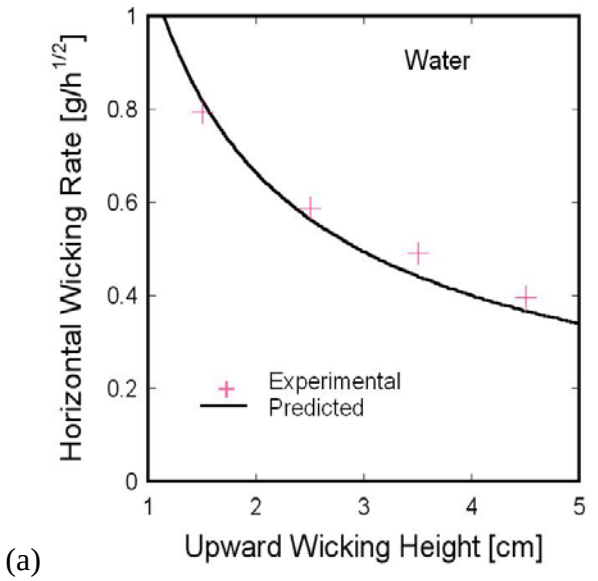

(a)

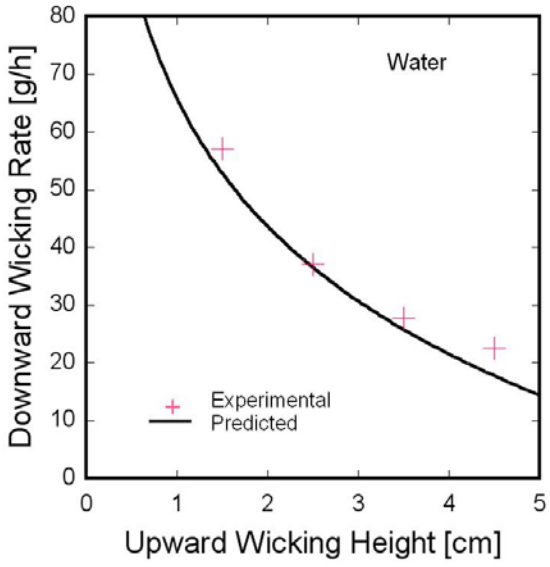

(b)

Figure 2.8 Predicted (solid line) and experimental (+) horizontal (a) and downward (b) wicking rates versus upward wicking height for water. The experimental wicking rates for water were measured at 90% relative humidity and were taken from the literature [49].

2.4 Conclusions

The integrated upward-horizontal-downward (UHD) wicking test was conducted on a polyester knit fabric with four different fluids characterized by different physical properties. Horizontal and downward wicking rates were different for the various fluids, but when analyzed to extract permeability versus saturation, the data fell onto a single master curve. Thus, the UHD test and analysis provides results that are independent of the fluid employed, validating the test as one that allows the measurement of the intrinsic properties of a fabric that govern wicking: effective capillary radius and permeability as functions of saturation. For this reason, the UHD wicking test differs from other wicking tests. The intensive properties yielded by the UHD test can be used to predict wicking rates for other Newtonian fluids. This was demonstrated by comparing calculated and experimental wicking rates for two fluids: 1-octanol and water. Such capabilities should prove quite valuable in engineering and design of wicking fabrics.

CHAPTER 3

CONTROL OF MICROFLUIDIC FLOW IN AMPHIPHILIC FABRICS[2]

3.1 Introduction

The research described in this chapter was inspired by work in microfluidics; the study of geometrically constrained fluids within micrometer-sized structures that consist of networks of interconnected channels and reservoirs [1, 11]. As described in Chapter 1, the small dimensions of microfluidic channels result in large surface-area-to-volume ratios, strong wall-fluid interactions, and rapid mass diffusion of solute particles [1]. As a consequence, manipulation of physical and chemical properties of the channels (*e.g.*, shape, connectivity, surface energy and wettability of walls) enables precise control over fluid transport. Microfluidic chips can thus be engineered to transport small volumes of fluids to precise locations on the chip, where (bio)chemical reactions can be carried out [11, 18].

The challenge with microfluidic devices is that their soft-lithography manufacturing process [1, 11], limits commercially viable use to specialized high-value applications with small volumetric throughput of liquids. Efforts towards cheaper

[2] The contents of this chapter has been published:
Owens, T. L.; Leisen, J.; Beckham, H. W.; Breedveld, V., "Control of Microfluidic Flow in Amphiphilic Fabrics", *ACS Applied Materials & Interfaces* 3(10), 3796-3803 (2011).

microfluidic devices have focused on replacement of PDMS with alternative substrate materials. Cheap, porous materials that can efficiently wick liquids via capillary action, like paper and cotton yarns, have emerged as primary candidates, because capillary flow eliminates the need for external power sources to generate flow [11],[19-21], [24-26].

Paper- and yarn-based microfluidic structures not only offer cheaper, more scalable production methods for microliter-scale microfluidic devices, but because of their economics, they also open up a pathway towards applications with much larger volumetric flow rates, while maintaining the inherent advantages of microfluidics. For example, the efficiency of an industrial-scale liquid–liquid extraction processes can be maximized when the interfacial contact area between immiscible liquid phases is large and the diffusion of solute from the bulk of each liquid to the liquid-liquid interface is rapid [27]. As stated above, the fundamental physical characteristics of microfluidic flow are very amenable to these requirements. Thus, faster, more efficient extractions with smaller reagent volumes could potentially be achieved if microfluidic devices can be produced sufficiently cheaply to be economically viable for processes with large volumetric flow rates.

The focus of this chapter is to investigate the feasibility of fabrics as large-scale microfluidic structures because existing textile manufacturing technologies offer proven economy-of-scale advantages. Fabrics are engineered porous structures that consist of interlocking woven yarns, which themselves are bundles of fibers or filaments. The voids in between these yarns create a network of microchannels. A woven fabric therefore contains two types of microscopic voids that can accommodate capillary flow: (1) the *intra*-yarn spaces between fibers or filaments within a yarn, and (2) the *inter*-yarn spaces

between the yarns in a fabric. By weaving hydrophobic and hydrophilic yarns together in a single fabric, we can thus create a network of microchannels with heterogeneous surface properties, which should allow for simultaneous flow of immiscible liquid phases with a large interfacial contact area. The textile manufacturing industry has developed scalable technologies to produce patterned fabrics that combine yarns of different types in repetitive geometrical structures with various degrees of complexity, ranging from simple plain weave structures to more complex architectures for specialty applications [56-59] and it is well-known that variations in fabric construction parameters and material properties significantly affect fluid movement in fabrics [60].

The main objectives of this chapter are to prove that: (1) careful design of woven amphiphilic fabrics yields a similar level of control over fluid motion as observed in microfluidic devices, and (2) co-flow of immiscible liquid phases can be achieved with a large interfacial contact area, which makes the fabrics suitable as microcontactor substrates for liquid-liquid extraction processes, both on the laboratory scale and, because of scalable manufacturing technology, on industrially relevant scales [61].

3.2 Experimental

3.2.1 Fabric Design

Capillary liquid flow in a porous medium is governed by the size, orientation and surface chemistry of the pores [3, 7]. The wicking flow rate of liquid into a fabric is controlled predominantly by yarn placement, the spacing between yarns, and their surface chemistries. A distinguishing feature of this study is that we systematically investigated

the effect of the placement of hydrophilic and hydrophobic yarns in amphiphilic fabrics to determine: (1) how effectively yarn placement can be used to control the flow path and flow rate of liquids into fabrics, and (2) if parallel flow of immiscible liquid phases can be achieved within an amphiphilic fabric. To systematically and unambiguously address these research questions, we limited the fabric architecture in our investigation to a plain weave, in which two sets of yarns ("weft" and "warp") intersect at right angles and in which each yarn alternately crosses over and under subsequent intersecting yarns. Furthermore, as will be described in detail below, we used two types of yarns with similar physical properties (diameter and fiber density), but different surface chemistries. Figure 3.1 depicts the weave patterns of five fabrics used in this study, with hydrophobic yarns shown in red (dark) and hydrophilic yarns in blue (light). Inspired by the standardized classification of surfactants in terms of hydrophilic/lipophilic balance, we developed a fabric nomenclature that captures the yarn pattern within a repeat unit in terms of the quantity and positional order of the two yarn types. Hydrophilic yarns are designated "H" and hydrophobic (or lipophilic) yarns "L". The fabric pattern is then specified by identifying a repeat unit for the fabric and listing the sequence of yarns within this repeat unit in both primary directions. For example, 2H-2L/4L (Figure 3.1b) describes a fabric in which pairs of like yarns (2H and 2L) alternate in one direction, while only hydrophobic yarns (4L) are present in the other, perpendicular direction.

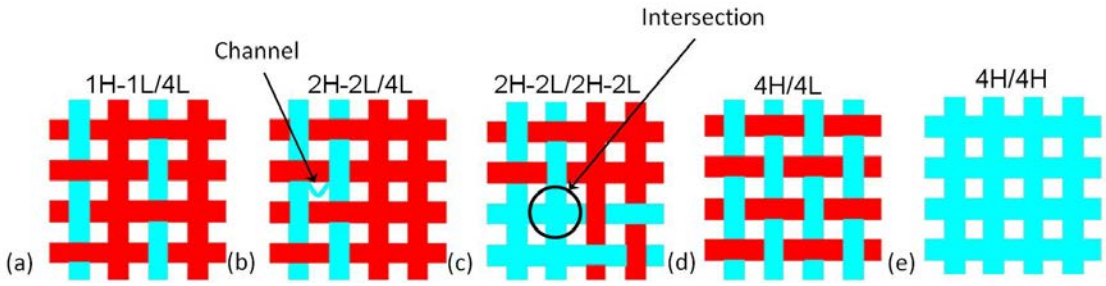

Figure 3.1 Schematics of five fabric samples examined in this study. The red (dark) yarns represent hydrophobic (or lipophilic) yarns (L), while the blue (light) yarns represent hydrophilic yarns (H): (a) 1H-1L/4L, (b) 2H-2L/4L, (c) 2H-2L/2H-2L, (d) 4H/4L (e) 4H/4H (purely hydrophilic control fabric). Highlighted are examples of a "channel" and an "intersection", key structural features of the amphiphilic fabrics with regards to fluid transport.

The fabric designs in Figure 3.1 highlight two structural features that were hypothesized *a priori* to affect fluid flow: "channels" and "intersections". A "channel" is defined as the void space between two parallel yarns. Because capillary flow relies on adhesive forces between the liquid and surrounding solid surfaces, capillary action is expected to be maximized when two yarns of the same surface chemistry are placed side by side; compare, for example, 1H-1L/4L in Figure 3.1a (no hydrophilic H-H channels) with 2H-2L/4L in Figure 3.1b (one hydrophilic H-H channel per repeat unit). Additionally, by using only one yarn type in a particular direction, the number of channels in that direction is maximized: fabric 4H/4L in Figure 3.1d possesses four vertical hydrophilic channels per repeat unit. It is important to reiterate that the term channel only refers to the *inter*-yarn void spaces, not to the *intra*-yarn voids between fibers within each yarn. As will be discussed in the Results section, capillary flow in *intra*-yarn void spaces does contribute to fluid flow. However, this first study of amphiphilic fabrics aimed to elucidate the effect of *inter*-yarn voids, which can be

engineered via the weave pattern. Hence, all fabrics in this study were designed to have constant yarn diameters and *intra*-yarn spacing.

The second key structural feature of amphiphilic fabrics with regards to liquid flow are the so-called “intersections”, perpendicular crossings of yarns (see *e.g.*, 2H-2L/2H-2L in Figure 3.1c. Intersections of like yarns enable fluid transfer between orthogonal yarns and this connectivity creates alternative pathways for fluid flow between locations.

With the above definition of channels and intersections in mind, five different fabric samples were constructed, each with varying numbers of hydrophilic channels and intersections. For example, fabric 1L-1H/4L (Figure 3.1a) has no intersections and no channels between hydrophilic (H) yarns. Fabric 2H-2L/4L (Figure 3.1b), on the other hand, has one hydrophilic channel per repeat unit, but no intersections between hydrophilic yarns; sample 2H-2L/2H-2L (Figure 3.1c) has two hydrophilic channels and four intersections between hydrophilic yarns per repeat unit; sample 4H/4L (Figure 3.1d) has four hydrophilic channels per repeat unit, but no intersections. Finally, sample 4H/4H is the control fabric consisting of all hydrophilic yarns. By comparing fluid flow paths and rates in these five fabrics, we can systematically study contributions of these structural features of the fabrics to microscopic fluid flow.

Because of the potential applications of amphiphilic fabrics as lab-scale microfluidic devices for small liquid volumes and as industrial scale continuously operated liquid-liquid microcontactors, the dynamics of liquid flow in these fabrics were evaluated for both scenarios. The water wicking rates and flow paths for the five fabric samples depicted in Figure 3.1 were analyzed via two methods: drop tests and upward

wicking tests. In the drop tests, a single drop of liquid is placed on the fabric; liquid absorption and flow into the fabric then occurs from this finite liquid reservoir, analogous to microfluidic chips for medical diagnostic screenings. In this set-up, flow channels within the fabric compete for the finite volume of available liquid and the microscopic flow is thus expected to be time-dependent. In upward wicking tests, on the other hand, one end of a fabric strip is immersed in a large liquid reservoir, so that a continuous supply of liquid is available; this scenario more closely resembles continuous liquid-liquid extraction set-ups. Studying the flow dynamics for finite and infinite reservoirs will provide insight into behavior that is relevant for both applications.

The final experiment described in this paper is a two-phase horizontal wicking test with two immiscible fluids. This experiment was critical in order to determine if the insights from tests with a single fluid can be related to simultaneous flow of immiscible liquids, which is required for achieving liquid-liquid extractions in amphiphilic fabrics.

3.2.2 Materials

Commercially available fibers were obtained and ring spun into yarns by Patrick Yarns (Kings Mountain, NC). Delcron Hydrotec® (DAK America) fibers (hydrophilic copolyester, 1.5 in length, 1.5 denier or 1.67×10^{-4} g/m) were spun to give white hydrophilic yarns (24 cotton count or 220 denier or 2.4×10^{-2} g/m) that were 230 μm in diameter with 146 fibers/cross section. Polypropylene fibers (1.4 denier or 1.56×10^{-4} g/m) from FiberVisions (Duluth, GA) were ring spun to give white hydrophobic yarns (26 cotton count or 202 denier or 2.2×10^{-2} g/m) that were 260 μm in diameter with 144 fibers/cross section. Twist levels (typically 12 to 18 turns/inch) were kept as low as

possible to maximize fluid flow yet allow sufficient cohesion for spinning and weaving. The yarns were woven at the Textile Technology Center of Gaston College (Belmont, NC) on a computer-controlled dobby rapier sample loom (SL7900, CCI Tech; New Taipei City, Taiwan) to give a plain weave fabric (20 × 72 in), with 75 yarns/in in both warp and weft directions, resulting in a cover factor of 90%. The fabric porosity ε was measured to be 0.65 and its thickness was found to be 0.04 cm. The yarns were arranged in the warp and the weft was inserted to give a large variety of systematically different patterns of hydrophilic and hydrophobic yarns. Black tag yarns were then inserted to mark borders between different weave patterns.

Water was deionized using a Millipore Direct-Q 5 ultrapure system. Anhydrous *n*-dodecane was used as purchased from Sigma Aldrich (purity > 99%). Liquid food dyes used to color the water were McCormick® (black) and Walmart Great Value® (orange), which were both purchased locally. The dye used to color the dodecane was powdered Dispersol Blue 4PA (ICI Americas; Charlotte, NC).

3.2.3 Methods

Drop Tests

In the drop tests (cf. Figure 3.2a), a small rectangular fabric sample (15 mm × 8 mm) was placed on a microscope slide and secured at each end using self-adhesive tape. A 5μL drop of water was then placed on hydrophilic yarns near the center of the fabric sample using an Eppendorf® 20 μL pipette. Dyed water (black) was used to increase the contrast between wetted and dried fabric for image analysis purposes, but control studies with non-dyed water were carried out to ensure that the dye did not affect

the water wicking properties. Drop tests were recorded from the top to visualize fluid flow paths and from the side to quantitatively monitor drop volume evolution. Video microscopy was performed using Lumenera (Ottawa, Ontario) LU135M monochrome and LU135C color cameras (for side and overhead views, resp.) in combination with a Leica Z6 APO zoom lens (Leica Microsystems; Buffalo Grove, IL), and Lucam Recorder image acquisition software (Astrofactum; Munich, Germany). The recorded images were analyzed with IDL (Interactive Data Language) image analysis software (ITT Visual Information Solutions; Boulder, CO), to determine the size of the diminishing water drop as a function of time. The volume of the liquid drop was calculated from the length of its base and its height, assuming that the drop had a spherical shape at all times; this assumption is reasonable due to the high surface tension of water and the small drop volumes in all tests.

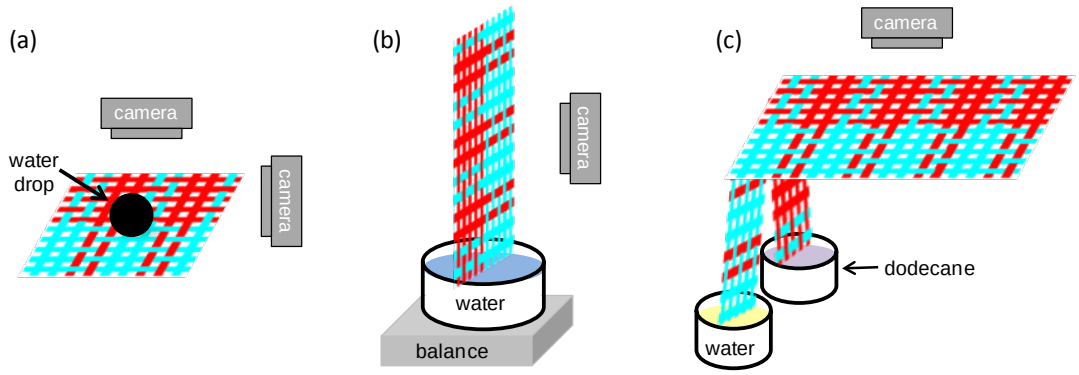

Figure 3.2 Experimental set-ups for monitoring fluid transport into fabrics: (a) drop test in which an overhead camera was used to capture flow path and a side-view camera was used to capture drop volume as a function of time, (b) upward wicking test from a reservoir in which a balance and camera were used, and (c) horizontal wicking test in which the end of a fabric strip was cut at the border between groups of parallel adjacent hydrophilic and hydrophobic yarns so that feeder strips could supply water and dodecane from two separate reservoirs.

Upward Wicking Tests

For upward wicking tests (cf. Figure 3.2b), 20 mm x 40 mm strips of fabric were used. The samples were hung vertically from a holding bridge constructed from FisherTechnik blocks (Studica, Inc; Sanborn, NY). In front of this holding bridge was a camera to record the vertical progression of the wetting front of water as it was being absorbed into the fabric sample. A water reservoir (with black dyed water) was placed on top of a balance so that the mass of liquid absorbed into the fabric could be recorded; both the water reservoir and the balance were placed on top of a lab jack, which was raised until the fabric was submerged to a ~1 cm depth at the start of each experiment. To minimize effects of air flow on balance measurements and to minimize variations in temperature and humidity, the experiments were conducted under a transparent Plexiglass cover. Analogous to the drop tests, a camera (Sony XC-ES50 with a Navitar 7000 Zoom Lens) was used to record the vertical progression of the wetting front into the fabric. The mass of liquid absorbed into the fabric was recorded via Labtronics Balance Talk XL data acquisition software (Labtronics Inc; Guelph, Ontario) on a computer connected to the analytical balance (Sartorius Acculab VIC, Data Weighing Systems, Inc; Elk Grove IL) via an RS232 serial port. Wicking data from the first 30 seconds of the test (ca. 1 cm of upward wicking distance) were fit with a straight line to determine the initial upward wicking rate. At times greater than 30 seconds, the slowing effects of gravity became apparent in the data.

Horizontal Two-phase Wicking Test

Horizontal two-phase wicking tests (cf. Figure 3.2c) were conducted on a 50 mm × 10 mm fabric sample of construction 5H-5L/2H-2L (also see Figure 3.6a). One end of the sample was placed on a microscope slide and secured to the slide using self-adhesive tape, creating a horizontal test section of ca. 15 mm. The rest of the fabric (~35 mm) was draped over the edge of the slide and cut lengthwise along the border between hydrophilic and hydrophobic yarns to create feeder strips that could be immersed into separate reservoirs for water and dodecane. Liquid flow was initiated by filling the reservoirs with the appropriate liquids. To distinguish between the two naturally clear liquids, water was dyed orange and dodecane was dyed purple. Overhead images of the wicking process were again recorded using a Lumenera LU135C color camera with Leica Z6 APO zoom lens to resolve the two liquid streams.

3.3 Results and Discussion

3.3.1 Drop Tests

Overhead drop tests revealed that flow paths and flow rates of water wicking into the amphiphilic fabrics can be controlled by the arrangement of hydrophilic and hydrophobic yarns. Figure 3.3 presents a comprehensive overview of the results of the drop tests for all five fabric samples: the top row of images (Figure 3.3a) is a schematic representation of the construction of each fabric, which is confirmed by the second row of UV-illuminated images (Figure 3.3b), in which the hydrophilic yarns appear bright because the polyester of which they are composed exhibits fluorescence; rows 3 − 6 (Figure 3.3c) present overhead views of the progression of fluid flow into the fabrics;

finally, the bottom row is a side-view snapshot of the water drops 50 seconds after being placed on the fabrics. In addition, the results from the quantitative drop volume analysis are shown in Figure 3.4.

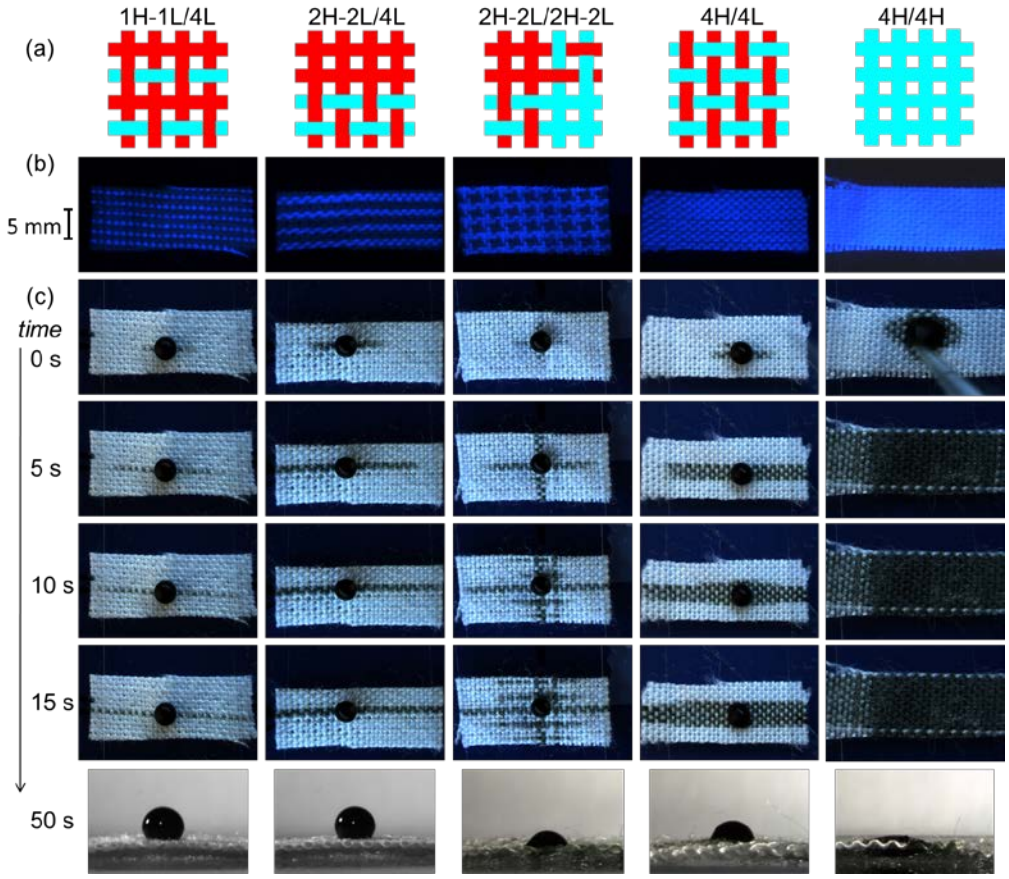

Figure 3.3 Single drops of water absorb into fabrics at rates and along paths governed by the arrangement and density of hydrophilic yarns: (a) fabric schematics, (b) UV-illuminated images in which hydrophilic polyester yarns are bright, and (c) time-resolved images of drop absorption. Each column represents a single fabric sample. Bottom row shows side view images of the water drop after 50 seconds.

As expected, the control fabric, 4H/4H, which contains no hydrophobic yarns that hinder the movement of water, exhibits very fast water flow in all directions and in all

yarns. The drop absorption rate of 4H/4H is two orders of magnitude larger than any other fabric sample in this study, as indicated by the absence of a drop in Figure 3.3c after 50 seconds and the data in Figure 3.4. This control fabric represents the mechanism of liquid absorption into fabrics that one encounters in everyday life in most ordinary fabrics. However, when comparing water flow in 4H/4H with the other fabric samples, it becomes clear immediately that addition of hydrophobic yarns and variations in fabric design (*i.e.*, placement of yarns) significantly alters the liquid flow rate and the flow path.

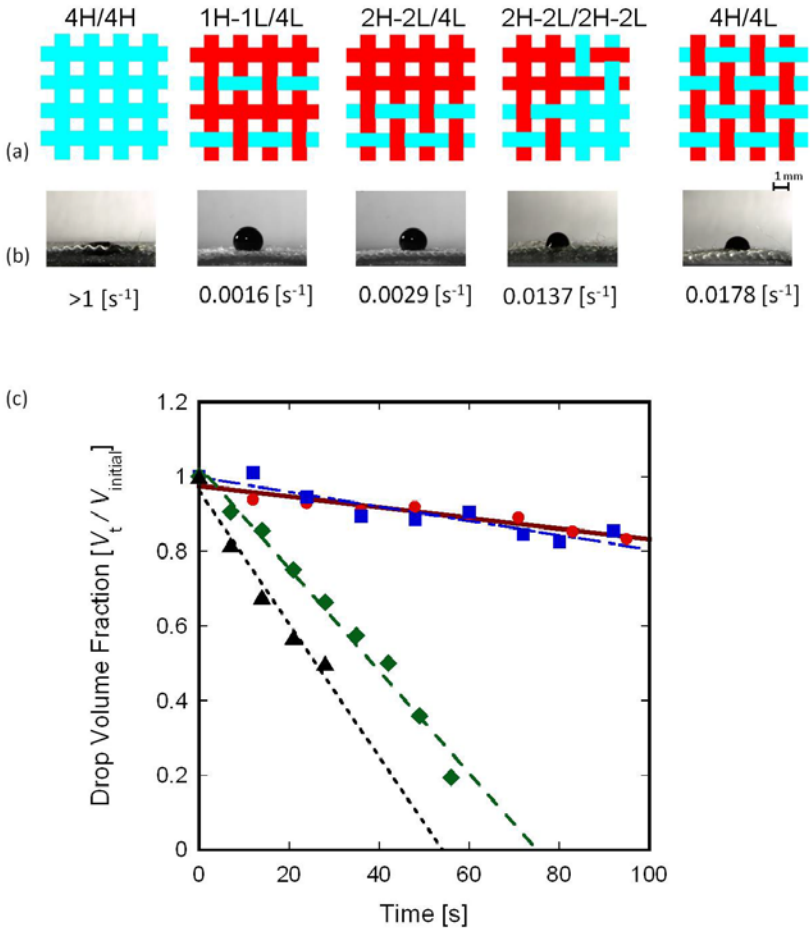

Figure 3.4 Quantitative analysis of water drop volume reduction versus time: (a) fabric schematics, (b) side view images of water drops 35 seconds after placement on fabrics; numbers below images are rates of drop volume reduction determined from (c) drop volume, normalized to initial volume, versus time for ●:1H-1L/4L, ■: 2H-2L/4L, ♦: 2H-2L/2H-2L, and ▲: 4H/4L; lines are linear least-squares fits and slopes are rates of drop volume reduction listed in (b). For the fully hydrophilic 4H/4H fabric, the drop was completely absorbed within 1 s.

In sample 1H-1L/4L, water flows anisotropically, only along the hydrophilic yarn on which the drop was initially placed. Similar behavior is observed for sample 2H-2L/4L, albeit with a wider fluid channel formed by the adjacent hydrophilic yarns. In both cases, water only flows anisotropically because there are no hydrophilic

intersections that facilitate liquid transfer in the perpendicular direction. Another important observation when comparing these two samples is the difference in the water absorption rates between 2H-2L/4L and 1H-1L/4L. The placement of the hydrophilic yarns in 2H-2L/4L creates a hydrophilic channel, which enables water flow between the hydrophilic yarns as well as within the yarns. As a result, more water can absorb in sample 2H-2L/4L than in 1H-1L/4L, as indicated by the darker color of the wetted strip in the images, at a higher rate. Figure 3.4 shows that the rate of water drop volume reduction is ~80% greater in sample 2H-2L/4L than in 1H-1L/4L.

Looking at the data for 2H-2L/2H-2L in Figure 3.3, we see again that water initially flows only along the hydrophilic yarns on which the drop was placed. However, once the water encounters intersections with perpendicularly oriented hydrophilic yarns, it can reach yarns that were not wetted by the initial drop placement by following the network of intersecting yarns; this flow pattern was not observed in samples 1H-1L/4L and 2H-2L/4L. Eventually, following the available fluid paths, water spreads throughout 2H-2L/2H-2L in a checkerboard fashion until the pattern of wetted channels mimics the fabric construction of the sample. Figure 3.4 shows that the presence of intersections in the fabric speeds up water absorption into the fabric; comparing the rate of absorption in 2H-2L/2H-2L with 2H-2L/4L, we notice a substantial increase by over 4 times.

Finally, analysis of the sample 4H/4L shows highly anisotropic wicking with preferential flow along the direction of the hydrophilic yarns. However, in contrast to 1H-1L/4L and 2H-2L/4L, water is able to slowly spread laterally to neighboring hydrophilic yarns that are outside the initial drop contact area, perpendicular to the H yarn orientation. The spreading occurs when the yarns are filled sufficiently with water to

allow flow across channels to neighboring yarns. It is noteworthy that the lateral spread of water is much faster in 2H-2L/2H-2L (and 4H/4H), which provide hydrophilic intersections and therefore orthogonal H yarns, while 4H-4L offers merely channels that must be filled and crossed. Figure 3.4 shows that the high channel density of 4H/4L results in a drop volume reduction rate that is ~30% larger than for 2H-2L/2H-2L, making sample 4H/4L the amphiphilic sample with the fastest drop absorption rate. Although intersections are clearly helpful for spreading the liquid across the fabric samples, the larger hydrophilic channel density and larger initial contact area between the drop and hydrophilic yarns in 4H/4L dominate the initial water absorption rate presented in Figure 3.4b and Figure 3.4c. It should be noted, however, that towards the end of the drop tests, when the finite size of the fabric samples becomes relevant, the absorption rate in 4H/4L slows down significantly as compared to sample 2H-2L/2H-2L, in which intersections offer alternative flow paths to the fluid. This is clearly shown in the bottom row of Figure 3.3c, where it is obvious that after 50 seconds the remaining drop on sample 4H/4L is larger than the drop on 2H-2L/2H-2L, despite the larger initial absorption rate. In conclusion, to increase the initial absorption rate of water, the addition of channels is more effective than the addition of intersections. Intersections, on the other hand, will facilitate spreading of the liquid throughout the entire fabric, thus increasing its absorptive capacity.

3.3.2 Upward Wicking Tests

The results from the upward wicking tests largely support the observations from the drop tests. Figure 3.5c displays the initial upward wicking rates for each fabric

sample, which were determined from a linear least squares fit to the mass versus time data recorded during the first 30 seconds of each test. Figure 3.5b shows images for each fabric sample 100 seconds after immersion into the dyed water.

Once again, the control fabric 4H/4H without hydrophobic yarns has by far the fastest upward wicking rate, over 5 times faster than any of the amphiphilic samples. Without hydrophobic yarns hindering the flow of the liquid, water can fully saturate the fabric, as indicated by the sharp wetting front in 4H/4H.

On the other end of the spectrum, in sample 1H-1L/4L, water only flows up into the hydrophilic yarns, which constitute every other vertical yarn, resulting in the slowest wicking rate. For sample 2H-2L/4L, the fraction of hydrophilic yarns in the vertical direction is the same, 50%, but the difference is that these yarns come in pairs, rather than as isolated yarns. The presence of hydrophilic channels in 2H-2L/4L has a significant effect on the wicking rate, which is 50% larger than for 1H-1L/4L, similar to drop test results presented in Figure 3.4b and Figure 3.4c.

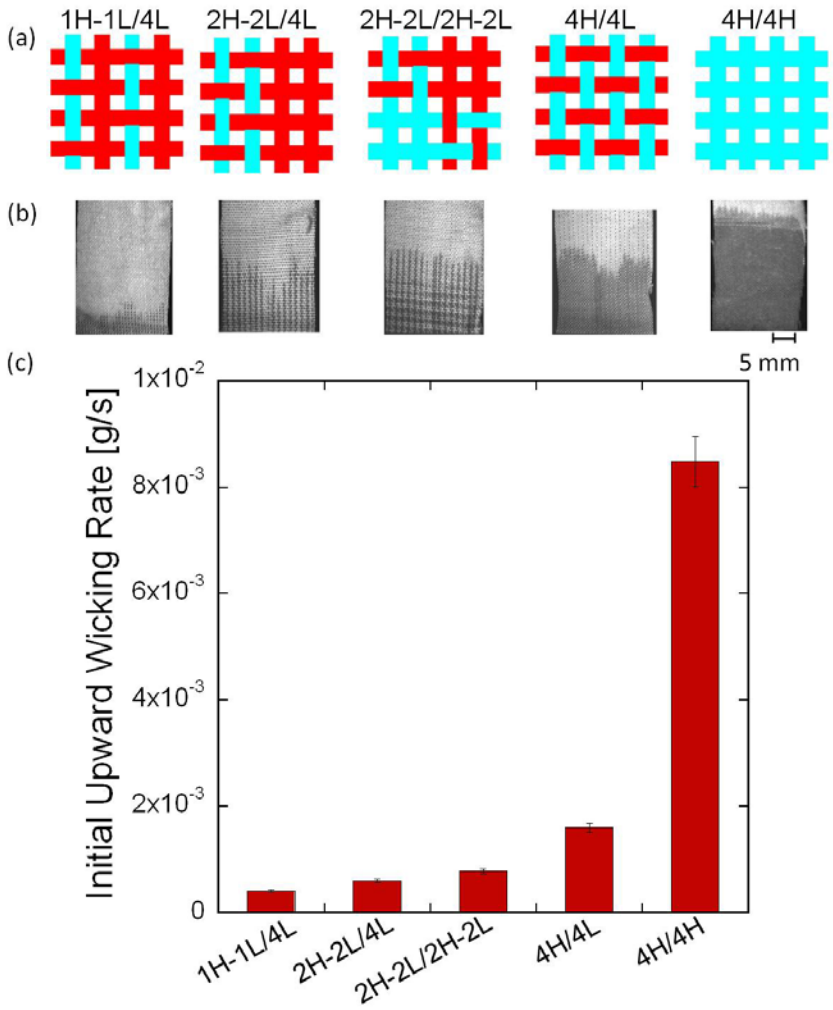

Figure 3.5 Upward wicking of water: (a) fabric schematics, (b) images showing flow patterns and wetting fronts after 100 seconds, and (c) initial upward wicking rates determined from linear least squares fit to first 30 seconds of mass versus time data.

The most complex fabric architecture, sample 2H-2L/2H-2L, exhibits interesting behavior in the upward wicking test. At the wetting front, water only flows vertically along pairs of hydrophilic yarns in that direction (cf. Figure 3.5b). However, behind the wetting front, water spreads in the transverse direction by transferring to orthogonal hydrophilic yarns at the intersections. This effect does not occur in samples 1H-1L/4L

and 2H-2L/4L since there are no orthogonal H yarns, similar to the observation in the drop test. As shown in Figure 3.5c, hydrophilic intersections in the fabric allow water to wick into the fabric at a faster rate (~30%) than for sample 2H-2L/4L.

From the bar graph in Figure 3.5c it can be seen that sample 4H/4L displays the fastest wicking rate among the amphiphilic fabrics, even 2 times faster than sample 2H-2L/2H-2L. The large number of hydrophilic channels in 4H/4L dominates the vertical wicking behavior. In these upward tests, where wicking occurs from an infinite reservoir, the need for lateral fluid spreading is not as critical as it was in drop tests on a finite fabric sample. In spite of the absence of intersections, liquid is still able to spread along the entire 4H/4L fabric length, because each hydrophilic yarn is in direct contact with the liquid reservoir. Hence, for upward wicking, the addition of channels has a larger effect on the wicking rate than the addition of intersections.

Figures 3.3-3.5 demonstrate unequivocally that weaving hydrophobic and hydrophilic yarns together into the same amphiphilic fabric allows for control over the flow path and rate of liquid absorption into the fabrics by engineering the fabric structure. The effects of changes in fabric structure on liquid flow path and flow rate were nominally the same for the drop tests and upward wicking tests, although the role of intersections is less important in the upward wicking tests. In conclusion, liquid flow can be controlled for both small drop volumes that are representative of microfluidic applications, and for wicking from reservoirs, which is more representative of large-scale industrial applications; there should not be significant differences between liquid flow dynamics upon scale up of the fabric.

3.3.3 Parallel Flow of Immiscible Phases - Horizontal Two-phase Wicking Tests

After concluding the single fluid experiments presented above, the next challenge was to test the second hypothesis behind this study, namely that amphiphilic fabrics should enable simultaneous co-flow of immiscible fluids. As described in the Methods section and illustrated in Figure 3.2c, a fabric strip was split into feeder strips that were immersed in water and dodecane, respectively. The series of images in Figure 3.6c display the wicking of water and dodecane into the horizontal section of the fabric, which had construction parameters 5H-5L/2H-2L. This fabric design was chosen because of the presence of channels and intersections for both yarn types. The larger groupings of 5 yarns in the primary flow direction (as compared to pairs in 2H-2L/2H-2L) were selected to facilitate visual observation of the liquid phases. When water (dyed orange) wets the fabric, it stains the white hydrophilic yarns yellow; as dodecane (dyed purple) wets the fabric, it stains the white hydrophobic yarns a faint purple. In the two-phase wicking test, water was allowed to start wicking before dodecane to compensate for its slower wicking rate and allow both liquids to simultaneously enter the fabric area within the camera field-of-view. As a result, the first picture in Figure 3.6c, at time zero, only shows water in the fabric, no dodecane. In the subsequent images, it can clearly be seen that water and dodecane flow in parallel, filling their respective yarns. After 65 seconds, both water and dodecane have reached the end of the viewing area.

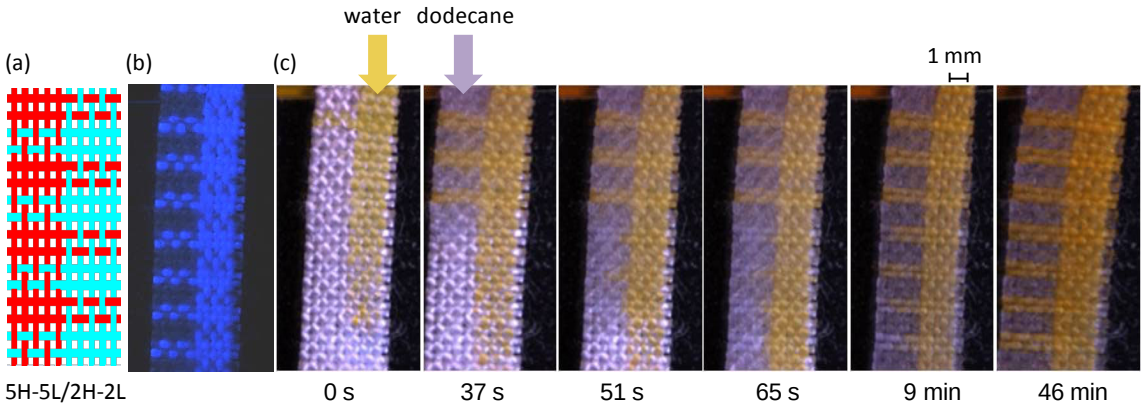

Figure 3.6 Co-flow of aqueous and hydrocarbon fluid in amphiphilic fabric 5H-5L/2H-2L: (a) fabric schematic, (b) UV-illuminated image of fabric that shows hydrophilic microchannels as bright regions, and (c) time-resolved overhead images that show water (stains yellow) wicks along the hydrophilic microchannels (pre-wicked into fabric already at t = 0) and dodecane (stains faint purple), which initially appears from the top left of image at 37 s as a darkening of the yarns, wicks along the hydrophobic microchannels. By 65 s, dodecane has wet the entire fabric not already wet by water, including perhaps some hydrophilic microchannels. By 46 min, water has filled all hydrophilic microchannels and the image exactly resembles the UV-illuminated image of the dry fabric shown in (b).

All hydrophilic yarns in the wicking direction are wetted with water. Dodecane has wetted all of the hydrophobic yarns in the wicking direction and the perpendicular direction; it even seems to have wetted the hydrophilic yarns that were not wetted by water yet, as indicated by the purple color.

Although dodecane was able to initially wet both hydrophilic and hydrophobic yarns, it does not prevent water from ultimately moving into the hydrophilic yarns, displacing the dodecane. The image after 9 minutes clearly shows that all transverse hydrophilic yarns are turning yellow and filling with water. The final image, taken after 46 minutes, shows that the co-flow of the two immiscible liquids is stable: neither liquid phase was able to displace the other. The intimate interfacial contact between phases was

maintained throughout the wicking experiment, which is very promising for liquid-liquid extraction experiments. In existing liquid-liquid extraction equipment, intense efforts (*e.g.*, agitating phases via sieve trays, mixer paddles, rotating disks) must be made to create and sustain large interfacial contact areas between immiscible liquid phases that are necessary for efficient extractions [61]. In our amphiphilic fabrics, parallel flow of immiscible phases is simply facilitated by the surface chemistry of the yarns and microscopic capillary flow. These fabrics therefore show potential for performing highly efficient liquid-liquid extractions. This would be facilitated by the highly scalable nature of this technology, and by the large and widespread existing infrastructure for its production. Modern looms allow high speed production of fabrics with constructions that range from simple (*e.g.*, plain weave) to enormously complex in terms of relative yarn arrangements and placement.

3.4 Conclusions

Wicking flow of aqueous fluids in micrometer-sized channels can be directed and controlled by precise placement of hydrophilic yarns into a woven fabric with hydrophobic yarns. The fluid is transported through voids between fibers that make up the yarns, and through microchannels between the yarns. Systematic variation in the numbers of adjacent parallel and orthogonal hydrophilic yarns allowed control of the areal density of inter-yarn microchannels that were hydrophilic, hydrophobic, and amphiphilic. Increasing density of inter-yarn hydrophilic microchannels significantly enhanced flow rates of aqueous fluids. The successful control of finite liquid volumes indicates that careful design of amphiphilic fabrics can be used to create simple

microfluidic structures for various end-use applications. Amphiphilic microchannels were created by adjacent placement of hydrophilic and hydrophobic yarns. Simultaneous co-flow of an aqueous and hydrocarbon fluid was demonstrated. This result, combined with the large interfacial contact area between immiscible fluids contained within an amphiphilic fabric, suggests these materials are potentially useful as large-area microcontactors for industrial-scale liquid-liquid extractions.

CHAPTER 4

ANALYSIS OF THE STRUCTURAL FEATURES AFFECTING MICROFLUIDIC FLOW IN AMPHIPHILIC FABRICS

4.1 Introduction

Manufacturing of technical textiles is a growing industry. Since the 1970s, textile applications have expanded from primarily aesthetic uses to applications where function is the main goal [31]. Fabrics have been manufactured with nano-coatings, fluorocarbon coatings, and surface roughness to create superhydrophobic, or self-cleaning fabric surfaces [32]. Microencapsulation of antimicrobial agents within textile fibers, yarns and fabrics has been shown to have potential for medical textiles that can prevent bacterial and fungal infections in patients [31-33]. Additionally, ground drains are commonly lined with geotextiles that act as filtration media to permit water flow, but prevent passage of soil particles [31]. Ultimately, the use of the geotextile minimizes the movement of ground surfaces, preventing subsidence.

Fundamental knowledge of the factors affecting fluid transport within a textile is necessary to specifically engineer textiles for the aforementioned niche applications. Textiles contain a distribution of capillary spaces; when liquid is brought into contact with such a capillary network, it will be transported into the void space if the forces of adhesion between the liquid and the capillary wall are greater than the forces of cohesion

between the molecules of the liquid. This capillary liquid flow, commonly known as wicking, is governed by the size, orientation and surface chemistry of the pores in the capillary network [3, 7]. Hence, the flow rate of liquid into a textile is controlled predominantly by filament placement, the spacing between filaments, and their surface chemistries. It follows that many researchers have recognized structural features as a main factor influencing the transport of fluid in textiles [62-64] .

In Chapter 3, we demonstrated that wicking flow of aqueous fluids in amphiphilic fabrics can be controlled by precise placement of hydrophilic yarns relative to hydrophobic yarns [65]. The fluid is transported through voids inside hydrophilic yarns, and through microchannels between adjacent hydrophilic yarns, while surrounding hydrophobic yarns act as barriers to aqueous flow. Additionally, simultaneous co-flow of an aqueous and a hydrocarbon fluid was demonstrated in microchannels where hydrophilic yarns were placed next to hydrophobic ones. This result, combined with the large interfacial contact area between immiscible fluids contained within an amphiphilic fabric, suggested that these materials are potentially useful for industrial-scale liquid-liquid extractions. The initial study yielded useful semi-quantitative information indicating that water wicking rates can be controlled through fabric design, in particular through the relative placement of hydrophilic and hydrophobic yarns. However, only a small number of fabric designs were tested in Chapter 3. A larger sample set is needed to elucidate the relationship between wicking rate and placement of hydrophilic and hydrophobic yarns in the fabric more clearly. Understanding the effect of yarn arrangement on wicking rate is necessary to further develop these amphiphilic fabrics for end applications like liquid-liquid extractions. Fundamental knowledge of the factors

affecting fluid transport in amphiphilic fabrics can be gained by conducting a systematic quantitative analysis of their structural features.

In this chapter, such a systematic study was conducted on 18 different woven amphiphilic fabrics. Five distinct structural features were identified by varying the number and placement of hydrophilic and hydrophobic yarns in each fabric. We refer to these features as H/L ratio, channels, intersections, yarn blockages and yarn orientation. Liquid flow rate was investigated with respect to each structural feature. Results show that each structural feature plays an important role in liquid transport, and provide guidance on how each feature can be optimized to create amphiphilic fabrics that are ideal for industrial-scale liquid-liquid extractions.

4.2 Experimental

4.2.1 Fabric Design

The fabrics investigated in this study were woven using a plain weave construction: two sets of yarns (“weft” and “warp”) were combined into finished fabrics by intersecting at right angles, in a pattern where each warp yarn passes over, then under, subsequent weft yarns. Two different yarns were used in our designs with similar physical properties (diameter and fiber density), but different surface chemistries (hydrophilic and hydrophobic) in order to investigate the effect of the amphiphilic patterns without altering other physical characteristics of the yarns. The fabric designs were integrated into a single 20” x 72” test fabric, by varying the placement and number of hydrophilic and hydrophobic yarns every 4 inches in the warp direction and every 18

inches in the weft direction of the fabric. As a result, the test fabric essentially yielded a matrix of different fabric designs, each 4” x 18” in size.

Figure 4.1 depicts the weave patterns of the 18 different fabrics used in this study, with hydrophobic yarns shown in red (dark) and hydrophilic yarns in blue (light). As described in Chapter 3, we devised a fabric nomenclature that captures the yarn pattern within a repeat unit in terms of the quantity and positional order of the two yarn types. Hydrophilic yarns are designated “H” and hydrophobic (or lipophilic) yarns “L”. The fabric pattern is then specified by identifying a repeat structure for the fabric and listing the sequence of yarns within this repeat structure in both primary directions. For example, viewing the image designated 2H-2L/4L in Figure 4.1, we see that the nomenclature describes a fabric construction in which pairs of yarns (2H and 2L) alternate in the warp direction, while only hydrophobic yarns (4L) are present in the weft direction, perpendicular to the warp. Figure 4.1 clearly shows that the fabrics differ in terms of the placement and number of hydrophilic and hydrophobic yarns. Some of the fabric designs have groupings of 5 identical yarns in the warp; these fabrics were primarily created to facilitate imaging of the fluid flow through video microscopy. It should be noted that the yarn diameter and fiber density are virtually the same for both yarn types. By keeping the yarn diameter and fiber density the same, while varying the amount and placement of the two types of yarns, flow rate studies on each fabric will allow us to (1) determine how wicking flow varies with the type and density of structural features, and (2) determine the best arrangement of hydrophobic and hydrophilic yarns to produce a fabric that is suitable for efficient liquid–liquid extractions.

The fabric groupings in Figure 4.1a through 4.1f highlight the most obvious structural feature, the relative amount of hydrophilic and hydrophobic yarns. We classified the fabrics by the ratio of the number of hydrophilic to hydrophobic yarns in the fabric (*i.e.* number of H yarns/number of L yarns). Figure 4.1a depicts the fabrics in Class 1 with the smallest H/L ratio: 0.33. Figure 4.1b shows the fabrics in Class 2, with the next largest H/L ratio: 0.71. Likewise, Figures 4.1c through 4.1e each depict the fabrics that fall into the remaining classes, 3-6; the higher the class number, the larger the H/L ratio, and the larger the amount of hydrophilic yarns per hydrophobic yarn in the fabric.

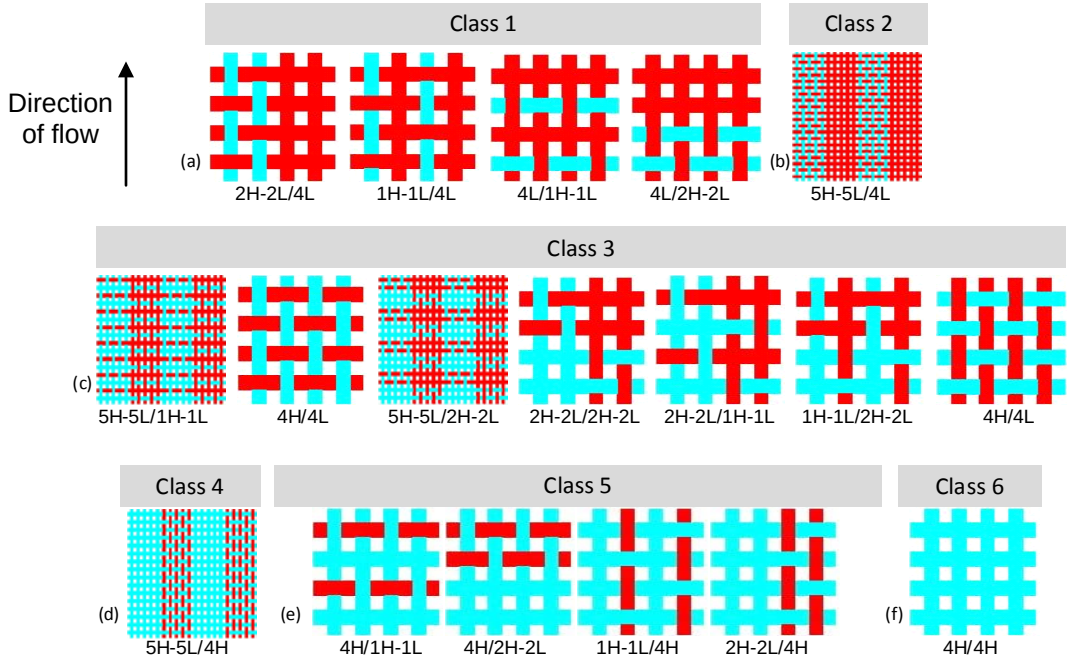

Figure 4.1 Schematic of 18 fabric samples examined in this study. The red (dark) yarns represent hydrophobic (or lipophilic) yarns (L), while the blue (light) yarns represent hydrophilic yarns (H). The fabrics are grouped according to class, which is defined by the ratio of the number of hydrophilic to hydrophobic yarns in the repeat pattern of each fabric. (a) Class 1: H/L= 0.33, (b) Class 2: H/L=0.71, (c) Class 3: H/L=1, (d) Class 4: H/L=1.4 (e) Class 5: H/L=3, (f) Class 6: H/L= ∞.

It is anticipated that increasing the number of hydrophilic yarns in an amphiphilic fabric should enhance aqueous fluid transport. However, upon the addition of extra hydrophilic yarns to the fabric, the H/L ratio is not the only structural feature that is affected. Depending on the orientation of the yarn and placement of the yarn with respect to each hydrophobic yarn, additional structural features arise: "channels" and "intersections" between hydrophilic yarns, the number of consecutive hydrophobic "blockage" yarns placed perpendicular to the primary direction of flow, and differences in yarn orientation.

A "channel" is defined as the inter-yarn void space between two parallel yarns of the same type (either H-H or L-L). Because capillary flow relies on adhesive forces between the liquid and surrounding solid surfaces, it is expected to be maximized when two yarns of the same surface chemistry are placed side by side; compare, for example, 1H-1L/4L in Figure 4.2 (no hydrophilic H-H channels) with 2H-2L/4L (one hydrophilic H-H channel per repeat unit). Water traveling in 2H-2L/4L can occupy an inter-yarn space that is surrounded by hydrophilic solid surfaces, whereas fluid in 1H-1L/4L can only flow through amphiphilic inter-yarn spaces that are surrounded by both H and L yarns. By using only one yarn type in a particular direction, the number of channels in that direction is maximized: fabric 4H/4L in Figure 4.2c possesses four hydrophilic channels per repeat unit. It is important to note that the term channel only refers to the inter-yarn void spaces, not to the intra-yarn voids between fibers within each yarn. Capillary flow in intra-yarn void spaces does contribute to fluid flow. However, this study of amphiphilic fabrics aimed to elucidate the effect of inter-yarn voids, which can

be engineered via the weave pattern. Hence, all fabrics in this study were designed to have constant yarn diameters and constant intra-yarn spacing.

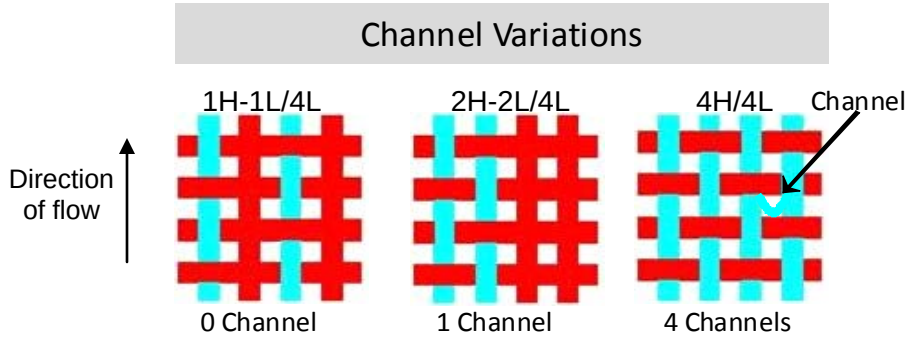

Figure 4.2 Schematic of fabrics used to investigate the effect of "channels" on liquid flow. Highlighted is an example of a channel, and the number of channels in each fabric: 1H-1L/4L (0 channel); 2H-2L/4L (1 channel); 4H/4L (4 channels).

The third key structural feature of amphiphilic fabrics are "intersections"; perpendicular crossings of yarns (see *e.g.*, 2H-2L/1H-1L in Figure 4.3a). Intersections of like yarns enable fluid transfer between orthogonal yarns and this connectivity creates alternative pathways for fluid flow between locations. Compare, for example, 2H-2L/4L in Figure 4.3a (no intersections) with 2H-2L/1H-1L (4 intersections). Additional perpendicular hydrophilic yarns increase the number of intersections: see for example, fabric 2H-2L/4H in Figure 4.3a (8 intersections). Lastly, if there is more than one channel in the repeat structure of the fabric (see *e.g.* 4H/4L, 4H/1H-1L and 4H/4H in Figure 4.3b) the number of intersections is doubled upon the addition of perpendicular crossing of hydrophilic yarns. Compare 2H-2L/1H-1L in Figure 4.3a (4 intersections) with 4H/1H-1L in Figure 4.3b (8 intersections).

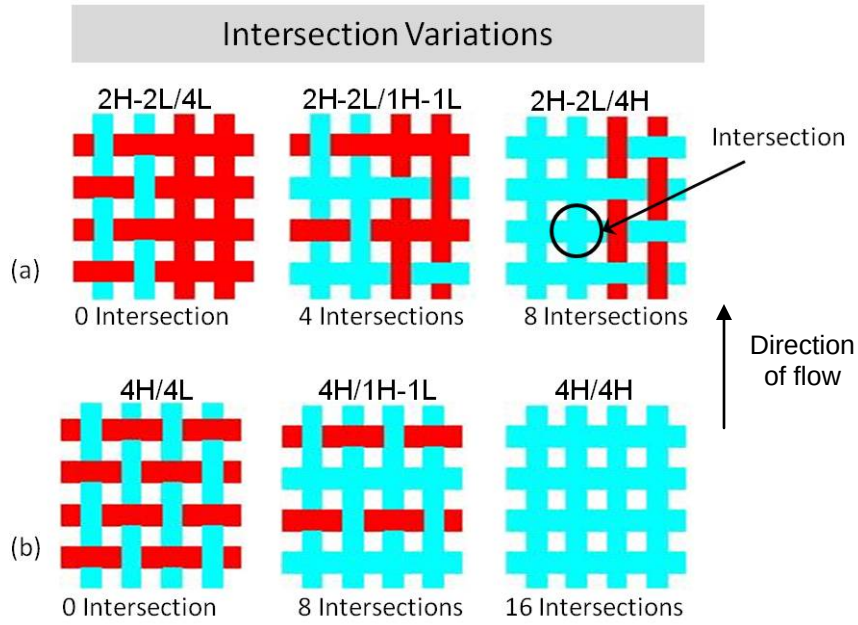

Figure 4.3 Schematic of fabrics used to investigate the effect of "intersections" on liquid flow. Highlighted is an example of an intersection. (a) Fabrics with 1 channel: 2H-2L/4L (0 intersections); 2H-2L/1H-1L (4 intersections); 2H-2L/4H (8 intersections). (b) Fabrics with 4 channels: 4H/4L (0 intersections); 4H/1H-1L (8 intersections); 4H/4H (16 intersections).

Another structural feature of amphiphilic fabrics is the number of consecutive "blockage" yarns. A "blockage" yarn is a yarn placed perpendicular to the direction of liquid flow that has a surface chemistry opposite that of the wetting fluid. Blockages are essentially the opposite of intersections in that they inhibit fluid transfer between orthogonal yarns and thus limit the pathways of fluid flow. Figure 4.4 illustrates blockages in several different fabrics; it displays three different fabric sets.

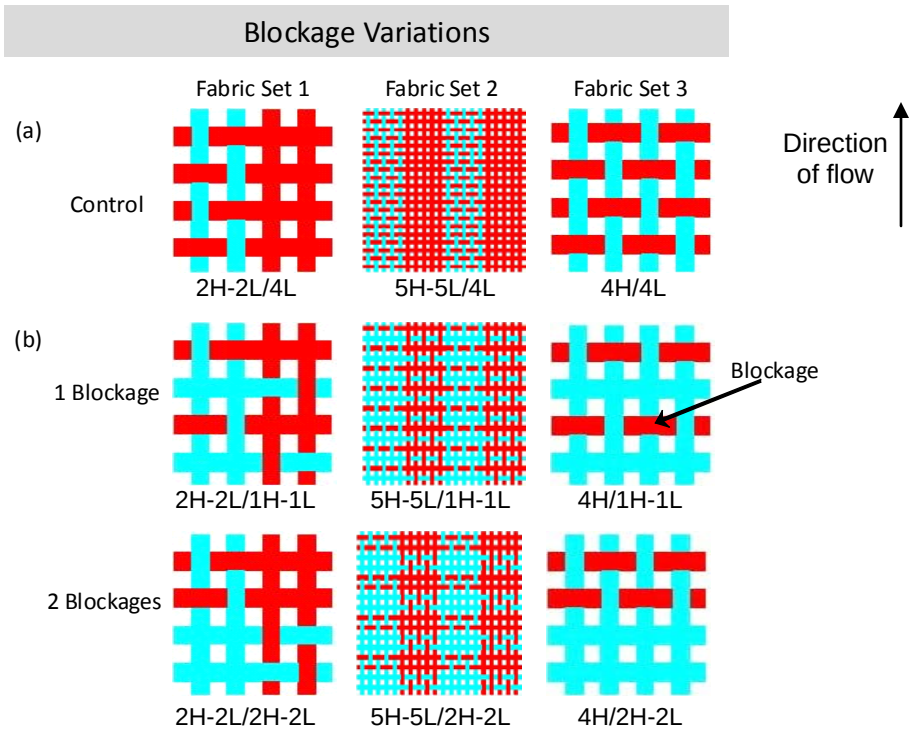

Figure 4.4 Schematic of fabrics used to investigate the effect of blockage yarns on liquid flow. Fabrics were evaluated in sets of 3. (a) Displays the control fabrics for each fabric set. Control fabrics were used to provide a base wicking rate, as they have a similar structure; they were not used to quantify the effect of blockages because they have fewer hydrophilic yarns and thus a different H/L ratio. (b) Shows the fabrics in each data set with 1 blockage (2H-2L/1H-1L, 5H-5L/1H-1L, 4H/2H-2L) and 2 blockages (2H-2L/2H-2L, 5H-5L/2H-2L, 4H/2H-2L). Also highlighted in (b) is an example of a "blockage" yarn.

Each fabric set is composed of 2 different fabrics, both with the same basic structure (*i.e.* same H/L ratio, same number of channels and intersections), and 1 control fabric. As shown in the figure, for aqueous upward flow, blockages can be quantified by counting the number of consecutive hydrophobic yarns in each fabric perpendicular to the direction of flow. This is readily illustrated by comparing fabric 2H-2L/1H-1L in Figure 4.4b (1 blockage yarn) with fabric 2H-2L/2H-2L (2 blockage yarns). The same

comparison can be made on fabrics with 4 channels (see e.g., 4H/1H-1L and 4H/2H-2L in Figure 4.4b). It is important to note the difference between the control fabrics (Figure 4.4a) and the other 2 fabrics in each fabric set. In fabric set 1, the control fabric has 1 channel and 4 blockages. The rest of the fabrics in fabric set 1 also have 1 channel, but 1-2 blockages. In comparing the fabric pattern of the control fabric with the other 2 fabrics, we see that 2 horizontal hydrophilic yarns have been removed from the fabric structure, which also reduces the number of intersections. To ensure that only the effect of blockages is considered in the analysis, and not variations in intersections or H/L ratio, the quantitative discussion about blockages will only focus on the two fabrics in each data set with the same basic structure.

The last structural feature under investigation is the hydrophilic yarn orientation. For fabrics investigated in this study, the primary direction of water flow is the warp direction of the fabric. In Figure 4.5a, however, the hydrophilic yarns in fabrics 4L/1H-1L, 4L/2H-2L, and 4L/4H are oriented purely in the weft direction.

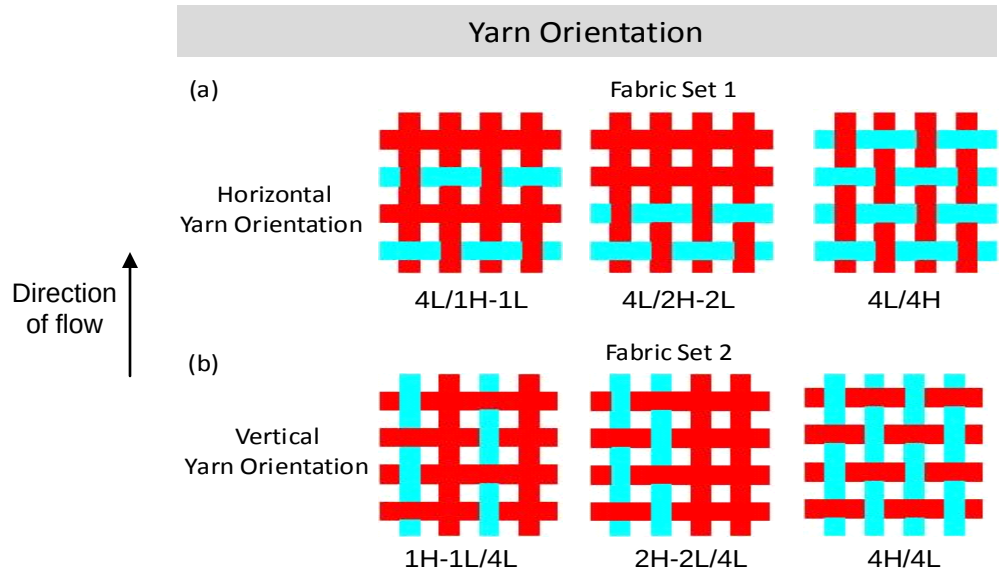

Figure 4.5 Schematic of fabrics used to investigate the effect of yarn orientation on liquid flow; (a) displays fabrics with purely horizontal yarn orientation (4L/1H-1L, 4L/2H-2L, 4L/4H) and (b) displays fabrics with purely vertical yarn orientation (1H-1L/4L, 2H-2L/4L, 4H/4L).

In Figure 4.5b we see that fabrics 1H-1L/4L, 2H-2L/4L, and 4H/4L, have the same number and placement of hydrophilic and hydrophobic yarns as the fabrics in 4.5a, except that the hydrophilic yarns are now oriented purely in the flow (warp) direction. By comparing the wicking rates of fabric sets 1 and 2 in Figure 4.5, the effect of yarn orientation on wicking rate can be explored.

4.2.2 Materials

Commercially available fibers were obtained and ring spun into yarns by Patrick Yarns (Kings Mountain, NC). Delcron Hydrotec® (DAK America) fibers (hydrophilic copolyester, 1.5 in length, 1.5 denier or 1.67×10^{-4} g/m) were spun to give white hydrophilic yarns (24 cotton count or 220 denier or 2.4×10^{-2} g/m) that were 230 μm in

diameter with 146 fibers/cross section. Polypropylene fibers (1.4 denier or 1.56×10^{-4} g/m) from FiberVisions (Duluth, GA) were ring spun to give white hydrophobic yarns (26 cotton count or 202 denier or 2.2×10^{-2} g/m) that were 260 μm in diameter with 144 fibers/cross section. Twist levels (typically 12 to 18 turns/inch) were kept as low as possible to maximize fluid flow yet allow sufficient cohesion for spinning and weaving. The yarns were woven at the Textile Technology Center of Gaston College (Belmont, NC) on a computer-controlled dobby rapier sample loom (SL7900, CCI Tech; New Taipei City, Taiwan) to give a plain weave fabric (20 × 72 in), with 75 yarns/in in both warp and weft directions, resulting in a cover factor of 90%. The fabric porosity ε was measured to be 0.65 and its thickness was found to be 0.04 cm. The yarns were arranged in the warp, and the weft was inserted to give a large variety of systematically different patterns of hydrophilic and hydrophobic yarns. Black tag yarns were inserted to mark borders between different weave patterns.

Water was deionized using a Millipore Direct-Q 5 ultrapure system. Locally purchased liquid McCormick® food dye (black) was used to color the water.

4.2.3 Methods

For upward wicking tests (cf. Figure 4.6), 20 mm x 40 mm strips of fabric were used. The samples were hung vertically from a holding bridge constructed from FisherTechnik blocks (Studica, Inc; Sanborn, NY). A camera was positioned in front of this holding bridge to record the vertical progression of the wetting front as water was being absorbed into the fabric sample. A water reservoir (with black dyed water) was placed on top of a balance so that the mass of liquid absorbed into the fabric could be

recorded as a function of time; both the water reservoir and the balance were placed on top of a lab jack, which was raised until the fabric was submerged to a ~1 cm depth at the start of each experiment. To minimize effects of air flow on balance measurements and to minimize variations in temperature and humidity, the experiments were conducted under a transparent Plexiglass cover. A camera (Sony XC-ES50 with a Navitar 7000 Zoom Lens) was used to record the vertical progression of the wetting front into the fabric. The mass of liquid absorbed into the fabric was recorded via Labtronics Balance Talk XL data acquisition software (Labtronics Inc; Guelph, Ontario) on a computer connected to the analytical balance (Sartorius Acculab VIC, Data Weighing Systems, Inc; Elk Grove IL) via an RS232 serial port. Wicking data from the first 30 seconds of the test (ca. 1 cm of upward wicking distance) were fit to a straight line to determine the initial upward wicking rate. At times greater than 30 seconds, the slowing effects of gravity became apparent and wicking rates started to vary.

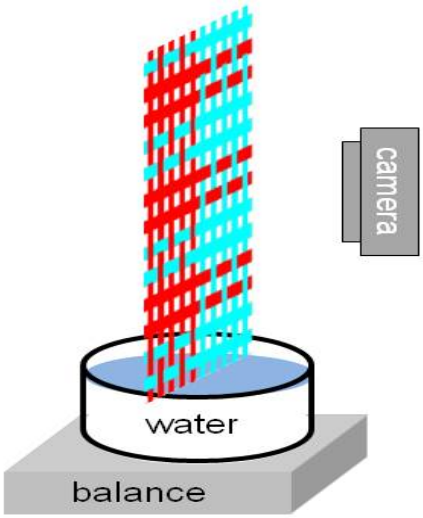

Figure 4.6 Upward wicking experimental set-up for monitoring fluid transport into fabrics. Upward wicking tests were done from a reservoir; a balance and camera were used to record each test.

4.3 Results and Discussion

An investigation of the first structural feature, H/L ratio, revealed that upward wicking rate shows a weak correlation with the fraction of hydrophilic yarns. Figure 4.7 displays the upward wicking rates of all 18 fabric samples tested ranked from 1-18, in order of increasing wicking rate. Shown above and below the bar graph are the fabric schematics. The number next to each schematic represents the fabric rank, the color of each number designates the class of the fabric sample, *i.e.* H/L ratio. Additionally, the inserted graph displays the average upward wicking rate of all fabrics in each class versus H/L ratio. From the information shown in Figure 4.7 we can conclude that a correlation exists between wicking rate and H/L ratio, but that the predictive power is weak. The error bars in the inset represent the standard deviation of wicking rate within each fabric class, which is quite significant (standard deviation ~70%), indicating that not all data

points within each class adhere to the trend. The same can be seen in the bar graph, where the rank order of the fabrics is certainly not strictly by class; some fabrics in a lower class wick faster than those from a higher class. This crude analysis indicates that, not surprisingly, the fraction of hydrophilic yarns does affect the wicking of a fabric, but that the H/L ratio is not the only factor determining the wicking rate of an amphiphilic fabric. To gain a more detailed understanding fluid flow in amphiphilic fabrics, we have to investigate how wicking rate is affected by the placement of the hydrophilic yarns in the fabric via more narrowly defined features, such as channels, intersections, yarn blockages, and yarn orientation.

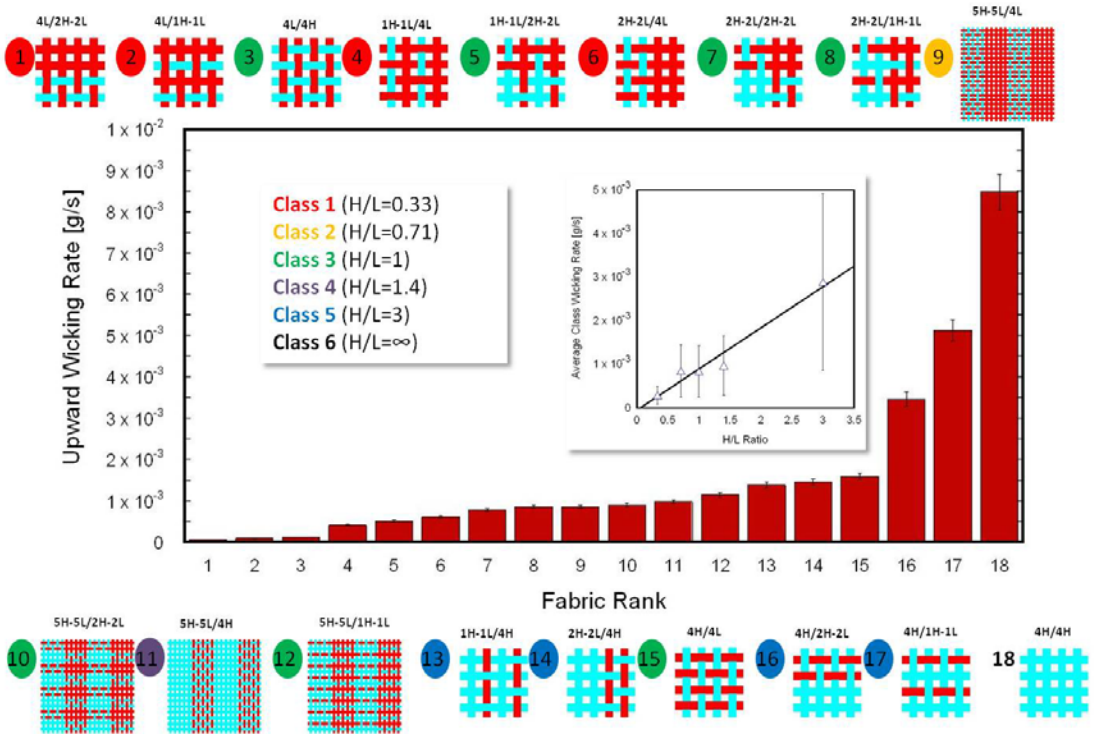

Figure 4.7 Analysis of fabric class (*i.e.* H/L ratio); upward wicking rates of all 18 fabric samples, ranked in order of increasing wicking rate. Shown above and below the bar graph are the schematics of all fabrics tested; the number to the left of each schematic is the fabric rank, the color of each number designates the class of the fabric sample. The inserted graph displays the average upward wicking rate of each class (Δ) versus H/L ratio.

Figure 4.8 illustrates the importance of channels for the wicking rate of an amphiphilic fabric. Upward wicking rate is plotted versus the number of channels and the number of hydrophilic yarns in the repeat pattern of three fabric designs shown in Figure 4.2. Each data point represents the wicking rate for one fabric. Figure 4.8 reinforces that structural features, such as, channels are important in determining wicking rate, not just the number of hydrophilic yarns in the fabric. In Figure 4.8, we see that when wicking rate is plotted versus the number of hydrophilic yarns as the structural feature of interest, the data do not exhibit any clear trend. However, the number of

channels is very good predictor with the data following a linear correlation. In the experimental design section of this paper, channels were defined as the void space between two parallel yarns of the same surface chemistry. The number of hydrophilic yarns itself does not classify the distribution of void space between two parallel yarns, while the number of channels does. As a consequence, the latter is a much more predictive quantity, as shown by the graph. This confirms the idea that a "channel" geometry is a key structural feature affecting fluid flow in amphiphilic fabrics.

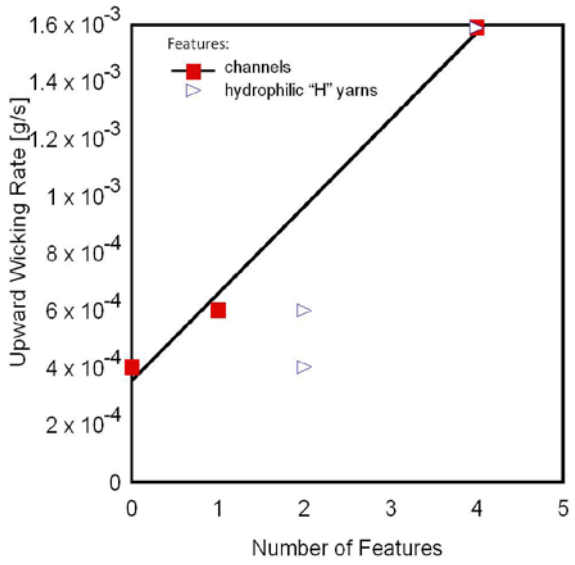

Figure 4.8 Analysis of the effect of channels; upward wicking rate is plotted versus number of features: in the repeat unit: hydrophilic channels (■) and hydrophilic yarns (►).

The third structural feature our experiments focused on was intersections. Figure 4.9 presents a plot of upward wicking rates versus the number of intersections for two

sets of fabrics, grouped according to the number of channels in the weaving patterns, which are shown in Figure 4.3. From the plot, we see the importance of intersections to fluid transport. For both groups of fabrics, both with 1 and 4 channels, wicking rates increase strongly with the number of intersections, roughly according to a linear correlation. The guide line for the fabrics with 1 channel has a smaller slope than the guide line for the fabrics with 4 channels. This result suggests that intersections have a larger effect on wicking rate in fabrics with more hydrophilic channels, which can be explained by the fact that intersections open up additional pathways for liquid transport in a fabric through lateral flow between channels. Adding an intersection to a fabric with more channels will open up more pathways for liquid to flow, thus having a more pronounced impact on wicking rate.

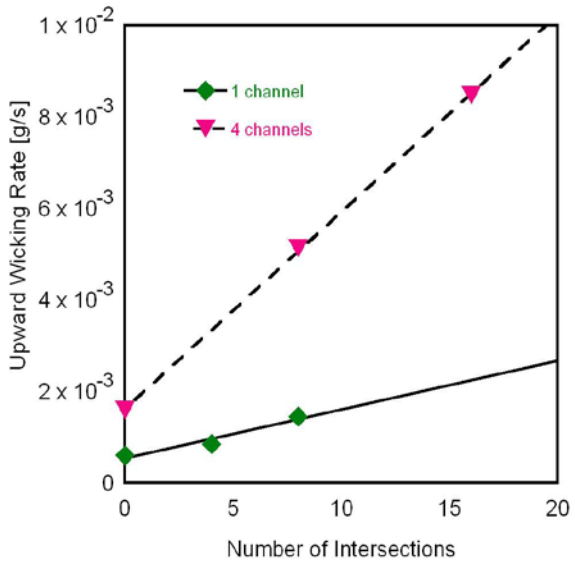

Figure 4.9 Analysis of the effect of intersections on wicking rate; upward wicking rate is plotted versus number of intersections for fabrics with 1 channel (♦) and 4 channels (▼) in the repeat unit, respectively (see Figure 4.3).

Looking at the data in Figure 4.10 we see that the fourth structural feature of amphiphilic fabrics, blockages, hinders liquid transport. Upward wicking rate is plotted as a function of the number of blockages for the three fabric sets discussed in the Experimental Design section (Figure 4.4). Each fabric set is composed of 2 different fabrics, both with the same basic structure, and a control fabric. From the plot in Figure 4.10, we can conclude that when the number of blockages is increased from 1 to 2, the upward wicking rate decreases, and this occurs for all the fabric sets studied. The wicking rate of a fabric with multiple channels decreases more due to additional blockages than a fabric with fewer channels as indicated by the slopes of the guide lines. This makes sense because yarn blockages are essentially the opposite of intersections; they inhibit fluid transfer between orthogonal yarns and thus hinder the pathways of fluid flow. This is why for blockages we see the opposite relationship to wicking rate as was observed for intersections. The trends in Figure 4.10 are only based on two data points per fabric set because there were few fabrics woven which varied only in number of blockages. To determine if we could confidently conclude that the effect of blockages follows a clear trend, we plotted the wicking rates for the control fabrics in the same graph. The figure shows that the control fabrics adhere to the same trend, even though one might expect their rates to decrease more strongly because of the loss of 2 hydrophilic yarns in addition to the extra blockages.

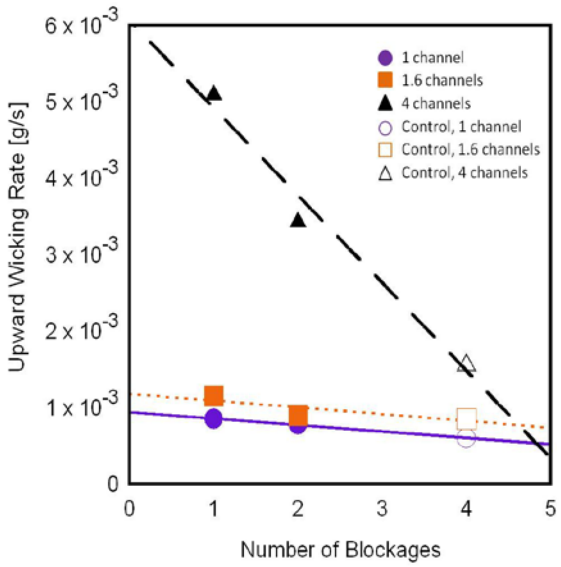

Figure 4.10 Analysis of the effect of blockages. Upward wicking rate is displayed versus number of blockages for fabrics with 1 channel (●),1.6 channels (■) and 4 channels (▲); the open symbol in each group of fabrics represents the control fabric (see Figure 4.4)

The final structural feature that we investigated, yarn orientation, probably has the most obvious effect on wicking rate. Figure 4.11 displays the effect of yarn orientation on fluid transport in amphiphilic fabrics. The figure shows images of the wetting front of fabrics 4L/1H-1L, 4L/2H-2L, and 4L/4H after 1 min of submersion into a liquid reservoir, in direct comparison with fabrics 1H-1L/4L, 2H-2L/4L, and 4H/4L. It is absolutely clear that no wetting front is established in any of the fabrics with horizontal hydrophilic yarns, while wetting is very apparent in the fabrics with vertical hydrophilic yarns. Not surprisingly, this result indicates that yarn orientation is critical for achieving upward wicking in amphiphilic fabrics; at least some wetting yarns must be oriented parallel to the direction of flow. This result is further supported by the wicking rates values plotted in Figure 4.7. We see that fabrics with hydrophilic yarns oriented in the

horizontal direction (4L/1H-1L, 4L/2H-2L, 4L/4H) have the lowest upward wicking rates, roughly an order of magnitude smaller than those for the fabrics with hydrophilic yarns in the vertical direction. The small uptake of liquid in fabrics 4L/1H-1L, 4L/2H-2L, and 4L/4H is not even due to upward wicking, but due to gradual wetting of the hydrophilic yarns that are submerged below the liquid level in the fluid reservoir.

Figures 4.8 through 4.10 all show approximately linear trends of wicking rate as a function of number of channels, intersections and yarn blockages. This would indicate that every channel, intersection or yarn blockage that is added to the fabric has the same effect on wicking rate. Channels are the void space between two yarns, so upon the addition of every channel the same additional volume for fluid flow is added to the system. Therefore, the observed linear trend can easily be explained. However, the situation for intersections and yarn blockages is far less clear cut. These features either open up or close off pathways for liquid flow. One may have predicted that the addition of the first intersections to a fabric design would have a greater effect on wicking rate than additional ones, because the first intersections open up more new pathways for liquid flow. As a consequence, it is hard to imagine that the later addition of extra intersections has the same effect on fluid flow as the first intersections. A similar discussion can be made for yarn blockages. Nevertheless, a linear trend is what we observe in Figures 4.9 and 4.10. The result is interesting and implies that every intersection and yarn blockage is important to liquid flow, a conclusion which is not necessarily intuitive when we think about the contribution of one intersection or yarn blockage to an entire fabric network. This shows how important a detailed quantitative analysis is to understanding the dynamics of liquid flow in amphiphilic fabrics.

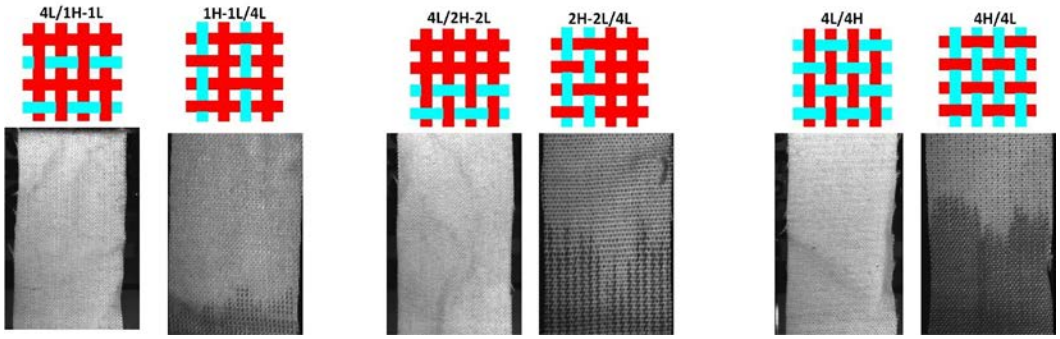

Figure 4.11 Analysis of the effect of yarn orientation. Depicts the wetting front of fabrics 4L/1H-1L, 4L/2H-2L, 4L/4H, which do not facilitate upward wicking, after 1 minute of submersion into a liquid reservoir, compared with fabrics 1H-1L/4L, 2H-2L/4L, and 4H/4L resp., which do facilitate upward wicking.

In summary, to understand the ranking of the fabrics in Figure 4.7 we must consider the effect of each structural feature: H/L ratio, channels, intersections, hydrophobic blockages, and yarn orientation. The fabrics with lowest, essentially negligible wicking rates are those with purely horizontal hydrophilic yarn orientations; next in line are the fabrics that have vertical hydrophilic yarns but no channels or intersection; then follow those with increasing numbers of channels and intersections. The fabrics with the fastest wicking rates are those that have the largest H/L ratio, vertical yarn orientations and the largest numbers of channels and intersections. Also notice that the fabrics with fewer blockages always have larger wicking rates than their corresponding structures with more blockage yarns. Every feature discussed in this study contributes to the liquid transport properties of amphiphilic fabrics. By using what has been learned from this study it is obvious which fabric patterns should be used for applications with liquid-liquid extractions: 5H-5L/1H-1L, 5H-5L/2H-2L, 5H-5L/4L and 2H-2L/2H-2L. The selected fabrics have 1:1 or close to 1:1 H/L ratios which should

yield the highest contact area between aqueous and organic phases during extractions. These fabrics also have enough channels and intersections to attain moderate flow rates through the fabric, a variable which should be considered for industrial-scale liquid-liquid extractions.

4.4 Conclusions

The arrangements of hydrophilic and hydrophobic yarns in a woven amphiphilic fabric define key structural features that significantly affect wicking flow. During wicking, fluid is transported through voids between fibers that make up the yarns of a fabric, and through voids between the yarns. For an amphiphilic fabric, these voids can be described by the structural features: H/L ratio, channels, intersections, yarn blockages and yarn orientation. Increasing H/L ratio, channels and intersections, but decreasing yarn blockages, improves the flow rate of aqueous fluids. Additionally, wetting yarns must be oriented parallel to the direction of flow to promote wicking. Optimization of all features can be used to create an amphiphilic fabric that is ideal for industrial-scale liquid-liquid extractions.

CHAPTER 5

AMPHIPHILIC FABRICS AS LIQUID-LIQUID CONTACTORS FOR SOLVENT EXTRACTIONS

5.1 Introduction

Liquid-liquid extraction is a versatile technique with a wide range of commercial applications. It is a process that facilitates the removal of a chemical species (solute) from one liquid phase (raffinate) to another (extract), based on the solute having a higher relative solubility in the extract [27, 61]. Once the raffinate and the extract phases are brought into contact, the solute will diffuse into the extract. Lab-scale extractions are often carried out in small batch extractors or separatory funnels, while large-scale industrial extractions are conducted in multistage continuous extractors. Liquid-liquid extraction is utilized in the processing of numerous chemicals, including, petrochemicals, pharmaceuticals and agricultural chemicals, and for wastewater treatment [27, 61].

Traditional techniques used for water treatment, including flocculation, precipitation and filtration, are effective in reducing organic pollutants to a level suitable for disposal into public sewerage or natural waterways, but they fail to reduce the concentration of heavy metals below regulatory limits [66]. More recently, researchers have been using liquid-liquid extraction to lower heavy metal concentrations in wastewater streams. Extractions can be carried out with organic diluents containing acid

or chelating extractants [66]. For high concentration contaminates, aromatic oxime molecules and organophosphates may be used to remove metals such as Cu(II), Au(I), Pb, or Ni, and rare earth metal species. Solvent extraction methods are improvements over traditional techniques, but they still have some disadvantages. For example, liquid-liquid extraction equipment can be expensive to implement and can require large amounts of energy to operate [67].

Liquid-liquid extraction equipment and energy costs can be reduced by carrying out extractions with amphiphilic fabrics. In the previous chapters of this thesis it was shown that amphiphilic fabrics show potential for use as large-scale microfluidic structures. We found in Chapters 3 and 4 that transport of aqueous fluids into an amphiphilic fabric can be controlled by the arrangement of hydrophilic and hydrophobic yarns. We also found that simultaneous parallel flow of two immiscible phases can be achieved in a fabric with adjacent hydrophilic and hydrophobic yarns. The characteristics of microfluidic flow include large surface area to volume ratios and rapid mass diffusion. Therefore, an amphiphilic fabric should be able to facilitate efficient liquid-liquid extraction using less energy than traditional techniques. Furthermore, large sheets of fabric can be produced relatively cheaply due to the economies of scale of the textile industry [34].

To develop amphiphilic fabrics for use in industrial-scale solvent extractions, the obvious next steps are to (1) show that liquid-liquid extractions can be conducted in an amphiphilic fabric and to (2) quantify the efficiency of these substrates as extraction media. Mass transfer of the solute from the raffinate stream into the extract phase, is the major limiting factor affecting the efficiency of a liquid-liquid extraction. Mass transfer

rates at a liquid-liquid interface are generally a function of the contact area between liquid phases, liquid velocities, and solute concentration [67, 68]. By investigating the extraction efficiency of a model system over a range of solute concentrations using amphiphilic fabrics that vary with respect to fabric design and wicking rates, we can gain a general idea of how extraction efficiency is affected by these parameters. This information will enable us to speculate about the interfacial dynamics of liquid-liquid extractions in amphiphilic fabrics even in the absence of detailed flow velocity and interfacial geometry data. Furthermore, comparison of the results for extractions in amphiphilic fabrics with more traditional methods like batch extractors, will show how the performance of amphiphilic fabrics stacks up against traditional liquid-liquid extraction techniques.

In this thesis chapter, we will first show that liquid-liquid extractions can be conducted in an amphiphilic fabric by visualizing the extraction of acetic acid from hexane into water via video microscopy in three amphiphilic fabrics with different weaving patterns. An acid-base indicator was added to the aqueous phase, so that a color change of the water in the yarns of the fabric occurred upon the extraction of acetic acid. Subsequently, to quantify the efficiency of solvent extractions in amphiphilic fabrics for water treatment applications, the extraction of copper ions from water into solutions of di-(2-ethyl-hexyl)phosphoric acid in dodecane was investigated. Again, the copper ion extraction was carried out using amphiphilic fabrics with three different weaving patterns to study the effect of fabric design; it was also carried out in a batch extractor. During each fabric extraction liquid flow rates were recorded. The efficiencies of liquid-liquid extractions in amphiphilic fabrics and a batch extractor were calculated and analyzed

with respect to superficial velocities and/or solute concentration in order to determine the feasibility of amphiphilic fabrics for industrial-scale processes.

5.2 Experimental

5.2.1 Fabric Design

Figure 5.1 depicts schematics of the four amphiphilic fabric samples that were used for the extraction studies reported in this chapter: 5H-5L/4L, 5H-5L/1H-1L, 5H-5L/2H-2L, and 2H-2L/2H-2L. Previous research reported in Chapter 4 has shown that moderate to fast water flow rates can be achieved in these amphiphilic fabrics. The fabrics also have intricately interlaced hydrophilic and hydrophobic yarns that should provide for a larger contact area between immiscible phases during two-phase wicking, than the other amphiphilic fabrics that were engineered for this thesis. The relatively large flow rates and large contact areas of the fabrics in Figure 5.1 make these fabrics good candidates for studying the efficiency of liquid-liquid extractions with respect to superficial velocity and perceived contact area. The dry specific contact area, a_d; $a_d = A/\varepsilon V_t$, where A, the total dry contact area between immiscible phases for each fabric, was calculated by summing the contact area in the amphiphilic channels and the contact area at perpendicular crossings of yarns in each fabric. The dry specific contact areas for fabrics 5H-5L/4L, 5H-5L/1L-1L and 5H-5L/2L-2L were all found to be 1.37 mm^{-1}, and for fabric 2H-2L/2L-2L the contact area was 2.94 mm^{-1}. Obviously, these contact areas are not as large as would be ideally desired for an industrial process; packed columns have surface areas ranging from ~50-1000 m^{-1} [67]. The surface area of a typical homogenous fabric ($\varepsilon \sim 75\%$, fiber diameter 20μm) is ~50,000 m^{-1} [69, 70], this surface

area is largely due to the surface area created by the surface of the fibers within each yarn of the fabric. Therefore, future generations of amphiphilic fabrics have the potential to have large specific contact areas if the yarns of the fabric are composed of bicomponent synthetic fibers that have amphiphilic properties on the length-scale of individual fibers. However, for the fundamental studies outlined in this thesis fibers with homogenous surface chemistry were used and the specific contact areas reported were sufficient.

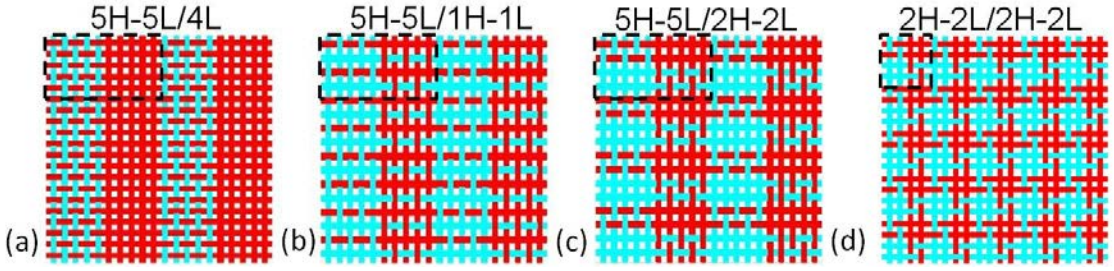

Figure 5.1 Schematics of fabrics used for solvent extraction studies; (a) 5H-5L/4L (b) 5H-5L/1H-1L (c) 5H-5L/2H-2L (d) 2H-2L/2H-2L. The repeat unit of each fabric is enclosed within the dashed lines.

5.2.2 Materials

Commercially available fibers were obtained and ring spun into yarns by Patrick Yarns (Kings Mountain, NC). Delcron Hydrotec® (DAK America) fibers (hydrophilic copolyester, 1.5 in length, 1.5 denier or 1.67×10^{-4} g/m) were spun to give white hydrophilic yarns (24 cotton count or 220 denier or 2.4×10^{-2} g/m) that were 230 μm in diameter with 146 fibers/cross section. Polypropylene fibers (1.4 denier or 1.56×10^{-4} g/m) from FiberVisions (Duluth, GA) were ring spun to give white hydrophobic yarns (26 cotton count or 202 denier or 2.2×10^{-2} g/m) that were 260 μm in diameter with 144

fibers/cross section. Twist levels (typically 12 to 18 turns/inch) were kept as low as possible to maximize fluid flow yet allow sufficient cohesion for spinning and weaving. The yarns were woven at the Textile Technology Center of Gaston College (Belmont, NC) on a computer-controlled dobby rapier sample loom (SL7900, CCI Tech; New Taipei City, Taiwan) to give a plain weave fabric (20 × 72 in), with 75 yarns/in in both warp and weft directions, resulting in a cover factor of 90%. The fabric porosity ε was measured to be 0.65 and the thickness was found to be 0.04 cm. The yarns were arranged in the warp and the weft was inserted to give a large variety of systematically different patterns of hydrophilic and hydrophobic yarns. Black tag yarns were then inserted to mark borders between different weave patterns.

Water was deionized using a Millipore Direct-Q 5 ultrapure system. Anhydrous *n*-dodecane (purity > 99%), copper(II)sulfate pentahydrate (trace metals basis; purity > 99.9%), anhydrous sodium acetate (purity >99%), anhydrous acetic acid (ACS grade; purity >99%) and anhydrous hexane (purity >95%) were used as purchased from Sigma Aldrich. Di-(2-ethyl-hexyl)phosphoric acid (D2EHPA) and thymol blue sodium salt (ACS grade) were used as purchased from VWR international.

5.2.3 Methods

Qualitative studies were conducted with fabrics 5H-5L/2H-2L, 5H-5L/4L, and 2H-2L/2H-2L to confirm if there was sufficient contact between liquid phases to promote an extraction and to identify if the location of the liquid-liquid interface could be controlled by the placement of hydrophilic and hydrophobic yarns. Quantitative studies were conducted with fabrics 5H-5L/2H-2L, 5H-5L/1H-1L, and 2H-2L/2H-2L to

determine the extraction efficiencies in amphiphilic fabrics and compare them with a traditional batch extractions.

Methods for Qualitative Extraction Studies

The extraction of acetic acid from hexane into water was evaluated via video-microscopy in fabrics 5H-5L/2H-2L, 5H-5L/4L, and 2H-2L/2H-2L. The acid-base indicator thymol blue was added to the aqueous phase. Upon extraction of acetic acid into water, thymol blue changes the color of the water from yellow-green to pink. By monitoring the color change of the water, while allowing both the aqueous and organic phases to wick into the fabric, we could determine the extent of the extraction as a function of time and location within the fabric.

Solution Preparations

The aqueous phase was prepared by dissolving several drops of 0.06 wt% thymol blue in deionized water. Thymol blue is an acid-base indicator and in aqueous solution changes from a yellow-green (pH ~7) to pink (pH~2) upon addition of an acid. The organic phase was prepared by mixing 9.6 mL of acetic acid with 6.4 mL of hexane. The acetic acid concentration in hexane was high to ensure that a large amount of acid was available for transport into the aqueous phase and thus highlight the color change of the aqueous phase in the fabric.

Experimental Procedure and Set-Up

The extraction was conducted using a horizontal two-phase wicking set-up (cf. Figure 5.2). To conduct two-phase horizontal wicking, fabric samples of construction

5H-5L/2H-2L, 5H-5L/4L, and 2H-2L/2H-2L (cf. Figure 1) were cut into 60 mm × 16 mm strips. One end of each sample was placed on a microscope slide and secured to the slide using self-adhesive tape, creating a horizontal test section of ca. 20 mm. The rest of the fabric (~40 mm) was draped over the edge of the slide and cut lengthwise to create two feeder strips that were immersed into separate reservoirs for the water/thymol blue mixture (feeder strip width ~8mm) and the acetic acid/hexane mixture (feeder strip width ~8mm). Liquid flow into the fabric was initiated by filling the reservoirs with the appropriate liquids. To determine the extent and location of the extraction in the fabrics the color change of the water upon contact with the organic phase was monitored via video microscopy. Overhead images of the horizontal test section were recorded using a Lumenera (Ottawa, Ontario) LU135C color camera with Leica Z6 APO zoom lens (Leica Microsystems; Buffalo Grove, IL) and Lucam Recorder image acquisition software (Astrofactum; Munich, Germany).

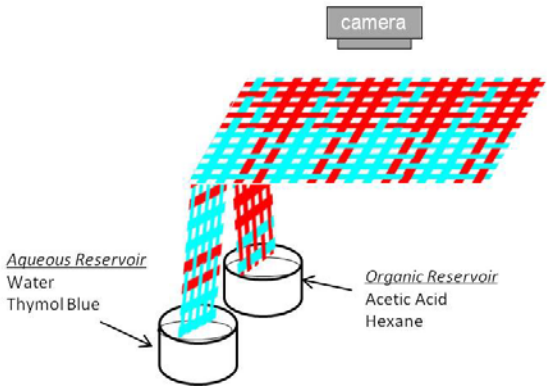

Figure 5.2 Two-phase horizontal wicking set-up.

Methods for Quantitative Extraction Studies

The extraction efficiency of the removal of copper ions from water into solutions of di-(2-ethyl-hexyl)phosphoric acid (D2EHPA) in dodecane was investigated in fabrics 5H-5L/2H-2L, 5H-5L/1H-1L, and 2H-2L/2H-2L. The extraction is essentially an ion exchange process between dissolved copper ions and hydrogen ions from D2EHPA. The experiments were carried out in the presence of an acetate buffer in the aqueous phase in order to control the pH of the solution, so that the equilibrium conditions are shifted in favor of the copper ion removal from the aqueous phase. The extraction mechanism can be summarized with the following scheme [71-73]:

$$\underset{\text{Copper Cation}}{Cu^{2+}_{aq}} + \underset{\text{Acetate Anion}}{CH_3COO^{-}_{aq}} + \underset{\text{D2EHPA Dimer}}{(H_2R_2)_{org}} \leftrightarrow \underbrace{\left(CuCH_3COO \cdot (HR_2)\right)_{org}}_{\text{Copper Complex}} + \underset{\text{Hydrogen Cation}}{H^{+}_{aq}} \quad (1)$$

where *R* represents D2EHPA.

The efficiency of a liquid-liquid extraction is mainly determined by the rate at which the solute is transferred through the liquid phases, the contact area and time between phases. Separation processes involving two liquids require consideration of mass transfer dynamics in both phases. The two-film theory for mass transfer is commonly used as the framework for analyzing mass transfer coefficients and interfacial dynamics of liquid-liquid extractions [67, 68]. This theory is based on the assumption that the resistance to mass transfer is restricted to stagnant films on either side of the interface between the two fluids (cf. Figure 5.3), while the interface itself provides no

resistance. Within this framework the mass transfer of a solute between two liquid phases (Q) can be defined in terms of bulk concentrations [68]:

$$Q = N_A \bullet a = K_L a\left(C_{A_b}^{(1)} - C_{A_b}^{(2)} \right) \qquad (2)$$

where N_A is the molar flux of solute A, a is the interfacial contact area between liquid 1 and liquid 2, K_L is the overall mass transfer coefficient of solute A, and $C_{Ab}^{(1)}$ and $C_{A_b}^{(2)}$ are the bulk concentrations of the solute in the raffinate and extract, respectively.

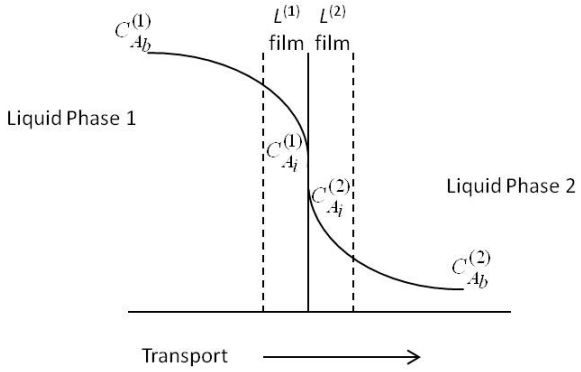

Figure 5.3 Typical concentration profile at the interface between two liquids as solute A diffuses from liquid 1 to liquid 2.

It is important to note here that in the absence of empirical data mass transfer coefficients must be determined using correlations [68, 74]. According to most of the correlations available in literature the value of the mass transfer coefficient for fluid-fluid

systems is dependent on fluid properties, fluid velocity, the diffusion coefficient of the solute, and the geometry of the system [74]. For the study outlined in this chapter, we did not have a good understanding of the wet interfacial contact area between the liquid phases, we only had an estimate of the dry contact area; wet contact area can only be determined from in situ imaging studies or detailed computational fluid dynamics analysis. Wet contact area information is needed to precisely determine the velocity of the fluids and estimate the geometry of the extraction system, thus the overall mass transfer coefficient was not known. However, if we look at equation 2, we can see that another variable affecting mass transfer rate is solute concentration. And while the exact fluid velocity cannot be estimated without wet contact area information, we can measure fluid flow rate and the cross sectional area of the fabric; these parameters can be used to find superficial velocity, V_s. By carrying out the copper ion extraction at a range of initial copper concentrations, in amphiphilic fabrics that provided for different fluid flow rates, the efficiency of the extraction can be studied with respect to superficial velocity and solute concentration. Results will not allow us to describe the dynamics of mass transfer in amphiphilic fabrics in detail, but they will provide enough information for us to characterize the efficiency of the system at a range of conditions and speculate about the dynamics of mass transfer.

The efficiency of an extraction can be determined by measuring the amount of the solute in the raffinate phase before and after the extraction. The percent efficiency, %E, of the copper ion extraction from water was calculated using equation 3.

$$\%E = \left(1 - \frac{[Cu_{aq}]_f}{[Cu_{aq}]_i} \right) \times 100 \quad (3)$$

Where $[Cu_{aq}]_i$ and $[Cu_{aq}]_f$ are the initial and final concentrations of copper ions in the aqueous (raffinate) phase, respectively.

Solution Preparations

For the copper ion extraction experiments, the aqueous phase was prepared by dissolving a pre-weighted amount of $Cu_2SO_4 \bullet 5H_2O$ in acetate buffer media (pH ~ 4.3) to provide copper ion concentrations of 50 ppm-200 ppm. The organic phase was prepared by dissolving D2EHPA in dodecane to create a 100mM solution.

Experimental Procedure and Set-Up

The fabric extractions were conducted using a vertical two-phase wicking set-up (cf. Figure 5.4). To conduct vertical two-phase wicking, 51 × 22 mm fabric samples were cut of designs 5H-5L/2H-2L, 5H-5L/1H-1L, and 2H-2L/2H-2L (also see Figure 5.1). One end of each fabric sample (~30 mm) was cut lengthwise to create feeder strips that could be immersed into separate reservoirs for the water/copper/acetate mixture (feeder strip width ~14 mm) and the D2EHPA/dodecane mixture (feeder strip width ~8 mm). A special reservoir was created into which a fabric could be inserted and hung vertically, to ensure that liquids would only have to wick downwards through the fabric (cf. Figure 5.4). The reservoir was constructed from PDMS by pouring uncured, liquid PDMS into a mold consisting of two hemi-cylinders glued onto a microscope slide,

separated by about 5 mm. Once the PDMS was cured in the oven at 70^{o}C and removed from the mold a dual-feed reservoir was formed with separate organic and aqueous sections. The feeder strips were connected to the liquids through a slit in the bottom of the PDMS reservoir that provided a tight, leak-free fit. The reservoir with the fabric was then attached to a holding bridge constructed of Fishertechnik building blocks (Studica, Inc; Sanborn, NY). Once the reservoir was securely in place one section was filled with the aqueous phase (~4 mL). The fabric was allowed to saturate with the aqueous phase until liquid began dripping from the bottom of the fabric. A reservoir was placed underneath the fabric on top of a balance to record the flow rate through the fabric. The mass of liquid dripping from the fabric was recorded via Labtronics Balance Talk XL data acquisition software (Labtronics Inc; Guelph, Ontario) on a computer connected to the analytical balance (Sartorius Acculab VIC, Data Weighing Systems, Inc; Elk Grove IL) via an RS232 serial port. Once the water was dripping at a steady rate, the organic reservoir was filled (~3 mL) to initiate the co-flow and extraction. At this time, the reservoir beneath the fabric, which had been accumulating untreated water, was replaced with a new reservoir. This was done to ensure that the treated aqueous phase was not re-contaminated by allowing it to mix with the untreated water in the exit reservoir. Approximately 2 minutes after the aqueous reservoir was empty, the extraction was stopped. The contents of the exit reservoir were poured into a separatory funnel and left undisturbed for at least 30 minutes to ensure complete separation of phases.

After separation, the aqueous phase was collected and analyzed to determine its copper ion concentration using a Buck Scientific 210 VGP Flame Atomic Absorption Spectrometer (Buck Scientific Inc.; East Norwalk, CT). To prepare the raffinate solutions

for the spectroscopy studies they were diluted with deionized water between 1.5 to 10 times depending on their initial concentration, so that the concentration range of the copper ions fell within the linear analysis region of the instrument (1-5 ppm Cu). Standard solutions were also prepared at concentrations of 1, 2, 3, 4 and 5 ppm copper. The absorbance of each sample was determined from an average of 5 readings with instrumental error of ~5%. A calibration curve of absorbance versus copper concentration was created using the standard copper solutions (1, 2, 3, 4, and 5 ppm Cu). Using the calibration curve and the absorbance readings of the raffinate samples, the final copper concentration in the aqueous phase after each extraction was determined.

For batch extractions, equal volumes of the organic and aqueous phases (4 mL each) were placed in a 20 mL vial. For batch extractions with externally applied energy, the vial was sealed and repeatedly inverted for 10 minutes; for batch extractions without applied energy the vial was sealed and left sitting undisturbed for 10 minutes. After all extractions the contents of the vial were poured into a separatory funnel and left undisturbed for at least 30 minutes to ensure complete separation of phases. After at least 30 minutes, the aqueous phase was collected for analysis of the copper ion concentration using a Buck Scientific 210 VGP Flame Atomic Absorption Spectrometer.

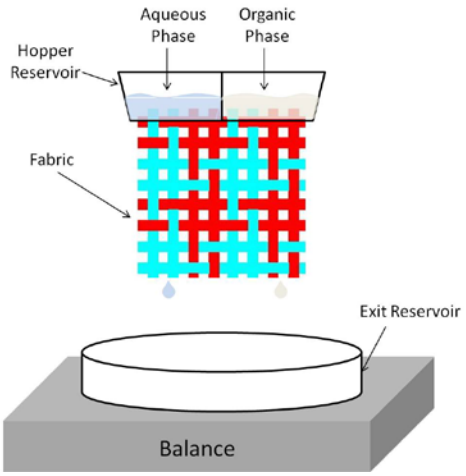

Figure 5.4 Two-phase vertical wicking set-up**.**

It is important to note here that although 30 minutes of separation time is significantly larger than the length of time of the extractions, the liquid phases are not in intimate contact when inside the separatory funnel, so mass transfer within the 30 minutes should be much smaller than the mass transfer between phases during the extractions. Nevertheless, we still conducted several batch extractions in vials with varying residence times. The results showed that for extractions conducted with residence times ranging from 5 – 30 minutes and then an additional 30 minutes for phase separation, there are significant differences in extraction efficiency; ~50-90%, respectively. This indicates that the variations in extraction efficiencies reported in this study are due to the extraction process, not the separation step.

5.3 Results and Discussion

5.3.1 Qualitative Extraction Studies

The series of images in Figure 5.5 displays the progression of the extraction of acetic acid from hexane into water in fabrics 5H-5L/4L, 5H-5L/2H-2L, and 2H-2L/2H-2L. As described in the Methods section and illustrated in Figure 5.3, each fabric strip was cut lengthwise to create feeder strips that were immersed in aqueous and organic phases, respectively. When water (dyed with thymol blue) wicked into the fabric, it stained the white hydrophilic yarns yellow-green; as hexane (mixed with acetic acid) entered the fabric it came into contact with the aqueous phase; acetic acid was transferred into the aqueous phase, causing the yellow-green water to turn pink. In these experiments the aqueous phase was allowed to wick before the organic phase to compensate for its slower wicking rate and thus ensure that both liquids entered the horizontal fabric area within the camera field-of-view simultaneously. As a result, the column of images in Figure 5.5b, only show the aqueous phase in the fabric, as hexane has not wicked into the fabric yet. In the first column of the next series of images, Figure 5.5c, the organic phase has been allowed to wet the fabric and the organic wetting front is just coming into view near the top portion of the images, as is indicated by a slight color change of the water. The rest of the images in each row show the progression of the extraction as the organic phase wicks through each fabric sample and transfer of acetic acid takes place.

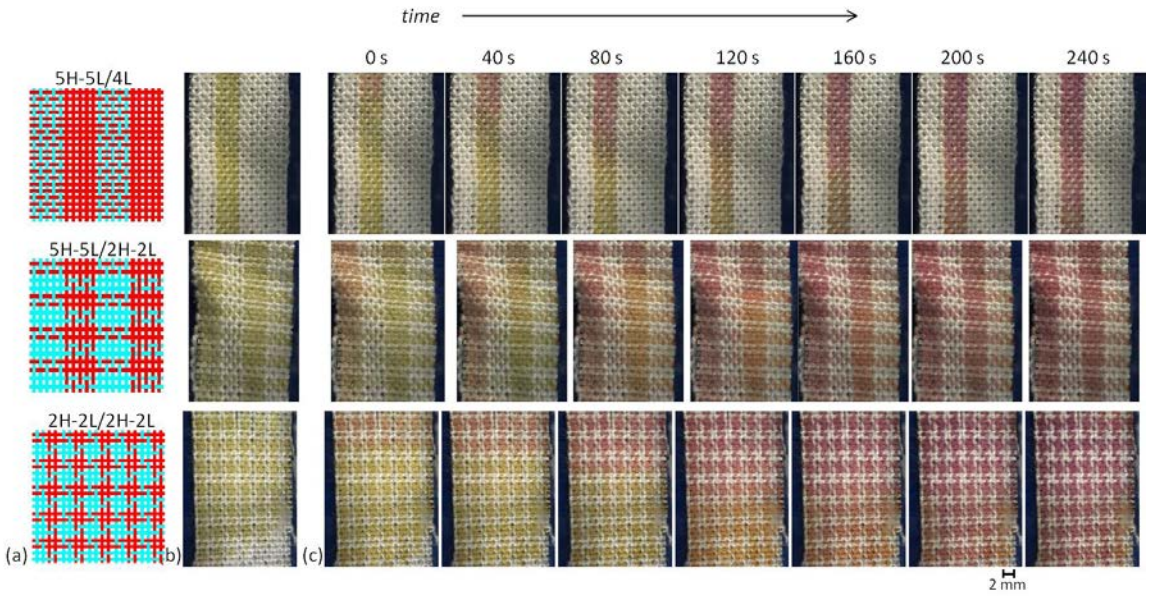

Figure 5.5 Progression of acetic acid extraction into water within amphiphilic fabrics. (a) fabric schematics, (b) fabric images showing water (stains yellow-green) pre-wicked into fabrics (c) time-resolved overhead images of acetic acid extraction; in the image at 0 s hexane has reached the pre-wicked hydrophilic yarns which are saturated with water/thymol blue mixture; as acetic acid is transferred from the hexane phase into the aqueous phase, the water pH is lowered and the indicator changes color from yellow-green (pH 7) to pink (pH 2).

Throughout the extraction in each of the fabrics in Figure 5.5, the water phase changes from yellow-green color (pH ~7) to orange-pink color (ph ~5) and then to hot pink (pH~2) toward the end of the extraction. This observation clearly indicates that there is sufficient intimate contact between the aqueous and organic phases in the amphiphilic fabrics to promote significant transport of acetic acid into the water phase. Additionally, because the aqueous phase is confined to the hydrophilic yarns, the interface for acetic acid transfer is located only at the hydrophilic yarns, where the aqueous and organic phases are in contact. As we change the placement of the hydrophilic yarns in the fabric, the interface for mass transfer also changes. Comparison

of the images of the extraction process with the weaving patterns shows unambiguously that the location of the color changed phase in the fabric exactly matches the placement of the hydrophilic yarns in the fabric throughout the extraction. Hence, it can be concluded that the contact area for liquid-liquid extraction in an amphiphilic fabric can be controlled by the placement of the hydrophilic and hydrophobic yarns woven in the fabric.

The extraction system used for this study was suitable for visual analysis, however for quantitative studies the concentration of the solute in the aqueous phase should be precisely and accurately determined. The concentration of metal ions in water is easily determined using flame atomic absorption spectroscopy (FAAS). This technique is precise, accurate and highly selective. The following section details the results of copper ion extractions from water, with the copper ion concentration analyzed via FAAS.

5.3.2 Quantitative Extraction Studies

Figure 5.6 displays the efficiency of the extraction of copper ions from water using D2EHPA diluted in dodecane plotted as a function of initial copper ion concentration. The fabrics used for the extractions were 5H-5L/2H-2L, 5H-5L/1H-1L and, 2H-2L/2H-2L, displayed in Figure 5.6a. Below each fabric schematic is the superficial velocity of the liquid phases calculated from the total flow rate data recorded during each extraction. Each velocity is an average of 5 separate trials with error of ~ 15%. Also reported is the Reynolds number, which characterizes the flow regime of the liquid in each fabric; all fabrics have creeping liquid flow. Residence times (τ) are reported in the Figure 5.6 caption and were found using the liquid flow rate (v) and the

volume of the liquid phase in the fabric (V) during the extraction; $\tau = V/v$ [75]. Figure 5.6b shows the extraction efficiencies for all three fabrics tested, and Figure 5.6c compares the efficiency of the copper ion extraction in fabric 5H-5L/2H-2L, with values obtained for batch extraction in vials. Data are shown for the batch extractions conducted with and without applied energy (*i.e* agitation). Agitation is used commonly in industrial liquid-liquid extractions to improve efficiency; create flow in the phases and increase contact area between phases. In this study, energy was applied to the system by constantly inverting the batch extractor. Batch extractions were also conducted without applied energy to provide a more direct comparison to the fabric extractions, which do not require the input of any external energy to promote contact between phases, other than gravitational and capillary forces that drive wicking flow.

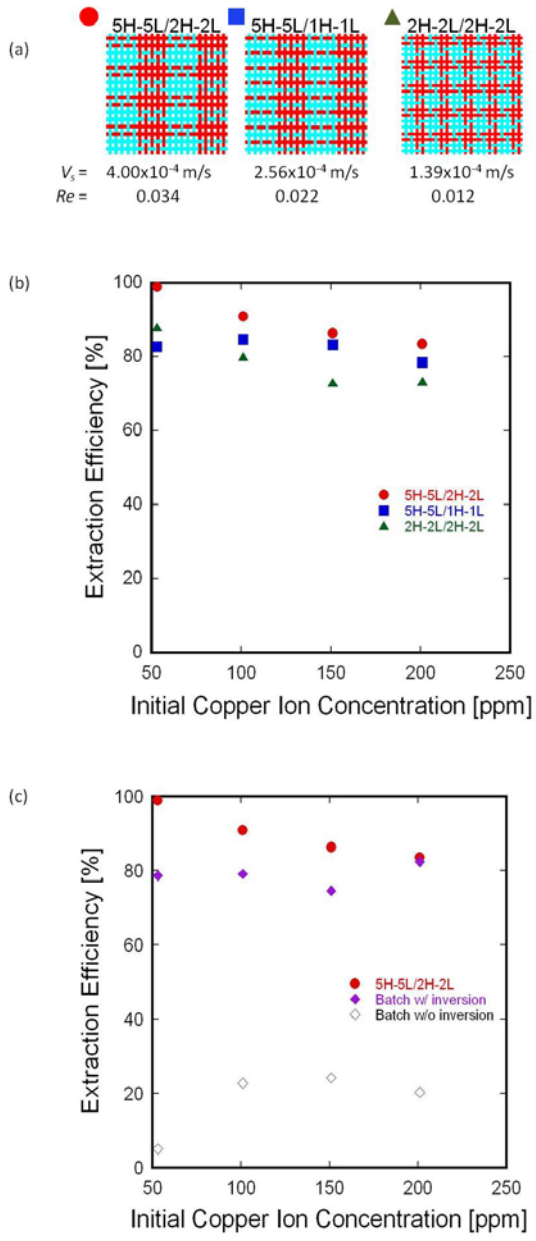

Figure 5.6 Extraction efficiency versus initial copper ion concentration (a) schematic of the three fabrics used for copper ion extraction studies; values below each schematic are superficial velocity and Reynolds number for each fabric, the aqueous phase residence time for each fabric shown was ~5 min, ~8 min, ~24 min, respectively (b) extraction efficiencies for the three fabrics tested (c) comparison of extraction efficiency between fabric 5H-5L/2H-2L and batch extractions with and without applied energy (*i.e.* agitation)

From Figure 5.6b we see that with amphiphilic fabrics we can achieve extraction efficiencies between 75% and 98% for the range of conditions probed in these experiments. Figure 5.6c shows that the batch efficiencies are lower than the efficiencies for the extractions in fabric 5H-5L/2H-2L. The efficiencies for the batch extractions with applied energy were ~80% and without applied energy they were ~20%. The very low efficiency at 50ppm copper ion concentration for the batch extractor without applied energy is most likely due to the reduced contact area between phases. According to the characteristics of mass transfer between two liquids the reduced contact area would have a larger affect on dilute solute concentrations due to the lack of a concentration driving force in the bulk of the liquid phases. The data in Figure 5.6 suggests that amphiphilic fabrics show promise for use in industrial-scale extractions, in particular at low contamination levels. These fabrics could possibly reduce energy costs associated with extraction equipment, while still achieving the high efficiencies that are necessary for complete extractions.

The efficiency data reported for the fabrics in Figure 5.6b were good, but they also showed some unexpected trends. At first sight the trend of the effect of fabric construction seems counter-intuitive. We see that fabric 2H-2L/2H-2L has the lowest extraction efficiency, the values for fabric 5H-5L/1H-1L are slightly higher and fabric 5H-5L/2H-2L performs the best. The weaving pattern of fabric 2H-2L/2H-2L suggests that more intimate contact should occur between phases than in the other fabrics, due to the more intricate network of hydrophilic and hydrophobic yarns; 2H-2L/2H-2L has a specific contact area of ~ 2.94 mm^{-1}, while the specific contact area of fabrics

5H-5L/2H-2L and 5H-5L/1H-1L was ~1.37 mm^{-1}. From a classic understanding of mass transfer, as what was summarized in the Methods section, a larger contact area between immiscible phases should lead to larger mass transfer rates of solute and thus a more efficient extraction. The data in Figure 5.6b show the opposite effect. Furthermore, if we look at the superficial velocities reported for each fabric in Figure 5.6a, we see that higher efficiencies correspond with higher velocities of the liquids. This is another unexpected result, because larger velocities imply a shorter residence time in the fabric and a shorter contact time between phases, which is usually detrimental to mass transfer efficiency.

When analyzing the results in Figure 5.6a and 5.6b we must obviously consider other factors that complicate the dynamics of mass transfer between phases. In a paper done by Dessimoz *et. al*., researchers showed that for two-phase flow in a microchannel, instabilities at the liquid-liquid interface play an important role in the mass transfer dynamics between phases [76]. Their research shows that interfacial tension and viscous forces control the stability of the interface between two immiscible liquids. The competition between these main forces can be quantified using a dimensionless number, the capillary number (Ca) to describe each phase; $Ca = \eta v/\sigma$, where η is fluid viscosity, v is the linear velocity of the fluid, and σ is the liquid-liquid interfacial tension. As the capillary number decreases, the tension forces become more dominate. The interfacial tension reduces the interfacial contact area and slug flow is observed (cf. Figure 5.7a). As the capillary number increases, viscous stresses become more relevant. The viscous forces extend and drag the fluid along the walls of the microchannel and the liquids flow in parallel streams (cf. Figure 5.7b). In this study, fluid properties remain unchanged, so

the velocity of the fluid is the only factor that varies the capillary number and thus controls if slug flow or stream flow will dominate.

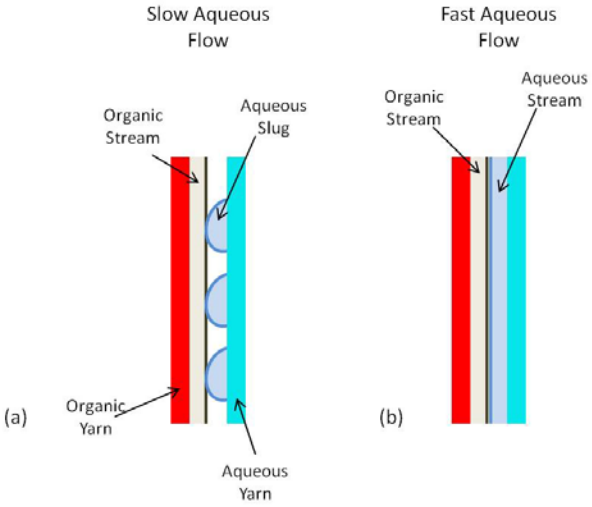

Figure 5.7 Possible flow patterns in amphiphilic microchannel at slow and fast aqueous flow rates. (a) aqueous slug flow at low flow rates reduces contact area between organic and aqueous phases, whereas (b) aqueous stream flow maximizes contact area between organic and aqueous phases; flow concept derived from research done by Dessimoz *et. al* [76].

The superficial velocities listed in Figure 5.6a show that fabric 5H-5L/2H-2L wicks liquid faster than 5H-5H/1H-1L and 2H-2L/2H-2L. If there were any instabilities at the interface between the two phases created by competition of interfacial tension and viscosity difference between the immiscible fluids it is possible that, 5H-5L/2H-2L provides a better extraction efficiency in spite of shorter residence times and a less intricate amphiphilic network. 5H-5L/2H-2L has the fastest superficial velocity, possibly allowing the aqueous phase to flow next to the organic phase in streams rather than slug

flow. Fluid flowing in streams would likely provide a higher contact area between phases than fluid flowing along the amphiphilic channels as slugs.

Another observation from the copper extraction suggests that the extraction efficiency in amphiphilic fabrics is highest at dilute concentrations of solute. Figure 5.6b shows this trend for every fabric tested. If we look at the extractions carried out in a traditional batch extractor as in Figure 5.6c we see that contrary to the fabric extractions, the efficiency of the batch extractor has little dependence on initial copper concentration. This indicates that the concentration dependence observed in the fabric must be a characteristic of the dynamics of liquid-liquid extractions in amphiphilic fabrics.

The concentration dependence observed in the fabrics can be explained by considering the difference between the concentration profile for a traditional extractor versus a microchannel. Mass diffusion at a liquid-liquid interface in an extractor generally follows the concentration profile in Figure 5.2: concentration gradients are located in concentration boundary layers on both sides of the interface, with homogenous bulk concentrations. However, because microchannels are so small, the concept of a bulk phase is unrealistic and concentration gradients should occur throughout the entire liquid phase. Hence, the concentration driving force for mass transfer might become higher in a microchannel than in a batch extractor so that dilute concentrations of copper result in higher extraction efficiencies in a microchannel than in a batch extractor. Although the trend of efficiency versus initial copper ion concentration in Figure 5.6c was unexpected, it could be very useful for high-value applications, where pure product streams are needed. The dynamics of liquid-liquid extractions at dilute solute concentrations in amphiphilic fabrics could prove valuable and should be further investigated.

The amphiphilic fabrics used for these extraction studies should be further developed for the removal of dilute concentrations of metal ions from water, a process which is commonly used for wastewater treatment. We have shown here that these fabrics perform well at dilute solute concentrations. Well-made fabrics can typically be used up to 25 times before they show signs of ware. An amphiphilic fabric can be designed with hydrophobic and hydrophilic yarns intersecting in one portion of the fabric and not intersecting in another portion of the fabric. In the intersecting portion, an extraction can be conducted and as the liquid phases are transported to the non-intersecting portion, the phases could be separated. The simultaneous extraction and separation of phases could prevent the need for a separation step at the end of the process. It is clear that the flow rate of water in the fabrics used in these studies is not fast enough to be sufficient for an industrial process, but flow rates can be significantly improved upon increasing the size of the fabric, in particular the length. Increasing the length will increase the hydrodynamic pressure in the fabric and cause the liquids to drip from the fabric faster.

5.4 Conclusions

The rate of solute mass transfer between two liquids depends on the size of the interfacial contact area, contact time between the two phases, flow rates and solute concentration. In traditional solvent extraction equipment energy is applied to increase the contact area between phases for more efficient extractions. However, this study shows that a large contact area between immiscible phases can be maintained without apply energy when organic and aqueous phases wick along the hydrophilic and hydrophobic

yarns in an amphiphilic fabric. Results from qualitative solvent extraction experiments show that there is sufficient contact between liquid phases in an amphiphilic fabric to facilitate mass transfer and achieve liquid-liquid extraction. These studies also showed the contact area between phases can be controlled by varying the arrangement of hydrophilic and hydrophobic yarns in the fabric. Results from quantitative studies showed that extractions in amphiphilic fabrics can be conducted at efficiencies of up to ~98%. In comparison, the efficiency of the copper ion exactions in a traditional batch extractor without applied energy is ~20%. Because of the high solvent extraction efficiencies that can be achieved without applying energy, amphiphilic fabrics show great promise as a new technology that can reduce costs and energy requirements for industrial-scale solvent extractions.

For further development of amphiphilic fabrics for industrial applications some ambiguities need to be addressed. In the extraction studies outlined in this thesis chapter, only a general idea existed of the contact area between phases based on the location of hydrophilic and hydrophobic yarns in each amphiphilic fabric; no in situ measurements of interfacial geometry have been performed. As it follows, counter-intuitive relationships between extraction efficiency, estimated dry contact area, and superficial velocities were observed. An estimation of wet interfacial contact area and linear velocity profiles are necessary to draw concrete conclusions about the dynamics of mass transfer in amphiphilic fabrics. Imaging studies such as MRI and computational fluid dynamics should be carried out to determine the wet contact area between phases across a range of process conditions, so that a more detailed quantitative analysis of the interfacial dynamics of two-phase flow in amphiphilic fabrics can be made. Additionally, although it

was unexpected that the extraction efficiency in amphiphilic fabrics would increase at dilute solute concentrations, this trend could prove valuable for high-value applications and should be further investigated.

CHAPTER 6

CONCLUSIONS AND RECOMMENDATIONS

6.1 Conclusions

This thesis is based on the idea that the interlocking yarns of a fabric create a network of microchannels similar to a microfluidic device and that weaving hydrophilic and hydrophobic yarns together into the same fabric allows for precise control over fluid transport into the fabric based on the placement of the two yarn types in the woven structure. The goal of this thesis was to conduct fundamental experimental studies to prove this hypothesis and to show the feasibility of using amphiphilic fabrics for large-scale applications, such as industrial liquid-liquid extractions. To achieve this goal, a novel class of amphiphilic fabrics was designed and manufactured. Their fluid transport properties were then investigated with a single fluid, as well as in co-flow of immiscible fluids.

As a prelude to the amphiphilic fabric studies, an initial study aimed to quantify the intensive performance properties of fabrics in the form of permeability-saturation curves. Accurate knowledge of these fundamental properties is needed for predicting process conditions and scale-up parameters for industrial applications. Chapter 2 showed that a new technique, the integrated upward-horizontal-downward (UHD) wicking test, provides the intensive properties of a fabric. To validate this technique, the UHD test was performed on a plain knit jersey fabric using fluids that varied in viscosity, surface tension, and density (*i.e.* dodecane, tetradecane and hexadecane). Results showed that

there was no significant difference between the permeability, effective capillary radius and saturation data for any of the fluids tested, thus confirming that the UHD test yields intensive, fluid-independent fabric characteristics. Based on the intensive properties derived from the wicking experiments on alkanes, accurate predictions could be made about liquid flow rates of other fluids (*i.e.* water and 1-octanol) into the same fabric, which provided further proof of the value of the UHD test.

After the development of the rigorous wicking test, the attention shifted to the design of amphiphilic fabrics. Chapter 3 described the design, construction and testing of amphiphilic fabrics with the simplest possible weave geometry (plain weave), but with variable patterns of hydrophilic and hydrophobic yarns. The number of adjacent hydrophilic yarns was systematically varied in both primary directions of the fabric (*i.e.* warp and weft directions) to change the fraction of inter-yarn microchannels that were hydrophilic, hydrophobic, and amphiphilic, respectively. Initial testing, including drop tests and upward wicking tests, was performed on 5 specific amphiphilic weaving patterns. Results showed clearly that the inter-yarn microchannels have a much greater contribution to wicking flow than the intra-yarn microchannels inside each porous yarn. Furthermore, it was found that wicking flow of aqueous fluids in these fabrics can be controlled, both with regards to directionality and magnitude, by precise placement of hydrophilic yarns relative to the hydrophobic yarns. Increasing the density of inter-yarn hydrophilic microchannels significantly enhanced flow rates of aqueous fluids. Unprecedented simultaneous co-flow of an aqueous fluid and a hydrocarbon fluid was demonstrated in the amphiphilic fabric. A key observation was that neither fluid was able

to displace the other and that each fluid accurately followed the flow paths defined by yarns of the corresponding surface chemistry.

Although the initial studies provided clear proof-of-concept data on the ability of amphiphilic fabrics to sustain co-flow of immiscible phases, further studies were needed to develop a more quantitative understanding of the effect of fabric design on wicking flow rates. In Chapter 4, a comprehensive study on 18 amphiphilic fabric patterns was conducted to identify the design parameters that affect liquid transport into amphiphilic fabrics and to determine which fabrics would be best candidates for use in liquid-liquid extractions, an application that requires both large interfacial contact area and sustained flow of the two immiscible phases. It was found that the arrangements of hydrophilic and hydrophobic yarns in a woven amphiphilic fabric can be defined through 5 key structural features that significantly affect wicking flow: the H/L ratio (balance between hydrophobic and hydrophilic yarns), density of inter-yarn channels between yarns of the same type, density of intersections between like yarns, yarn blockages due to intersecting yarns of the opposite type, and yarn orientation. Increasing the H/L ratio, channel density and intersection density, and decreasing the number of yarn blockages all improved the upward wicking flow rate of aqueous fluids. Additionally, a somewhat expected finding was that wetting yarns must be oriented parallel to the direction of flow to promote wicking. Based on these studies, four fabrics with optimized structural features were selected for initial testing of liquid-liquid extractions in amphiphilic fabrics.

To prove the feasibility of using amphiphilic fabrics in industrial-scale liquid-liquid extractions, the next steps were (1) to show that this process can be carried out in an amphiphilic fabric and (2) to quantify the efficiency of extractions in fabrics to prove

competitiveness. In Chapter 5, the extraction of acetic acid from hexane into water, in the presence of an acid-base indicator, was visualized via video microscopy for amphiphilic fabrics with three different weaving patterns. From these qualitative solvent extraction experiments it was concluded that sufficient contact area exists between immiscible liquid phases in the amphiphilic fabrics to facilitate mass transfer and achieve liquid-liquid extraction. These studies also showed that the interfacial contact between phases could be controlled by the placement of hydrophilic and hydrophobic yarns in the fabric. Subsequently, quantitative extractions of copper ions from water using dilute solutions of D2EHPA in dodecane were conducted to obtain quantitative extraction data. It was found that extractions in our first-generation amphiphilic fabrics varied between ~75 and ~98%. In contrast, the extraction efficiency of a comparable batch process without supply of external energy was only ~20%. Even when moderate amounts of external energy were provided to a batch extraction by inverting the vial, the extraction efficiencies were lower than for the amphiphilic fabrics.

The studies outlined in this thesis have shown that controlled microfluidic transport in an amphiphilic fabric can be achieved through the arrangement of hydrophilic and hydrophobic yarns and that these fabrics have potential to reduce equipment and energy costs when used as contactors for industrial-scale liquid-liquid extractions. To continue development of amphiphilic fabrics for industrial use there are additional studies that should be completed.

6.2 Recommendations

The liquid-liquid extraction studies outlined in Chapter 5 showed that fabric extraction efficiency increases in fabrics with larger superficial fluid velocities and when alternations between hydrophilic and hydrophobic yarns are less frequent. These results are counter-intuitive, since one would expect that efficiency would decrease if the contact area and residence time are decreased. However, this expectation is based on extrapolation of experiences with traditional extraction processes. The unique characteristics of two-phase flow in amphiphilic fabrics could easily give rise to unexpected complications; for example, the location and stability of the liquid-liquid interface are unknown. Instabilities may affect the contact area between two phases at small flow rates and the location of the interface could vary as a function of fluid velocity. Obviously, more detailed studies to identify the shape of the liquid-liquid interface would be critical to fully understand the dynamics of mass transfer in amphiphilic fabrics. Therefore, it is recommended that MRI imaging studies and computational fluid dynamics studies are conducted on two-phase flow in amphiphilic fabrics. With MRI studies we can use spatially resolved spectroscopy to probe the interfacial contact area of the extraction as a function of position and time, which is particularly useful for a non-transparent system. Although the MRI studies will not yield high-resolution images, they can provide valuable bench marks for computational studies. Computational fluid dynamics will allow us to model the motion of the fluids involved in the extraction system, so that we can quickly determine the effect that variations in fabric design have on the interfacial dynamics and mass transfer of the liquid-liquid system.

The liquid-liquid extraction studies also showed that extraction efficiency of the amphiphilic fabrics increased at dilute solute concentrations. This characteristic could be very useful for high value applications where pure product streams are necessary, but further studies need to be performed to validate and explain these experimental findings. Additional experimentation of solvent extractions at solute concentrations below 50 ppm should be explored; results would confirm the trend and test for feasibility in commercial applications.

Finally, a two-phase upward-horizontal-downward (UHD) wicking test should be conducted on all the amphiphilic fabrics that are ideal for use with liquid-liquid extractions. Initially, completing two-phase UHD experiments with amphiphilic fabrics was an objective of this thesis. However, during testing we found that the rate of aqueous transport along the hydrophilic yarns was not adequate to support planar flow throughout the upward, horizontal, and downward test sections. Towards the middle of the horizontal test section the rate of aqueous wicking became so slow that it was of the same magnitude as the evaporation of water from the surface of the fabric. Hence, the liquid wicking rate was insignificant and no rate data could be obtained to calculate effective capillary radius and permeability. This is unfortunate, because the UHD tests could have provided valuable permeability-saturation relationships for each amphiphilic fabric. Such information is useful for predicting process conditions upon scale up (*e.g.* liquid flow rates) and optimizing fabric design (*e.g.* yarn density and diameter).

It is recommended that a new series of amphiphilic fabrics will be manufactured with better performing hydrophilic yarns; in particular the water contact angle and the durability of the wetting properties of these yarns were not ideal in our current studies.

Research has shown that chemically altering the surface of synthetic fibers can improve their moisture absorption properties significantly; plasma treatment of PET yarns have been shown to yield water contact angles as low as 43^{o} [77, 78] . A direct comparison of the wicking rates of water in the plain knit fabric used in Chapter 2 with the fully hydrophilic plain weave fabric used in Chapter 3, suggests that knitted fabric constructions can facilitate larger aqueous wicking rates than woven ones. In the introductory chapter of this thesis it was shown that bicomponent synthetic fibers can also be manufactured that combine amphiphilic properties on the length-scale of individual fibers, and that knitted fabrics can be constructed with complex patterns. For example, the milanese knit was composed of two loops one from different sets of warp yarns, both knitted diagonally into the fabric. If we, construct an amphiphilic fabric with a milanense knit, using bicomponent side by side fibers made of plasma treated PET (hydrophilic fiber) and polypropylene (hydrophobic fiber), intimate intra-yarn and inter-yarn contact between immiscible phases could be achieved within the fabric. A liquid-liquid extraction conducted in such a system has the potential to be incredibly efficient. Furthermore, because the fabric construction and fibers should outperform our first generation fabrics, two-fluid UHD tests should be feasible with those new fabrics. From these UHD tests, the fundamental permeability-saturation relationship for amphiphilic fabrics could be calculated so that accurate predictions about fabric design and processing conditions can be made upon scale-up to industrial-sized liquid-liquid extractions.

As stated in the introduction of this thesis, recent advances towards cheaper microfluidic devices have largely been driven by the desire to deploy point-of-care (POC) diagnostic screening kits in developing countries for detection of common diseases.

Cheap, porous materials that can efficiently wick liquids via capillary action, like paper and cotton yarns, have emerged as primary candidates. The established infrastructure of the textile manufacturing industry also makes amphiphilic fabrics appealing as substrates for point-of-care medical diagnostic devices. The studies in Chapter 3 showed that flow of aqueous liquids proceeds exclusively along hydrophilic yarns. The repetitive nature of the woven fabrics, however, does not provide great flexibility in the design of microfluidic devices. Alternatively, a plain weave fabric consisting solely of hydrophobic yarns can easily be embroidered with hydrophilic yarns in virtually any pattern. A complex network of hydrophilic channels and reservoirs could thus be integrated into a hydrophobic fabric using standard embroidery patterns. Such embroidered POC devices could easily and cheaply be mass-produced. The work in this thesis has already shown control of microfluidic flow can be achieved by the placement of hydrophilic and hydrophobic yarns in a woven fabric, which is likely directly applicable to embroidered amphiphilic fabrics.

REFERENCES

1. Beebe, D.J., G.A. Mensing, and G.M. Walker, *Physics and applications of microfluidics in biology.* Annual Review of Biomedical Engineering, 2002. **4**: p. 261-286.

2. Patnaik, A., *Wetting and Wicking in Fibrous Materials.* Textile Progress, 2006. **38**(1): p. 100.

3. Bear, J., *Dynamics of Fluids In Porous Media*1972, New York: Elsevier.

4. Alam, S., et al., *Effect of Orientation of Glass Fiber on Mechanical Properties of GRP Composites.* Journal of the Chemical Society of Pakistan, 2010. **32**(3): p. 265-269.

5. Or, D. and M. Tuller, *Capillarity*, in *Encyclopedia of Soils in the Environment*, H. Daniel, Editor 2005, Elsevier: Oxford. p. 155-164.

6. Chatterjee, P.K. and B.S. Gupta, *Chapter I Porous structure and liquid flow models*, in *Textile Science and Technology*, P.K.C.a.B.S. Gupta, Editor 2002, Elsevier. p. 1-55.

7. Dullien, F.A.L., *Porous Media Fluid Transport and Pore Structure*. Second Edition ed1979, San Diego, CA: Academic Press.

8. Charbenau, R.J., *Groundwater Hydraulics and Pollutant Transport*. First Edition ed2006: Waveland Press Inc.

9. Welty, J.R., et al., *Fundamentals of Momentum, Heat, and Mass Transfer*. Fourth Edition ed2001, New York, NY: John Wiley & Sons, Inc.

10. Ehrfeld, W., V. Hessel, and H. Lowe, *Microreactors New Technology for Modern Chemistry*. First Edition ed2000, Mainz, Germany: WILEY-VCH.

11. Rivet, C., et al., *Microfluidics for medical diagnostics and biosensors.* Chemical Engineering Science, 2011. **66**(7): p. 1490-1507.

12. Whitesides, G.M., *The origins and the future of microfluidics.* Nature, 2006. **442**(7101): p. 368-373.

13. Whitesides, G.M. and A.D. Stroock, *Flexible methods for microfluidics.* Physics Today, 2001. **54**(6): p. 42-48.

14. Zimmerman, W.B.J., *Microfluidics: History, Theory, and Applications* 2006: SpringerWien New York.

15. Ehrfeld, W., V. Hessel, and H. Lowe, *Microreactors New Technology for Modern Chemistry*. First Edition ed2000, Mainz, Germany: WILEY-VCH.

16. Nagrath, S., et al., *Isolation of rare circulating tumour cells in cancer patients by microchip technology.* Nature, 2007. **450**(7173): p. 1235-U10.

17. Chen, Z.Y., et al., *A microfluidic system for saliva-based detection of infectious diseases.* Oral-Based Diagnostics, 2007. **1098**: p. 429-436.

18. Hansen, C.L., et al., *A robust and scalable microfluidic metering method that allows protein crystal growth by free interface diffusion.* Proceedings of the National Academy of Sciences of the United States of America, 2002. **99**(26): p. 16531-16536.

19. Balu, B., et al., *Patterning of superhydrophobic paper to control the mobility of micro-liter drops for two-dimensional lab-on-paper applications.* Lab on a Chip, 2009. **9**(21): p. 3066-3075.

20. Lu, Y., et al., *Rapid prototyping of paper-based microfluidics with wax for low-cost, portable bioassay.* Electrophoresis, 2009. **30**(9): p. 1497-1500.

21. Martinez, A.W., et al., *Patterned paper as a platform for inexpensive, low-volume, portable bioassays.* Angewandte Chemie-International Edition, 2007. **46**(8): p. 1318-1320.

22. Fu, E., et al., *Controlled reagent transport in disposable 2D paper networks.* Lab on a Chip, 2010. **10**(7): p. 918-920.

23. Fu, E.L., et al., *Transport in two-dimensional paper networks.* Microfluidics and Nanofluidics, 2011. **10**(1): p. 29-35.

24. Reches, M., et al., *Thread as a Matrix for Biomedical Assays.* ACS Applied Materials & Interfaces, 2010. **2**(6): p. 1722-1728.

25. Li, X., J.F. Tian, and W. Shen, *Thread as a Versatile Material for Low-Cost Microfluidic Diagnostics.* ACS Applied Materials & Interfaces, 2010. **2**(1): p. 1-6.

26. Ballerini, D.R., X. Li, and W. Shen, *Flow control concepts for thread-based microfluidic devices.* Biomicrofluidics, 2011. **5**(1): p. 13.

27. Green, D.W. and R.H. Perry, *Perry's Chemical Engineer's Handbook,* in *8th Edition*, McGraw-Hill, Editor 2008.

28. Wilson, K., *A History of Textiles* 1979, Boulder, Colorado: Westview Press, Inc.

29. *Introduction to Textiles Study Guide*, N.C.C.f.A.T. Technology, Editor 2001, North Carolina Center for Applied Textile Technology: Belmont, NC.

30. Hillstrom, K. and L.C. Hillstrom, *The Industrial Revolution in America Automobiles, Mining and Petroleum, Textiles*, 2006, ABC-CLIO and Greenwood Press.

31. Horrocks, A.R. and S.C. Anand, *Handbook of Technical Textiles* 2000: Woodhead Publishing.

32. Holme, I., *Innovative technologies for high performance textiles.* Coloration Technology, 2007. **123**(2): p. 59-73.

33. Anita, S., et al., *A study of the antimicrobial property of encapsulated copper oxide nanoparticles on cotton fabric.* Textile Research Journal, 2011. **81**(10): p. 1081-1088.

34. Wulfhorst, B., T. Gries, and D. Veit, *Textile Technology*. English Edition ed2006, Cincinnati, Ohio: Hanser Gardner Publications, Inc.

35. Gioello, D.A., *Understanding Fabrics: From Fiber to Finished Cloth* 1982, New York: Fairchild Publications Division of Capital Cities Media, Inc.

36. Spencer, D.J., *Knitting Technology*. Second Edition ed1989, Elmsford, New York: Pergamon Press, Inc.

37. *Erica's Stitches*. Sunday, November 29, 2009; Available from: http://emcstitches.blogspot.com/2009_11_01_archive.html.

38. Miller, B. and I. Tyomkin, *An Extended Range Liquid Extrusion Method for Determining Pore Size Distributions.* Text. Res. J., 1986. **56**(1): p. 35-40.

39. Bear, J., *Dynamics of Fluids In Porous Media* 1972, New York: Elsevier.

40. Dullien, F.A.L., *Porous Media: Fluid Transport and Pore Structure*. 2nd ed1992, London: Academic. 574.

41. Hong, C.J. and J.B. Kim, *A study of comfort performance in cotton and polyester blended fabrics. I. Vertical wicking behavior.* **8**(2): p. 218-224.

42. Morent, R., et al., *Measuring the wicking behavior of textiles by the combination of a horizontal wicking experiment and image processing.* Review of Scientific Instruments, 2006. **77**(9): p. 6.

43. Liu, Q., R.S. Parnas, and H.S. Giffard, *New set-up for in-plane permeability measurement.* Composites Part a-Applied Science and Manufacturing, 2007. **38**(3): p. 954-962.

44. Miller, B., *Criticlal Evaluation of Upward Wicking Tests,* 2000, International Nonwovens Journal: Princeton, NJ. p. 10.

45. Patnaik, A., et al., *Wetting and Wicking in Fibrous Materials.* Textile Progress, 2006. **38**(1): p. 1-105.

46. Ataie-Ashtiani, B., S.M. Hassanizadeh, and M.A. Celia, *Effects of Heterogeneitics on capillary pressure-saturation-relative permeability relaitonships.* Journal of Contaminant Hydrology, 2002. **56**: p. 175-192.

47. Fagerlund, F.F., A. Niemi, and M. Oden, *Comparison of relative permeability-fluid saturation-capillary pressure relations in the modelling of non-aqueous phase liquid infiltration in variably saturated, layered media.* Advances in Water Resources, 2006. **29**: p. 1705-1730.

48. Masalmeh, S.K., *The effect of wettability heterogeneity on capillary pressure and relative permeability.* Journal of Petroleum Science and Engineering, 2003. **39**: p. 399-408.

49. Simile, C.B. and H.W. Beckham, *Permeability-Saturation-Capillary Pressure Relations in Textile Fabrics from an Integrated Upward-Horizontal-Downward Wicking Test.* The Journal of the Textile Insitute, 2011. accepted.

50. Ghali, K., B. Jones, and J. Tracy, *Experimental-Techniques for Measuring Parameters Describing Wetting and Wicking in Fabrics.* Textile Research Journal, 1994. **64**(2): p. 106-111.

51. Adamson, A. and A. Gast, *Physical Chemistry of Surfaces*. 6 ed1997, Canada: John Wiley & Sons. 364-580.

52. Washburn, E.W., *The Dynamics of Capillary Flow.* The Physical Review, 1921. **17**(3): p. 273-283.

53. Simile, C.B., *Critical Evaluation of Wicking in Performance Fabrics*, 2004, Georgia Institute of Technology.

54. Miller, B., *Critical Evaluation of Upward Wicking Tests.* International Nonwovens Journal, 2000: p. 35-40.

55. Yaws, C.L., *Yaws' Handbook of Thermodynamic and Physical Properties of Chemical Compounds* 2003: Knovel.

56. Coskuntuna, E., A.J. Fowler, and S.B. Warner, *Fibrous structures with designed wicking properties.* Textile Research Journal, 2007. **77**(4): p. 256-264.

57. Bajaj, P., *Finishing of textile materials.* Journal of Applied Polymer Science, 2002. **83**(3): p. 631-659.

58. Gupta, D., P. Siddhan, and A. Banerjee, *Basic dyeable polyester: a new approach using a VUV excimer lamp.* Coloration Technology, 2007. **123**(4): p. 248-251.

59. Zhu, S.Q. and D.E. Hirt, *Improving the Wettability of Deep-Groove Polypropylene Fibers by Photografting.* Textile Research Journal, 2009. **79**(6): p. 534-547.

60. Patnaik, A., et al., *Wetting and Wicking in Fibrous Materials.* Textile Progress, 2006. **38**(1): p. 105.

61. Watson, J.S., *Separation methods for waste and environmental applications* 1999, New York: Marcel Dekker.

62. Lee, K.J., S.H. Kim, and K.W. Oh, *Organic solvent absorption characteristics of split-type microfiber fabrics.* **5**(4): p. 280-288.

63. Mhetre, S. and R. Parachuru, *The effect of fabric structure and yarn-to-yarn liquid migration on liquid transport in fabrics.* Journal of the Textile Institute, 2010. **101**(7): p. 621-626.

64. Patil, U.J., C.D. Kane, and P. Ramesh, *Wickability behaviour of single-knit structures.* Journal of the Textile Institute, 2009. **100**(5): p. 457-465.

65. Owens, T.L., et al., *Control of Microfluidic Flow in Amphiphilic Fabrics.* ACS Applied Materials & Interfaces, 2011. **3**(10): p. 3796-3803.

66. Kentish, S.E. and G.W. Stevens, *Innovations in separations technology for the recycling and re-use of liquid waste streams.* Chemical Engineering Journal, 2001. **84**(2): p. 149-159.

67. Seader, J.D. and E.J. Henley, *Separation Process Principles*. Second Edition ed2006, Hoboken, NJ: John Wiley & Sons, Inc.

68. Hines, A.L. and R.N. Maddox, *Mass Transfer Fundamentals and Applications* 1985, Upper Saddle River, NJ: Prentice Hall PTR.

69. Wickramasinghe, S.R., M.J. Semmens, and E.L. Cussler, *Better Hollow Fiber Contactors.* Journal of Membrane Science, 1991. **62**(3): p. 371-388.

70. Yang, M.C. and E.L. Cussler, *Designing Hollow-Fiber Contactors.* Aiche Journal, 1986. **32**(11): p. 1910-1916.

71. Ren, Z.Q., et al., *Extraction equilibria of copper(II) with D2EHPA in kerosene from aqueous solutions in acetate buffer media.* Journal of Chemical and Engineering Data, 2007. **52**(2): p. 438-441.

72. Chang, S.H., T.T. Teng, and N. Ismail, *Extraction of Cu(II) from aqueous solutions by vegetable oil-based organic solvents.* Journal of Hazardous Materials, 2010. **181**(1-3): p. 868-872.

73. Chang, S.H., T.T. Teng, and N. Ismail, *Efficiency, stoichiometry and structural studies of Cu(II) removal from aqueous solutions using di-2-ethylhexylphosphoric acid and tributylphosphate diluted in soybean oil.* Chemical Engineering Journal, 2011. **166**(1): p. 249-255.

74. Green, D.W. and R.H. Perry, *Perry's Chemical Engineers' Handbook*, 1997, McGraw-Hill.

75. Davis, M.E. and R.J. Davis, *Fundamentals of Chemical Reaction Engineering* 2003: McGraw-Hill.

76. Dessimoz, A.-L., et al., *Liquid-liquid two-phase flow patterns and mass transfer characteristics in rectangular glass microreactors.* Chemical Engineering Science, 2008. **63**(16): p. 4035-4044.

77. Hossain, M.M., et al., *Contact angle determination on plasma-treated poly(ethylene terephthalate) fabrics and foils.* Journal of Applied Polymer Science, 2006. **102**(2): p. 1452-1458.

78. Gouveia, I.C., L.C. Antunes, and A.P. Gomes, *Low-pressure plasma treatment for hydrophilization of poly(ethylene terephthalate) fabrics.* Journal of the Textile Institute, 2011. **102**(3): p. 203-213.

VITA

TRACIE LEEANNE OWENS

Tracie LeeAnne Owens was born on February 13, 1984 in Berkeley, California. She attended Dublin High School in Dublin, California. She was a part of the Atlanta University Center Dual Degree Engineering Program. She received her Bachelor of Science in Chemistry from Spelman College and her Bachelor of Science in Chemical Engineering from Georgia Institute of Technology in May 2007. As an undergraduate student at Spelman she was the recipient of the ExxonMobil Women in Science and Engineering Scholarship. After finishing her undergraduate studies she was accepted into the doctorate program in the School of Chemical and Biomolecular Engineering at Georgia Tech, where she conducted research under the supervision of Dr. Victor Breedveld and Dr. Haskell Beckham. As a graduate student she received a GEM PhD Fellowship. Her doctoral thesis research was focused in the area of fluid dynamics as it relates to microfluidic flow and flow in porous media. More specifically, she designed and fabricated a microfluidic structure for use as a large-scale chemical separator. After graduating with a Ph.D in Chemical Engineering in December 2011 she will work for ExxonMobil Process Research in Clinton, New Jersey.